Modulation of BMP Signaling During Dorsal-Ventral Patterning in *Drosophila melanogaster*

A DISSERTATION

SUBMITTED TO THE FACULTY OF THE GRADUATE SCHOOL

OF THE UNIVERSITY OF MINNESOTA

BY

Christina Brakken-Thal

IN PARTIAL FULFILLMENT OF THE REQUIREMENTS

FOR THE DEGREE OF

Doctor of Philosophy

Hans Othmer and Michael O'Connor

February, 2014

Acknowledgements

I am very grateful to my advisers Hans Othmer and Michael O'Connor for letting me work on this thesis over the past several years. I appreciate all of their helpful conversations, feedback, support, and patience as I have gone through my graduate training. I want to thank the past and present members of the Othmer Group and O'Connor Laboratory for their comments and support while I have worked on these projects. I would like to thank the members of the Developmental Biology Center and the Mathematical Biology Group for their helpful comments throughout my training. Dr. Aidan Peterson has been extremely helpful in troubleshooting and advising my biology projects. I would also like to thank him for reading my thesis and his helpful and insightful comments. Mary Jane O'Connor has been very helpful in troubleshooting the sequencing of *nejire* in Chapter 2. Chapter 3 of this thesis was completed in close collaboration with Dr. Likun Zheng. We developed the models and ran the simulations together for this

project.

I am very greatful to several funding sources that supported my throughout my training. I would like to thank the Biotechnology Training Grant for the first 2 years of my funding. I would like to thank the Warwick Fellowship through the Graduate School for the third year of my funding. I would like to thank the Developmental Biology Training Grant for my fourth year of funding. I would like to thank the Musculoskeletal Training Grant for my fifth year of funding. It has been a pleasure to get to be a part of these training programs and they have enriched my graduate school experience immensely.

I would like to thank my family for their love and support in completing this thesis. I would like to thank my parents Steven Thal and Peggy Brakken Thal for their support, trust, and encouragement. I would like to thank my husband, Jeff Thaler, for all his help throughout my PhD. I want to thank him for letting me discuss my projects, reading my drafts of the thesis, and his support and encouragement throughout my training. I would like to thank Natalie Thaler and Peggy Brakken Thal for helping to take care of my son over the last few months in order to give me more time to complete my thesis. Without all of your help and support this thesis would not have been possible.

Dedication

This thesis is dedicated to my family. To my parents Steven Thal and Peggy Brakken Thal for their love and support through my many years of schooling. To my brother Sean Brakken-Thal for his love and encouragement. To my husband Jeff Thaler whose love and support throughout my entire thesis would not have made this possible.

Abstract

Bone Morphogenic Protein (BMP) signaling is a conserved pathway used for development and homeostasis. In the model system *Drosophila melanogaster* patterning of the dorsal surface is controlled by Decapentapolegic (DPP), a BMP protein that robustly stimulates the BMP signaling pathway in a narrow domain of cells on the dorsal surface of the embryo. The levels of Dpp are estimated to be between 10-100 molecules / nucleus, which would predict a significant level of noise in Dpp signaling. However this is not observed, so there must be mechanisms that dampen noise in signaling pathways. I used molecular biology, genetics, and mathematical modeling to identify possible mechanisms for feedback control of BMP signaling and to elucidate mechanisms to dampen stochastic fluctuations in signaling molecules. I have identified a new novel allele of *nejire* with a stop codon in the 12th exon. This mutation truncates part of the glutamine rich domain at the end of the protein. This new allele has a highly variable phenotype with all embryos showing varying degrees of loss of Dpp signaling in the pre-cephalic furrow embryos, and half showing recovery just before and during gastrulation. I also studied the phenotype of Crossveinless-2 (Cv-2) during dorsal surface patterning.

I found that *cv-2* is a Dpp response gene that is a negative inhibitor of Dpp signaling during dorsal surface patterning. Cv-2 null embryos have a 20% wider area of Dpp signaling on the dorsal surface, and this change leads to a larger amnioserosa later in development. Interestingly loss of Cv-2 leads to a slight increase in noise in the width of pMad, the intracellular signaling of Dpp receptor activation. I followed up on this finding with a 3D stochastic model of Dpp for a single nuclear compartment which suggests that competition for BMP from the receptor could increase noise in signaling. In addition, the stochastic model suggests that endocytosis of Dpp bound receptors and nuclear accumulation of transcription factors may be mechanisms to decrease noise and increase robustness of Dpp signaling.

Contents

List of Tables

List of Figures

Chapter 1

Introduction

1.1 Introduction

Cells transmit information from the extracellular environment into the intracellular environment through signaling pathways to change cell behavior. The basic mechanism involves ligands binding to receptors on the cellular membrane which then causes a change in the intracellular environment. Aberrant signaling has been implicated in many different human diseases ranging from developmental defects to cancer [1, 2, 3]. Since signaling pathways are ubiquitously used by most cell types, in order to develop targeted therapies it is important to understand their regulation and how they are modulated in different settings. In this thesis

I report on studies involving Bone Morphogenic Protein (BMP) signaling to understand how it is able to robustly pattern the dorsal surface of the *Drosophila* embryo. By studying cases of aberrant patterning we can learn how this signaling pathway is modulated. In particular, I will focus on studying feedback control and robustness of BMP signaling using molecular biology and mathematical modeling. I will quantitatively analyze BMP signaling in early *Drosophila* development to better understand its regulation and determine how noise influences Dorsal / Ventral (D/V) axis patterning.

The BMP ligands are members of the transforming growth factor-β (TGF-β) superfamily and they are critical for growth, differentiation, pattern formation, and adult homeostasis [4]. Even though there are differences across species with respect to downstream target genes that are regulated by TGF-β signaling in specific tissues, the general mechanisms of feedback and extracellular regulation are conserved. In vertebrate systems, the greater complexity in the number of ligands, receptors and downstream signaling components makes the study of BMP signaling more difficult due to redundancy. For example, BMP signaling is required for craniofacial patterning [5, 6]. However the contributions of signals from individual ligands to overall pattern can be difficult to determine due to redundancy. Thus, the mechanisms for how BMP signaling controls craniofacial patterning have remained elusive. In *Drosophila* the complexity in the numbers of the BMP signaling

components is much less than in vertebrates enabling a more direct assessment of how each component contributes to overall signaling network.

1.2 *Drosophila* as a Model System

Drosophila, commonly known as the fruit fly, is an ideal model system to better understand basic mechanisms that control signaling pathways. Lower organisms are easier to study due to their greater simplicity. However, the fundamental principles of how different biological processes function is often similar between lower organisms, such as *Drosophila*, and higher organisms, such as humans [7]. It has been estimated that approximately 75% of human disorders with a known genetic basis have genes with sequence similarities in *Drosophila* [7]. Thus, *Drosophila* can be used as a model system to study how these genes function in order to develop therapies for treatment or cure of the underlying genetic conditions.

Drosophila has been a major model system for genetics research for over a century [8]. The initial theory that inheritance involved transmission of chromosomes that contained genes coding for different traits was discovered using *Drosophila* as a model [8]. *Drosophila* was also one of the first organisms used in genome wide mutagenesis screens to look for new phenotypes affecting all aspects of development. Based on the rich history of genetics research in *Drosophila*, it was one of

the first model organisms to have its genome fully sequenced and annotated in 2000 [9, 10]. The *Drosophila* genome is 180 Megabases in size and contains at least 13,739 genes, whereas the human genome is approximately 3.08 Gigabases and contains about 20,000 genes [11]. The function of novel genes are often first identified in *Drosophila* facilitating the understanding of the roles of homologous genes in vertebrate systems [12].

For research in in the field of developmental biology, *Drosophila* is advantageous due to its simple growth requirements enabling the production of large numbers of animals at all stages of development. In addition, the breadth of available molecular biology and genetic techniques is unmatched by any other organism. The lifecycle of *Drosophila* is fairly rapid at approximately two weeks, making it easy to collect large amounts of data in relatively short time frame compared to vertebrate model systems. Mutagenesis screens are also easy to implement facilitating the identification of many interesting mutations. Many of these mutations result in lethality when homozygous but these mutations can be maintained in a self perpetuating stock through the use of balancer chromosome. [13]. The balancer chromosomes have multiple inversions to prevent recombination between chromosomes and dominant mutations that allows the investigator to trace chromosomal inheritance. Another important tool is the Gal4/UAS system that allows for tissue specific expression or knockdown of genes [14, 15].

P-element transposons can also be used for gene disruption experiments, mapping genetic mutations, and for making transgenic animals that contain new gene configurations[16]. The wide breadth of these tools makes *Drosophila* an ideal system for studying control of signaling networks.

The early development of the *Drosophila* embryo is unusual compared to those of other model systems. Instead of rapid cell division with complete cytokinesis, the first 13 early divisions in *Drosophila* embryos involve nuclear fission within a large common cytoplasm leading to the formation of a syncytial embryo consisting of about 6000 surface nuclei and 20 or so central nuclei. Initially, the nuclei are in the center of the embryo, and at nuclear division nine the nuclei migrate out to the periphery of the embryo, forming a monolayer underneath the plasma membrane (Figure 1.1). Cellularization of individual surface nuclei commences during the fourteenth division cycle at about 2 1/2-3 hours of development. Most of the studies described in this thesis involve characterization of signaling output in embryos that are between nuclear cycle 9 and 14. A general subdivision of domains begins around the time of nuclear division nine. However the positional information along both axes is further refined between nuclear divisions nine to fourteen. Exterior to the plasma membrane is the perivitelline (PV) space. Proteins are secreted into the PV space where they can diffuse and interact to send signals back to the cytoplasm and nuclei for patterning tissue boundaries along

both the Anterior / Posterior (A/P) and D/V axes.

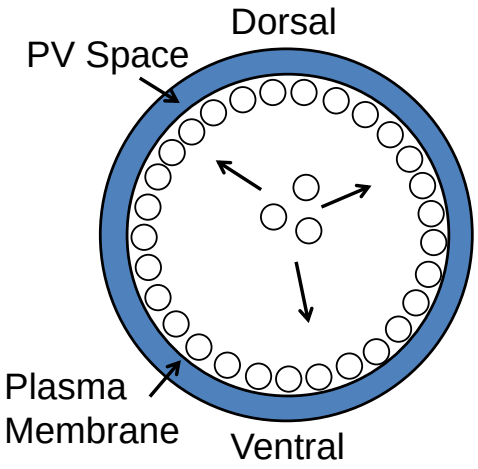

Figure 1.1: Cross-section of the Early *Drosophila* Embryo - During early embryogenesis nuclei are in a syncytium. At nuclear division nine, the nuclei migrate to the plasma membrane and form a monolayer under the plasma membrane. Above the plasma membrane is the PV space. Signaling molecules can be secreted from the cytoplasm into the PV space where they can diffuse, bind receptors and signal back to the nuclei.

1.3 BMP Signaling

1.3.1 BMP Signaling Pathway

During D/V patterning in the *Drosophila* embryo, BMP signals relay positional information to the nucleus based on the concentration of BMP ligand in the PV space. The strength of the signal controls the transcriptional output of target genes. The information flow can be separated into three major phases; first is

the formation of the active signaling complex in the PV space, the second is transducing a signal across the plasma membrane into the cytoplasm, and third is the passing of the signal into the nucleus such that various activator and repressor transcriptional complexes are assembled onto DNA (Figure 1.2).

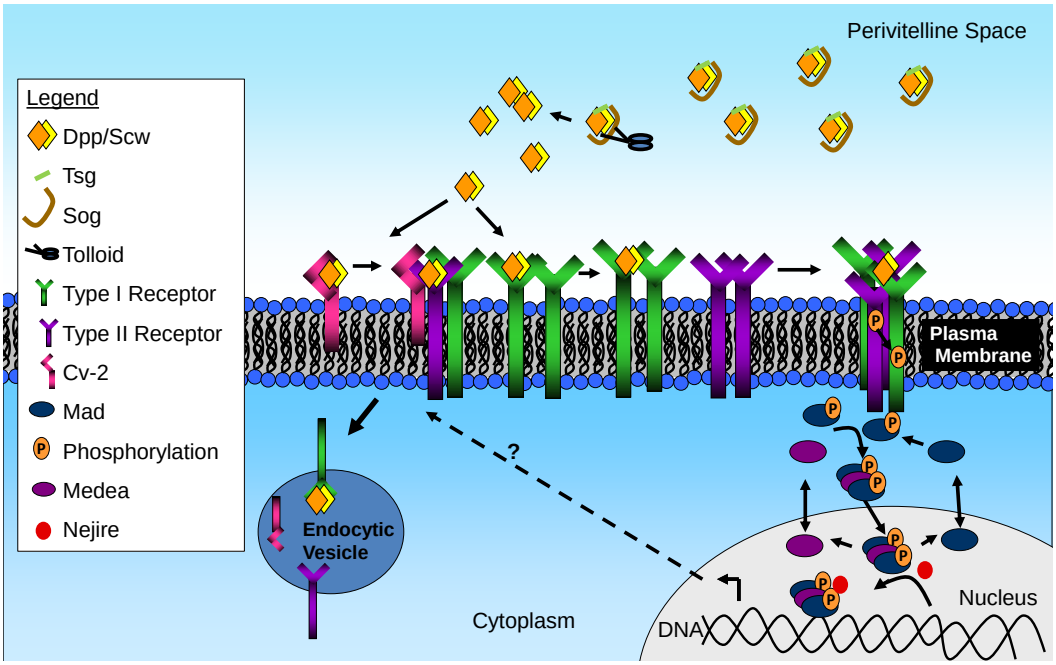

Figure 1.2: Model of the BMP Signaling Pathway - A dimer of BMP (orange and yellow) ligands is transported within the PV space by Sog (brown) and Tsg (light green) covering up BMP binding domains. At the dorsal midline Tld (black) cleaves Sog to release BMP to bind to the type I receptors (dark green) or Cv-2 (pink). The type I receptors recruit a dimer of type II receptors (dark purple) to form an active signaling complex. This leads the constitutively active type II receptor to phosphorylate (P) the type I receptor. Then the type I receptor phosphorylates Mad (dark blue) to pMad. Two pMad molecules combine with a co-smad, Medea, (light purple) to form an active transcription factor, which unidirectionally enters the nucleus. The active transcription factor can interact with cofactors (red) and turn on transcription. The produced proteins can feedback to regulate the overall BMP signaling pathway. One protein that is produced is Cv-2 (pink) which can bind BMP ligand and transfer it to the type II receptor. The receptors on the membrane are also endocytosed and can signal intracelluarly.

1.3.2 Formation of the Extracellular Signaling Complex

In early *Drosophila* development there is two BMP ligands present in the PV space: Decapentaplegic (Dpp), a homologue to vertebrate BMP-2 and 4, and Screw (Scw), a distantly related member of the BMP family within the large TGF-β superfamily. Dpp is produced over the dorsal 40% of the embryo [17] and Scw is produced uniformly in the embryo [18]. Dpp and Scw can form homodimers or heterodimers. The Dpp homodimer requires the type I receptor Thickvein (Tkv) to signal, and the Scw homodimer requires the type I receptor Saxophone (Sax) [19, 20]. The Dpp and Scw homodimers signal at a low level, that likely is responsible for specifying that portion of the dorsal surface destined to become dorsal ectoderm [21]. High levels of BMP signaling are produced by Dpp/Scw heterodimers. These molecules bind to a heterodimer of type I receptors, Tkv and Sax [21] (Figure 1.2) which in turn, recruit a dimer of the type II receptor, Punt (Pnt), to form an active signaling complex [22, 23, 24]). Pnt, Tkv and Sax are all serine/threonine kinases. Once the ligand/receptor complex is formed, Pnt activates the type I receptors by cross-phosphorylation (Figure 1.2). During canonical BMP signaling, the type I receptor then phosphorylates a cytoplasmic R-Smad (Mad in *Drosophila*) which in turn, complexes with a common Smad (Medea in *Drosophila*). The activated receptors on the membrane can also

undergo endocytosis (Figure 1.2). For TGF-β receptors, blocking clatharin mediated endocytosis prevents Smad, activation [25, 26, 27]. By analogy, endocytosis may also be an important component for activating BMP signaling.

1.3.3 Formation of the Active Transcription Factor

Once the type I receptors phosphorylates Mad to p-Mad [28] (Figure 1.2), two p-Mads combine with Medea in the cytoplasm and the complex translocates to the nucleus where it can either activate or repress transcription depending on the compliment of available cofactors [29] (Figure 1.2). The dynamics of intracellular Smad trafficking have only been studied using cell culture models and for Smad2 in response to TFG-β. Lacking more directly relevant in vivo data, I assume in this discussion that the dynamics of Mad trafficking in response to BMP signals during *Drosophila* D/V patterning are similar to those of Smad2 in cell culture systems. With this caveat, the pMad/Medea complex accumulates in the nucleus through non-uniform import and export across the nuclear membrane [30] (Figure 1.2). Mathematical models predict the pMad complex is unidirectionally transported into the nucleus; whereas, pMad and Medea are transported in and out of the nucleus with similar rates. The pMad phosphatase, which dephosphorylates pMad to Mad, is only located in the nucleus. Thus the net effect is an accumulation of the transcription factor in the nucleus. The net effect of the signaling pathway

is to turn on or off genes to specify the formation of different tissues along the dorsal surface. In chapter 2 of this thesis, I describe the identificationed of a new mutation in *nejire* (*nej*), a gene encoding a known Smad co-factor and analyze its effects on D/V patterning.

1.3.4 BMP Signaling in Human Disease

In humans BMP signaling contributes to the formation of limbs, muscle, heart, kidneys, teeth, and liver. When signaling goes awry it can lead to a wide spectrum of developmental defects [31]. For example, loss of BMP signaling during limb formation can lead to fusion or loss of joints in the digits of the hands and feet [32]. BMPs were initially discovered by their ability to promote new bone growth at implantation sites in rats. This finding lead to significant clinical interest and BMP-2 is now commercially available. It is frequently used to treat traumatic or degenerative bone injuries. However, there can be significant complications associated with these treatments that have called its use into question. It is difficult to prevent BMP-2 from diffusing away from the fracture site, which can lead to ectopic bone formation at inappropriate sites [33]. It has also been hypothesized that too much BMP-2 at the fracture site may lead to serious infections [33] and perhaps increased cancer rates. Thus it is important to better understand how to control BMP diffusion in order to prevent some of these complications.

BMP signaling is also essential for cardiac development and vascular angiogenesis [34]. Up-regulation of BMP signaling is a critical component in cancer metastases and tumor growth. Inhibition of BMP signaling either directly or indirectly is an area of research for therapeutic targets to prevent cancer from spreading [34]. BMP signaling is also important for proper kidney development and is expressed throughout the developing kidney [35]. In the adult kidney is has been shown to be a protective factor against renal fibrosis and is a target for preventing chronic kidney disease [36]. To create better targets for treating the diverse range of diseases described above that arise due to aberrant BMP signaling, it is essential to better understand how BMP signaling is fine tuned during normal development.

1.4 Pattern Formation

1.4.1 BMP as a Morphogen

In the developing embryo, morphogen gradients are one of the ways a homogenous set of cells is patterned into different tissues, and this mechanisms is conserved across species [37]. A morphogen gradient determines cell fate in a concentration dependent manner. During early development, one of the first events is patterning of the A/P and D/V axes by morphogen gradients. This is a critical step in development because it determines the foundations for the body plan that will

follow. In D/V axis patterning, BMP ligands are major morphogens important for specifying dorsal structures [38]. BMP is a morphogen because it forms a gradient on the dorsal surface and specifies at least four different regions of gene expression at different thresholds of signaling [39, 29, 38, 40] (Figure 1.3).

One of the most common analogies for how morphogens specify pattern through gene regulation is known as the French flag model [41]. In this model, cells (or nuclei in the case of an early *Drosophila* embryo) determine what genes are expressed by reading the concentration of the morphogen outside the cell. In *Drosophila* embryos, the highest level of BMP signaling specifies the amnioserosa, a tissue which is required for dorsal closure later in development [42] (Figure 1.3). Moderate levels of BMP specify the dorsal epidermis [38]. Within the dorsal epidermis there are at least three distinct gene expression thresholds that may act to further subdivide the epidermis into smaller unique units of development[39] (Figure 1.3). Despite much research aimed at elucidating the mechanism of BMP gradient formation it is still not fully understood, nor is it entirely clear how nuclei interpret the gradient to specify distinct tissue boundaries.

The French Flag model for how morphogen gradients act during tissue specification is obviously an oversimplification, since the patterning system must be able to compensate for genetic and environmental variability to reproducibly construct a functional embryo. If these variables produce any noise in morphogen

concentration or readout it could have a large effect on the position of boundaries. Lewis Wolpert, the founder of the French Flag Model, has proposed that there must be a mechanism for cell-cell communication during the formation of boundaries [43] to ensure their proper placement. However, during dorsal surface patterning there is no evidence of direct nuclei to nuclei communication to create these boundaries. Thus the boundaries are assumed to be determined from reading the concentration of the morphogen ligand, but the mechanism of how this happens is not clear.

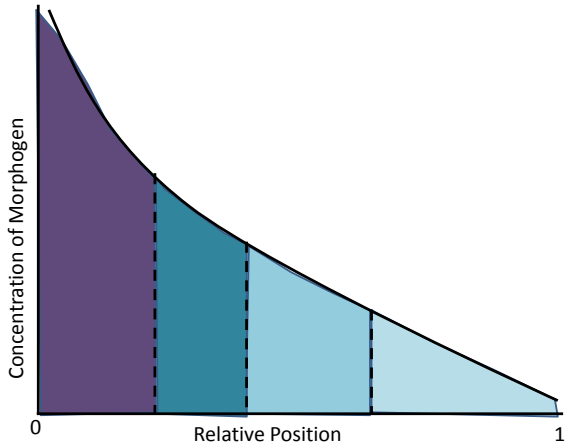

Figure 1.3: Morphogen Gradient Model - A morphogen gradient of BMP ligand is formed on the dorsal surface of the embryo. Zero represents the dorsal midline and 1 represents the lateral edge of the dorsal surface. High concentrations of BMP ligand specify the amnioserosa (purple) and lower levels specify the dorsal epidermis (turquoise). The dorsal epidermis is further subdivided into different regions depending upon the concentration of BMP ligand. The dotted lines represent the thresholds determining different boundaries between tissues.

1.4.2 Formation of the BMP Morphogen Gradient in the Early *Drosophila* Embryo

In the early embryo, the Dpp gradient is formed through interactions with extracellular modulators in the PV fluid. Dpp is produced and secreted into the PV space at uniform levels over the dorsal half of the embryo. However pMad, the downstream signal of BMP, follows a graded profile that starts wide and contracts over time to a narrow domain centered on the dorsal midline [44]. Thus, it is presumed that a gradient of Dpp is formed in the PV space that follows the gradient seen in pMad. The Dpp gradient is formed through a diffusion based mechanism in the PV space. The present model for how the sharpening of the dpp gradient occurs is as follows. First, Dpp forms a heterodimer with another BMP ligand Scw. In vitro studies show that this heterodimer is much more potent than either homodimers for producing high levels of pMad. The Dpp/Scw complex then binds to type IV collagen. Type IV collagen forms a scaffold for forming a complex that ultimately facilitates long range diffusion of Dpp/Scw [45, 46] (Figure 1.4). The levels of Dpp in the PV space are hypothesized to be low, so the type IV collagen may help to concentrate the ligand to increase its effective binding rate to Short Gastrulation (Sog), a BMP inhibitor that blocks the ability of BMP to bind to receptor. Sog binds to Dpp/Scw on collagen to form a Dpp/Scw/Collagen

tripartite complex (Figure 1.4). Upon Sog binding Dpp, Dpp is dislocated from type IV collagen and replaced with Sog binding the tripartite complex to type IV collagen (Figure 1.4). Then Twisted Gastrulation (Tsg) binds to the complex and dissociates it from type IV collagen allowing the Dpp/Scw/Tsg/Sog complex to diffuse and not rebind to collagen or receptor [46, 21] (Figure 1.4). The Dpp/Scw/Tsg/Sog complex also lengthens the lifetime of Dpp in the PV space by protecting it from receptor mediated degradation [47, 48]. The metalloprotease Tolloid (Tld) cleaves Sog and releases Dpp/Scw to either signal or rebind to BMP binding proteins [49, 50] (Figure 1.4). Sog levels are highest in the lateral domain of the embryo, which preferentially leads to transport of Dpp/Scw toward the dorsal midline [47, 51]. Tld levels are highest on the dorsal midline [49]. This favors the release and accumulation of Dpp/Scw on the dorsal midline. The overall binding rate for Dpp to its receptor is relatively low. In the absence of Sog type IV collagen may help transfer Dpp to its receptor [45, 46]. This complex set of reactions in the PV space allows for a gradient of Dpp/Scw to be formed with peak expression along the dorsal midline.

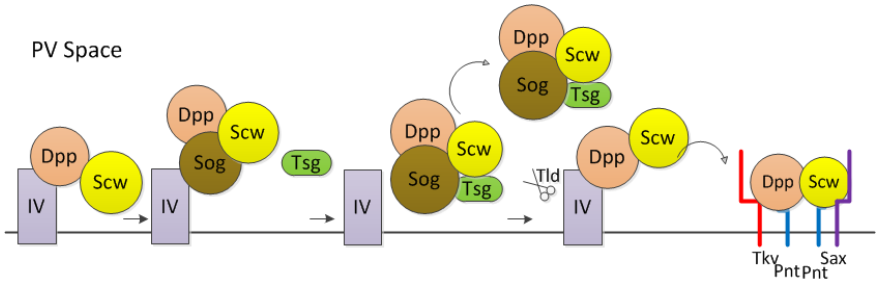

Figure 1.4: Model of the Formation of the Dpp/Scw Gradient - Dpp (pink) binds to type IV collagen (purple). Sog (brown) binds to Dpp/Collagen complex. When Scw binds to the complex, Dpp is released and Sog binds to collagen. Then, Tsg (green) binds to the Dpp/Scw/Sog complex and releases it from type IV collagen. The Dpp/Scw/Sog/Tsg complex can diffuse in the PV space. Tld (black) can release Dpp/Scw from Sog/Tsg. Dpp/Scw can rebind to collagen IV, which can help transfer it to its receptor complex of Tkv (red), Pnt (blue), and Sax (purple). Figure modified from [46].

The Dpp/Scw gradient is primarily studied by examining pMad expression profiles. Despite many production attempts, no high affinity antibodies exist to study Dpp in the PV space. Dpp-Green Fluorescent Protein (GFP) fusions have been generated to study Dpp profiles in the PV space. The Dpp-GFP fusions can rescue Dpp null embryos, but the GFP cannot be directly visualized in the PV space. The failure of directly visualizing Dpp-GFP in the PV space may be caused by the time delay required to form a functional chromophore. The half-life of GFP folding is estimated to be about 30 minutes and the formation of the Dpp gradient occurs at a similar rate. One work around that has been identified is that antibodies against GFP can be injected into the PV space, enabling the Dpp gradient to be visualized [22]. However this method is technically very difficult,

so the typical method for visualizing BMP gradient formation is indirect and involves examination the distribution of pMad since a high quality antibody is commercially available (Figure 1.5).

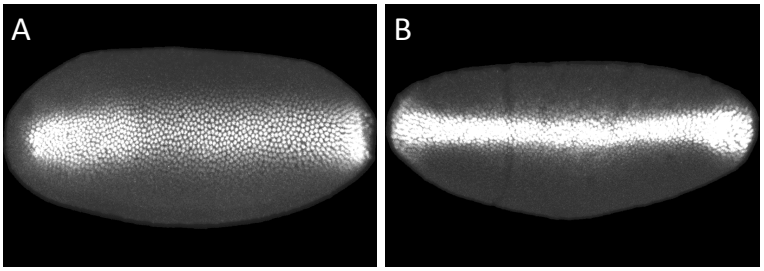

Figure 1.5: pMad Expression Profiles During Early and Late Embryogenesis - pMad profiles of the dorsal surface during early (A) and late (B) embryogenesis. Embryos are oriented with anterior to posterior from left to right. pMad profiles start broad and at low levels in the early embryo (A). In the later embryo, pMad profiles are narrower and more intense along the dorsal midline (B).

The boundaries between high and low signaling of the embryo are fairly sharp (Figure 1.5). The nuclei follow a fairly smooth gradient between high and low signaling. In wild type embryos, there is never a nucleus with high pMad levels in a region of nuclei with low pMad levels. The patterning of the embryos is also fairly consistent between embryos. This is somewhat surprising since the levels of Dpp required to achieve full activation of BMP signaling lead to an estimate of in vivo concentration to be on the order of 10-100 molecules / nucleus. Thus,

for such consistent and robust patterning to occur, there must be mechanisms to dampen any stochastic fluctuations due to low numbers of Dpp/Scw in the PV space. I will use mathematical modeling to study mechanisms that allow for this smooth output of pMad expression profiles in chapter 3.

1.4.3 Feedback in Forming the BMP Morphogen Gradient

In the early blastoderm, p-Mad concentration profiles are moderate and wide within the dorsal domain (Figure 1.5 A). In the late blastoderm, Dpp protein accumulation intensifies and contracts to a 5-9 nucleus wide dorsal stripe [44, 50] (Figure 1.5 B). The first models for D/V patterning predicted an intensification and widening of BMP signaling on the dorsal surface [47, 51]. Wang and Ferguson proposed that a positive feedback loop that increases the amount of BMP signaling in a local area could account for both the contraction and intensification of signaling [22], and mathematical models have confirmed that this could work [52]. The two best hypotheses for a positive feedback molecule that upregulates signaling is a co-receptor the preferentially binds BMP ligands and transfers it to the BMP receptor or a co-factor that directly upregulates the BMP receptors or their activity. Wang and Ferguson further speculated that feedback of a negative regulator of BMP signaling in the lateral regions of the embryo could also help to account for the contraction of signaling. However, the downstream targets that

give rise to the feedback in the embryo system have not been identified.

1.4.4 Comparison of BMP Signaling in Dorsal / Ventral Patterning in Early Embryogenesis and the Wing Disc

A clue to possible modulators that could account for the contraction and intensification in D/V patterning comes from analysis of BMP signaling during crossvein formation in the wing disc. The wing imaginal disc is a group of mitotic cells contained in the *Drosophila* larva that will form the adult wing during metamorphosis. During metamorphosis, two wing tissue types are formed the wing proper and the veins which act as structural rods to stiffen the wing so that flight is possible. There are also two types of veins; five longitudinal ones that run parallel to the proximal/distal axis and two crossveins which run perpendicular to the longitudinal veins (Figure 1.6). A high level of BMP signaling is required for formation of all veins (Figure 1.6) but the mechanism of crossvein formation is particularly interesting since they require a shuttling mechanism similar to what occurs in the early embryo [40]. However, there are some notable differences between the two systems. In D/V patterning the morphogen gradient is created within a region of uniform Dpp production; whereas in the crossvein the morphogen gradient is

created by diffusion away from Dpp produced in the longitudinal veins (Figure 1.6). Heparan sulfate proteoglycans (HSPGs) have been shown to be crucial for BMP signaling in the wing disc [53]. However, HSPGs are not required during embryonic dorsal surface pattering. In fact there is a translational block that prevents HSPGs from being expressed during the first three hours of development and ectopic HSPG expression actually disrupts D/V patterning likely by sequestering too much BMP into non-signaling complexes [54]. Two other genes that are needed for proper wing patterning but not D/V patterning are Pentagone, and Larval translucida (Ltl). Both code for proteins that bind to HSPGs and modulate BMP signaling through ill-defined processes but neither is expressed at high levels in the embryo [55, 56]. Interestingly, Ltl does genetically interact with a third protein that has been identified as essential for crossvein formation known as Crossveinless 2 (Cv-2) (Figure 1.6). Cv-2 is expressed in the early embryo and has also been shown to be a secreted factor that can bind to both BMP ligands and receptors [57]. Furthermore, Cv-2 expression is induced by BMP signaling potentially enabling it to be a feedback component that sharpens BMP gradients. Indeed, theoretical models that incorporate Cv-2 into the signaling paradigm as a molecule that acts as an exchange factor can generate the enhanced and sharpened gradients that are observed in the early embryo [52, 40, 57] (Figure 1.2). In this thesis I will examine the role of Cv-2 in dorsal surface patterning in Chapter

2.

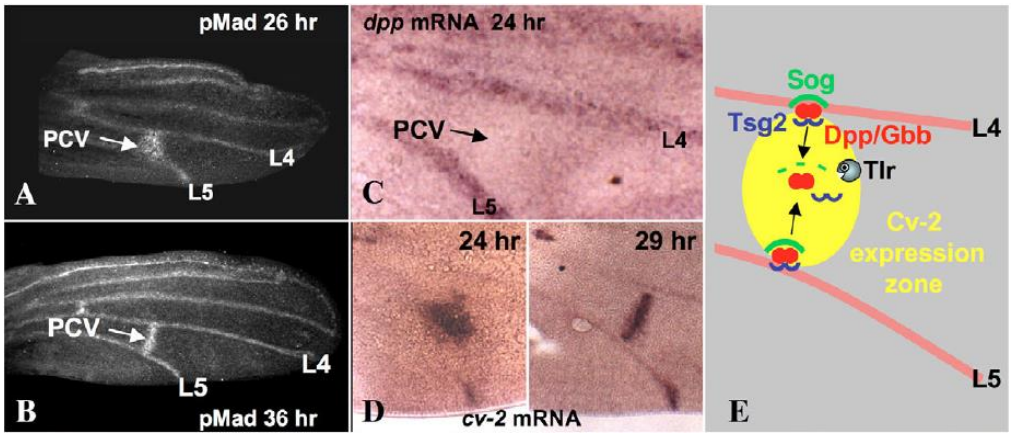

Figure 1.6: Crossvein Formation in the Wing Disc - pMad is expressed along the future position on the 5 longitudinal veins and 2 crossveins (A and B). In the posterior crossvein (PCV) pMad expression starts broad (A) and refines over time to the future position of the PCV (B). *Dpp* mRNA is not expressed in the region of the PCV (C) and must diffuse into the PCV region (E). *Cv-2* mRNA is expressed in a pattern that mimics pMad expression (D). The gradient of Dpp in the PCV is formed using many of the same molecules involved in the Dorsal Surface Dpp gradient (E). However unlike dorsal surface Dpp gradient formation, in the PCV the gradient is formed from Dpp in the longitudinal veins (E). Figure modified from [40].

1.5 Stochasticity in Biological Systems

Embryonic development has a remarkable property of being extremely robust, i.e. reliable and reproducible, despite fluctuations in the environment surrounding the embryo, noise in genome expression, and variations in the composition of the proteome. Despite these complications, the hatch rate of *Drosophila*, embryos is

nearly 80-90% in a laboratory setting [58, 59]. As the embryo matures into an adult some of the same issues still persist on a genetic, cellular, and organism level [60, 61, 62, 63]. The role of stochasticity in biological organisms is also important for understanding the development of disease processes [64] and how to increase efficacy and decrease side effects in drug discovery [60]. In order to better understand the stochastic nature of cells more work is needed to quantify the dynamics and concentrations of signaling molecules and to elucidate mechanisms of how cells adapt to or exploit noise.

Stochasticity in biological systems can occur at many different levels. In D/V patterning noise can come from low concentrations of BMP signaling molecules in the PV space leading to randomness of molecules interacting [61]. In the cytoplasm, stochasticity can arise from the randomness of pMad and Medea molecules interacting to form an active transcription factor. Noise can also arise from the process of transcription. Fluctuations in transcription are one of the most well studied areas of intracellular noise [61, 65, 66]. There can be noise in turning on and off gene expression, which can lead to a burst of mRNA molecules and downstream noise in the levels of protein produced. The contribution of noise to all levels of the BMP signaling cascade has not been carefully studied, nor have mechanisms that may enhance or decrease the inherent noise in the system been examined.

1.6 Feedback Loops in Signaling Networks

Signaling pathways are regulated at almost all levels and in many different ways. One common mechanism of regulation is positive and negative feedback of the signaling network on to itself. In positive feedback, an initial signal amplifies itself through modulation of the activity of one of the signal transduction components. In negative feedback the opposite occurs. Depending upon how positive and negative feedback loops are connected, a wide range of dynamic behaviors can be found. Bistability, defined as having two stable steady states, can be created from either a positive feedback loop or a double negative feedback loop [67]. A negative feedback loop can help to stabilize a protein at a constant level [67]. In a noisy environment, negative feedback is also a mechanism that can reduce noise [68, 69]. Under the right conditions, negative feedback loops can also create stable sustained oscillations [67]. In biology we can determine the structure of signaling networks, which often contain complex feedback loops. However, knowing the general structure of the networks does not allow us to easily predict the dynamics. Mathematical modeling can be used to predict the dynamics that are possible in different signaling network configurations.

1.7 Modeling in Dorsal / Ventral Patterning

1.7.1 Previous Models of Dorsal / Ventral Patterning

Mathematical modeling has been an important tool for understanding developmental biological systems. In D/V patterning, models have served a critical role for understanding the output of complex regulatory systems. A good model both explains the data and suggests new areas of study. In D/V patterning, three different types of models have been examined with respect to BMP signaling. The first set of models focused on describing mechanisms that helped direct the transport of Dpp within the PV space through specific interactions with other extracellular proteins, such that a steep gradient of Dpp developed at the dorsal midline [70, 47, 52]. Based on what was known at the time concerning the molecules involved and their biochemical activities, these models revealed that, something was missing in the model formulation since they could not explain the observed contraction and intensification of Dpp signaling along the dorsal midline. A second stochastic model addressed the issue of low levels of BMP signaling molecules and predicted that noise could be diminished in this system if there were a large number of receptors on the membrane surface [71]. However, this model did not look at factors downstream of the BMP receptors to see if there were other mechanisms that could also dampen the noise arising from low levels of signaling molecules. A

third model focused intracellularly on the Smad proteins and was primarily aimed at describing how nuclear accumulation of the Smad proteins occurs through an asymmetrical transport rate in and out of the nucleus [30]. As a component of this thesis I aim to integrate all the current models of BMP signaling into one model to examine how noise propagates through the BMP signaling network (Chapter 3). Through this study I hope to determine how the BMP signaling pathway consistently patterns the *Drosophila* embryo with sharp boundaries between areas of high and low pMad signaling as seen in Figure 1.5.

1.7.2 Stochastic Modeling of Dorsal / Ventral Patterning

Most of the models for BMP signaling have been based on deterministic differential equations. In these models the morphogen concentrations at particular points in space can be described over time using the partial differential equations:

$$\frac{\partial^2 X}{\partial t} = D\nabla^2 X + R(X) \tag{1.1}$$

where X is a molecule in the system, $D\nabla^2 X$ represents diffusion of species X, and $R(X)$ is a function containing the reactions of species X. If diffusion in the system is not taken into account, the description reduces to ordinary differential equations with just the reaction terms remaining. However, if noise is present in

the system, stochastic differential equations may be important to consider. Deterministic equations assume that large numbers of molecules are present, and that they follow the overall average behavior of the molecules through mass action kinetics. In stochastic equations, individual molecules are followed, and their behavior is described by a chemical master equation. If significant noise is present, these models can lead to different predicted behavior. In a system with multiple steady states, based on a set of initial conditions, the deterministic equations will normally give the same steady state solution. However with stochastic equations, the same set of initial conditions can lead to multiple different steady state solutions due to the noise in the system. Even in the case of one steady state in the system, a stochastic system can lead to a spread of solutions around a steady state as a result of noise in the system.

Noise due to low levels of signaling molecules could significantly influence the ability of the system to reproducibly generate a consistent gradient of BMP signaling. If there is noise in creating a gradient of BMP signaling, this may affect now nuclei determine their position along the D-V axis and may make sharp boundaries difficult to form. Thus, we propose that there must exit mechanisms to decrease noise in the system to create sharp reproducible boundaries of gene expression, and to study this we will create a stochastic model of BMP signaling that is based on previous deterministic models.

The stochastic nature of the system can be modeled with a Markov chain model. Let $X(t) = [X_1(t), X_2(t), \ldots, X_m(t)]$ be the number of molecules of each species in the system. $X(t)$ is a continuous time Markov chain if for any $0 < s_0 < s_1 < \ldots < s_n < s$ and possible states $i_0, \ldots, i_n, i, j$ we have

$$P(X(t+s) = j | X(s) = i, X(s_n) = i_n, \ldots, X(s_0) = i_0) = P(X(t+s) = j | X(s) = i). \tag{1.2}$$

This means that the probability of a reaction happening is independent of the history of the previous states. The Markov chain model for chemical reactions approaches the deterministic formulation for the system of reactions in the infinite volume limit of the Markov chain model [72]. If $X(t)$ is a Markov chain, then it satisfies the Chapman-Kolmogorov equation

$$p(x(t_n), t_n | x(t_{n+2}), t_{n+2}) = \int p(x(t_n), t_n | x(t_{n+1}), t_{n+1}) p(x(t_{n+1}), t_{n+1} | x(t_{n+2}), t_{n+2}) dx(t_{n+1}) \tag{1.3}$$

where $x(t_n)$, $x(t_{n+1})$, and $x(t_{n+2})$ are $X(t)$ at times t_n, t_{n+1}, and t_{n+2} respectively. This equation states that the probability of going between $x(t_n)$ and $x(t_{n+2})$ is the integral of all paths going from $x(t_n)$ to $x(t_{n+1})$ and then $x(t_{n+1})$ to $x(t_{n+2})$ for all $x(t_{n+1})$.

From the Chapman-Kolmogorov equation, we can derive the chemical master equation which governs the evolution of the probability that the system will be in a particular state as a function of time. The chemical master equation can be used to follow how the system evolves stochastically over time. For a system with R reactions and X species, the chemical master equation is

$$\frac{dP(X(t),t)}{dt} = \sum_{r \in R} a_r(X - \nu_r)P(X - \nu_r, t) - \sum_{r \in R} a_r(X,t) \tag{1.4}$$

where ν_r is the stoichiometric vector of reaction r and $a_r(X)$ is the reaction propensity of reaction r. The stoichiometric vector describes how the molecules of $X(t)$ change during the reaction. For example, for the reaction $x_1 + x_2 \rightleftharpoons x_3$, the stoichiometric vector for the forward direction is $[-1, -1, 1]$ for the vector $[x_1, x_2, x_3]$. The reaction propensity describes how likely it is that a reaction will occur. For a first order reaction, $a_r = k_r x$ where k_r is the kinetic rate constant. For a second order reaction where $x_i \neq x_j$, $a_r = V k_r x_i x_j$ where V is the volume of the system. For a second order reaction where $i = j$, $a_r = V k_r x_i(x_i - 1)/2$. The chemical master equation is a coupled set of ordinary differential equations (ODE) with one equation for every possible combination of molecules in the system. When there are no fluctuations in $X(t)$, the chemical master equation reduces to a continuous,

deterministic differential equation

$$\frac{dX(t)}{dt} = \sum_{r=1}^{R} \nu_r a_r(X(t)). \tag{1.5}$$

1.7.3 The Gillespie Algorithm

For a large system, the chemical master equation can have too many states to solve. Therefore simulations must be done to simulate a system based on the chemical master equation. The reactions in a stochastic biological system can be simulated using the Gillespie algorithm [73, 74]. In the Gillespie algorithm, all molecules and their positions are tracked over time. All reactions that occur are either unimolecular or bimolecular. Trimolecular reactions and larger must be broken down into a series of unimolecular or biomolecular reactions. This method assumes that the system is well mixed. The following steps describe the Gillespie algorithm:

1. Initialize the time $t = t_0$ and the system's state $x = x_0$.

2. Evaluate each reaction propensity, $a_r(x)$, for all $r \in R$ and find their sum, $a_0 = \sum_{j=1}^{R} a_j(x)$. a_0 is needed to find the time the next reaction will occur.

3. Generate p_1 and p_2 which are random numbers from URN$[0, 1]$.

4. Find the next time a reaction will occur, which is at $t + \tau$ where $\tau = \frac{1}{a_0(x)} ln(\frac{1}{p_1})$.

5. Find the next reaction that will occur by finding j, where j is the smallest integer that satisfies $\sum_{i=1}^{j} a_i x_i > p_2 a_0(x)$. j is the next reaction that will occur. This step is a way of randomly selecting the next reaction to occur from all possible reactions.

6. Update the time and the reaction that occur by replacing $t \leftarrow t + \tau$ and $x \leftarrow x + \nu_j$.

7. Iterate again, starting at step 2. The time steps for the Gillespie method are on the order of $\frac{1}{a_0(x)}$. $a_0(x)$ is often quite large which can make the simulations very slow.

The Gillespie algorithm needs to be modified to allow for it to be used in a system that is not well mixed. In this case, diffusion of molecules must be taken into account. A system can be broken into smaller compartments, where in each compartment the molecules are well mixed. Then diffusion can be treated like a chemical reaction in the Gillespie algorithm for moving between different compartments. For example, for a system of length L, we can break it up into M equally sized compartments of length $h = \frac{L}{M}$. The probability of moving between

compartments, d_i, for the ith molecule in the system with a diffusion constant of D_i is $d_i = \frac{D_i}{h^2}$.

1.7.4 Project Aims

In this thesis, I report on two studies aimed at understanding different aspects of BMP signaling as it relates to early D/V patterning in *Drosophila*. In the first project I examined the possible contribution of two genes to feedback control of BMP signaling during dorsal surface patterning. I identified a new allele of Nej, a protein that is thought to help the Smad complex form a more robust transcription factor in regions of high BMP signaling. I found that loss of Nej leads to variable BMP signaling output and discuss how this might occur. I also studied the role of Cv-2, a surface localized BMP binding protein, during D/V patterning and found that it acts in a negative feedback loop to inhibit BMP signaling. Cv-2 may also increase the amount of noise in BMP signaling during D/V patterning. The description of these projects is found in chapter 2. In a second project, I helped to create a novel three dimensional stochastic model to study how stochasticity might impact BMP signaling. In this model I integrated membrane, cytoplasmic, and nuclear dynamics of BMP signaling components to learn how noise might propagate through the system. The analysis of this model is found in chapter 3. Chapter 4 provides an overall discussion of the conclusions

reached by these studies.

Chapter 2

Crossveinless-2 and Nejire Modulate BMP Signaling

2.1 Introduction

The Bone Morphogenic Protein (BMP) signaling pathway is highly conserved and used in many developmental processes including embryonic axis specification, organogenesis and apoptosis. Embryonic axis specification is a critical first step in determining the developmental framework for the entire body plan. This process must be extremely robust and able to buffer against both extrinsic environmental variability during development and intrinsic genetic differences between individual embryos. This is especially true in *Drosophila melanogaster* as embryos undergo

external development, so they must be able to withstand a significant variation in environment conditions such as temperature and hydration state. In order to consistently pattern the embryo correctly in the face of these naturally occurring variations, there must be mechanisms that ensure robust development.

The dorsal surface of the *Drosophila* embryo is patterned by a morphogen gradient of Decapentaplegic (Dpp), a BMP family member [39, 29, 38, 40]. In this case Dpp is thought to act as a morphogen because it patterns the surface in a concentration dependent manner [39, 29, 38, 40, 21]. Dpp is produced uniformly over the dorsal surface of the embryo [17]. The Dpp gradient is formed through a series of extracellular modulators that shuttle Dpp to the dorsal midline [40]. Production of phosphorylated Mad (pMad), the intracellular transducer of the Dpp signal, is initially produced in a broad region within the dorsal domain of the early blastoderm embryo, but rapidly contracts and intensifies to a 5-9 nuclei wide stripe during nuclear divisions 12-14 [44, 50]. Peak signaling in the dorsal most 5-9 cells specify the amnioserosa, a tissue that is needed for coordinating gastrulation and proper dorsal closure later in development [42]. In the dorso-lateral regions of the embryo, that see a lower level of BMP signaling, the dorsal epidermis is specified [38, 21]. The boundary between high and low levels of signaling is very precise and forms a sharp border. In dorsal surface patterning no evidence has been found of nuclei to nuclei communication to help sharpen

this border. Instead the nuclei must interpret the concentration of Dpp in the perivitelline (PV) space, the region of the embryo above the plasma membrane. How the embryo robustly creates the boundary between the amnioserosa and dorsal epidermis is not completely understood.

During dorsal surface patterning, BMP signaling leads to changes in gene transcription. Some target genes produce products that directly help specify the features of the particular fated tissue and others appear to be involved in feedback signals that modulate BMP signaling. The primary BMP ligand in specifying dorsal tissue fate is Dpp, a homologue to vertebrate BMP-2 and 4 [40]. Dpp forms a heterodimer with Screw (Scw) (Dpp/Scw), a distantly related BMP family member [40, 75, 21]. Both Dpp and Scw are members of the TGF-β superfamily. The Dpp/Scw heterodimer primarily signals through a heterotetrameric complex composed of two type I and two type II serine/threonine receptors to phosphorylate Mad to pMad [28]. Two pMads combines with a co-smad Medea to form an active transcription factor [29]. The pMad/Medea complex interacts with other co-transcription factors to either turn on or off gene transcription. Some of the genes pMad/Medea controls may produce proteins that feedback to either inhibit or enhance BMP signaling. Although the major components of BMP signaling have been identified, we still do not understand the fine control of BMP signaling. Through studying the robustness of dorsal surface patterning we will better

understand the modulation of BMP signaling.

To understand robustness of dorsal surface patterning I identified two genes that may disrupt the consistent patterning of the embryo. I found a new mutation in the gene *nejire* (*nej*) that leads to a highly variable phenotype during dorsal surface patterning. I also studied the gene *crossveinless-2* (*cv-2*), which has been examined during wing disc patterning [76, 57] and proposed as a robustness mechanism for BMP signaling [71]. It has been shown that *cv-2* is expressed during dorsal surface pattering [57], but the Cv-2 phenotype has not been characterized.

2.1.1 The Role of Nejire in the BMP Signaling Pathway

In order for feedback in Dpp signaling to occur, an active transcription factor must be formed to turn on transcription. The basic structure of the Dpp transcription factor is two pMad molecules and a co-smad Medea. However, additional co-factors can assemble with the pMad/Medea complex to turn on or off specific genes. One of the co-factors for BMP signaling is Nej, a CREB binding protein (CBP) / p300 protein that acts as a general co-activator or inhibitor of transcription factors during development [77, 78, 79]. In most cases Nej acts as an activator of transcription. However Nej inhibits Wnt/Wingless signaling through acetylating a conserved lysine residue on *Drosophila* T-cell Factor [78]. In the early embryo Nej is an activator interacting with both Dorsal and Dpp to activate

ventral and dorsal surface patterning [77].

Nej is required for proper Dpp signaling during dorsal surface patterning, midgut development, tracheal patterning, and wing development [80]. Nej functions in a very region specific manner to control gene expression. In dorsal surface patterning, the activity of peak signaling of Dpp specifies the amnioserosa, and in this region both *race* and *hindsight* expression is lost. However in regions adjacent to the presumptive amnioserosa, *race* and *hindsight* expression is preserved [80, 39]. Nej does not affect patterning of the neurogenic ectoderm. Nej acts as a co-activator of the pMad/Medea complex through the C-terminal region of Nej binding to the C-terminal MH-2 region of Mad [80]. The N-terminal MH-1 region of Mad acts as an inhibitor of Nej binding [80]. Nej also regulates the transcription of *scw*, *twisted gastrulation* (*tsg*), and *tolloid* (*tld*), all of which are necessary for forming the Dpp morphogen gradient [81]. However Nej does not regulate all of the proteins required for Dpp gradient formation, as *short gastrulation* (*sog*) is not under the control of Nej [81]. Thus Nej acts in a region specific manor with Mad to activate transcription for regions of high signaling during dorsal surface patterning.

Nej serves several roles to promote transcription. The acetyltransferase activity of Nej promotes the activation of p-Mad through acting as a histone acetyltransferase to open the chromatin for transcription. Nej acetylates all four histones

[82] both directly [82, 83] and indirectly through combination of other acetyltransferases [84, 85, 86]. However Nej can also promote the formation of chromatin through acetylating Histone H3 Lysine 56 [87]. Nej also acts as a scaffold or bridge for other chromatin modifiers to assemble into an active transcriptional complex [88]. Since a wide range of proteins for several different signaling pathways interact with Nej, it may serve as an integrator between signaling pathways [88]. Nej may also acetylate other transcription co-activators in the complex. The wide range of functions Nej plays in the nucleus may allow Nej to interact in complex ways to turn on transcription in areas of high levels of Dpp signaling.

2.1.2 The Role of Crossveinless-2 in the BMP Signaling Pathway

Crossveinless-2 was first discovered in *Drosophila* [76] and has a vertebrate homolog BMPER and a related protein Kielin [89, 90, 91, 92]. Cv-2 is a secreted protein that has a N-termial cystine rich domain for BMP binding and a C-terminal von Willebrand Factor domain for membrane tethering [76]. The knockout and overexpression phenotypes were fairly perplexing until the mechanism of action was discovered. Cv-2 has been proposed to be both an activator [93, 94, 95, 91] and inhibitor [96, 97, 98, 99, 89, 92] of BMP signaling. Low expression of Cv-2

can promote signaling and overexpression can inhibit it. One proposed molecular mechanism of action for Cv-2 is that it binds BMP ligand and then transfers it to the type I BMP receptor, Thickveins (Tkv) [57]. Depending upon the relative binding rate of ligand to Cv-2 or its receptor and the transfer rate of BMP from Cv-2 to its receptor, Cv-2 can act as an inhibitor or activator of signaling by either sequestering or transferring ligand. Unlike many of the extracellular modulators of BMP signaling, Cv-2 acts locally to enhance or inhibit BMP signaling [57].

In *Drosophila*, Cv-2 has been primarily studied in the wing disc, a larval tissue that forms the adult wing. In the wing disc, a gradient of BMP diffusing from the longitudinal veins specifies the location of the crossveins [40, 76, 57, 100]. In Cv-2 null adults the crossveins are missing indicating that Cv-2 in this context enhances BMP signaling. In the posterior crossvein, Cv-2 is required to both initiate and sustain pMad expression. In the wing disc, Cv-2 is secreted and is indirectly attached to the cell surface through binding to heparin sulfate proteoglycans (HSPGs) via its vonWillibrand Factor domain located at the C-terminus. As described above, Cv-2 can also bind to the BMP type I receptor Tkv but the relative strengths of the interaction between the two binding partners is not known. In the early embryo HSPGs are not produced because of a translational block [54]. As a result, Cv-2 may not be as strongly tethered to the membrane surface as it is in wing imaginal tissue. Since the activity of Cv-2 (either pro BMP

or anti BMP) is highly context dependent, it is difficult to predict a priori how Cv-2 will affect BMP signaling during embryonic dorsal surface patterning.

Mathematical modeling of Cv-2 function during dorsal surface patterning has proposed that it may help shape the Dpp gradient through local activation of Dpp signaling [52, 57] and by increasing robustness of the signaling response in the face of potential fluctuations in Dpp protein levels [71]. During dorsal surface patterning, pMad profiles both contract and intensify along the dorsal midline due to a series of interactions between the Dpp/Scw heterodimer and various binding partners as well as the protease Tld. The end result of these interactions is a net flux of Dpp/Scw from the lateral regions toward the midline [44]. However based on the presently identified proteins and their known biochemical activities, mathematical models predict a widening and intensification of BMP signaling [70, 47] with time which is the opposite of what is actually observed. It has been proposed that a positive feedback circuit is needed to sharpen and intensify the pMad pattern [22]. The identity of the molecule(s) that provide the feedback is presently unknown, but modeling has shown that a cell surface localized BMP binding protein such as Cv-2 that can transfer BMP to its receptor can provide the necessary boundary sharpening and pMad intensification [52]. A second issue concerns the robustness of the system. Under most conditions, the D/V patterning mechanism is very robust even through estimates from cell culture data suggests

that the number of BMP molecules on the dorsal surface may be in the range of 10-100 molecules per nucleus [50]. This low number might be expected to result in stochastic fluctuations in the amount of signal perceived by each nucleus, which could make it hard to reliably pattern the dorsal surface. Mathematical models have demonstrated that a molecule with Cv-2 like activities could also function to dampen any stochastic fluctuations in BMP signaling [71]. Thus inclusion of a Cv-2 like molecule into the mathematical models helps reduce stochastic noise and solves the intensification and contraction problem inherent in the original models.

In this chapter, I will examine experimentally how BMP signaling is modulated in the early embryo by the transcription factor Nej and the BMP binding molecule Cv-2. I have identified a new allele of *nej*, and characterized its phenotype with respect to D/V patterning. I demonstrate that this allele causes extreme variability in formation of the pMad stripe suggesting that Nej may be essential for buffering noise. I will also show the effect on Cv-2 loss on the contraction and intensification of BMP signaling on the dorsal surface of the *Drosophila* embryo. I find that Cv-2 is induced by BMP signaling consistent with a potential feedback role but its loss does not dramatically affect pMad sharpening or intensity suggesting it is not likely to be the molecule that provides the positive feedback necessary to get proper dorsal patterning. As part of this study, I have also demonstrated the necessity for careful controls when analyzing subtle patterning phenotypes and

identified the best methodology to use for obtaining reproducible results.

2.2 Results

2.2.1 Nej Identification and Characterization

I received the Maternal Ventralizing Factor-1 (Mvent^1) fly line as a gift from Armen Manoukian. Mvent^1 contains a lethal mutation on the X chromosome that is hypothesized to create a dorsal surface patterning defect. A homozygous loss of function allele is lethal, but a stable stock can be maintained with the X balancer chromosome FM7. I have identified Mvent^1 as a new mutation in the gene *nejire* (*nej*). The Mvent^1 phenotype is highly variable ranging from no effect on D/V patterning to strongly ventralizing.

Identification of Nejire Mutation

I mapped the location of the *mvent*^{1} mutation using two different techniques. First, we used a duplication mapping technique (Figure 2.1). A series of duplications containing segments of the X chromosome transposed to the 3rd or Y chromosome was obtained from the Bloomington Stock Center. Males from these stocks were crossed to *mvent*^{1} balanced females and the progeny were examined

for presence of non-balanced (rescued) males [101, 102]. 80% of the Bloomington duplication series was used, but no rescue was observed. As an alternative mapping strategy, I next used a P-element mapping technique to find the general region of the mutation (Figure 2.2). In this method, the recombination frequency between a *white* (w^+) containing P-element inserted on a wild type chromosome and a gene of interest ($mvent^1$) on a w^- background will give a rough estimate of the distance between the P and the mutant gene. (Figure 2.2). The closer the mutation is to the P-element, the less likely the recombination event will occur between them. A rough P-element mapping narrowed the region containing $mvent^1$ to a location between the cytological interval 8A-10E (Table 2.1). A finer mapping narrowed the region to the cytological interval 8E7-9A1 with the most likely region being at 8F9 (Table 2.2). There are 18 genes located between 8E7-9A1. Nine genes have moderate to very high expression levels in the early embryo based on modENCODE temporal expression data, and two genes had no information. The two genes in the region 8F9 with high modENCODE expression data are *lethal (1)GO232* (*l(1)GO232*) (8F2-8F6) and *nejire* (*nej*) (8F7-8F9). L(1)G0232 is a non-membrane spanning tyrosine phosphatase, and Nej is a histone acetyltransferase known to interact with pMad [80]. Thus using P-element mapping I narrowed the search for the mutation to a small list of candidate genes, one of which included a gene known to interact with the BMP signaling pathway.

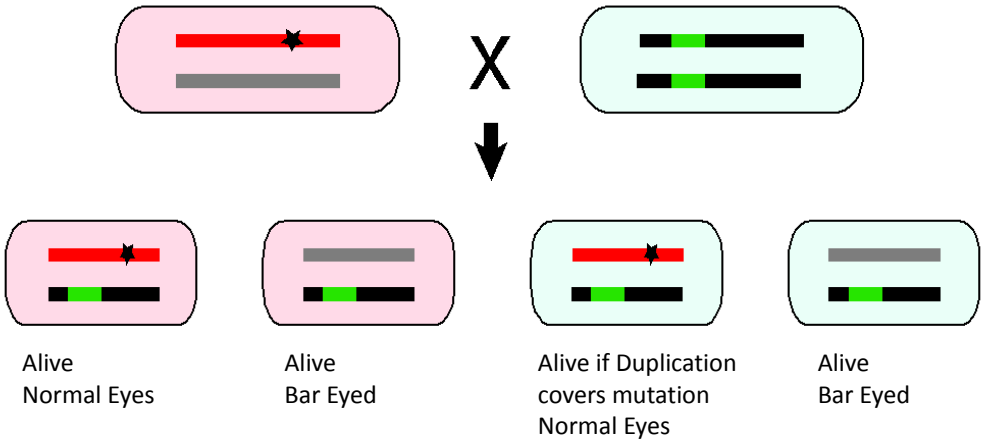

Figure 2.1: Duplication Mapping Technique- Virgin female (pink) flies containing a chromosome with the mutation (red star) and a balancer chromosome (grey) are crossed the males (blue) containing a duplication of the X chromosome (green). Males are scored for eye shape. Males with the balancer chromosome have bar eyes, whereas rescued males will have normal eyes.

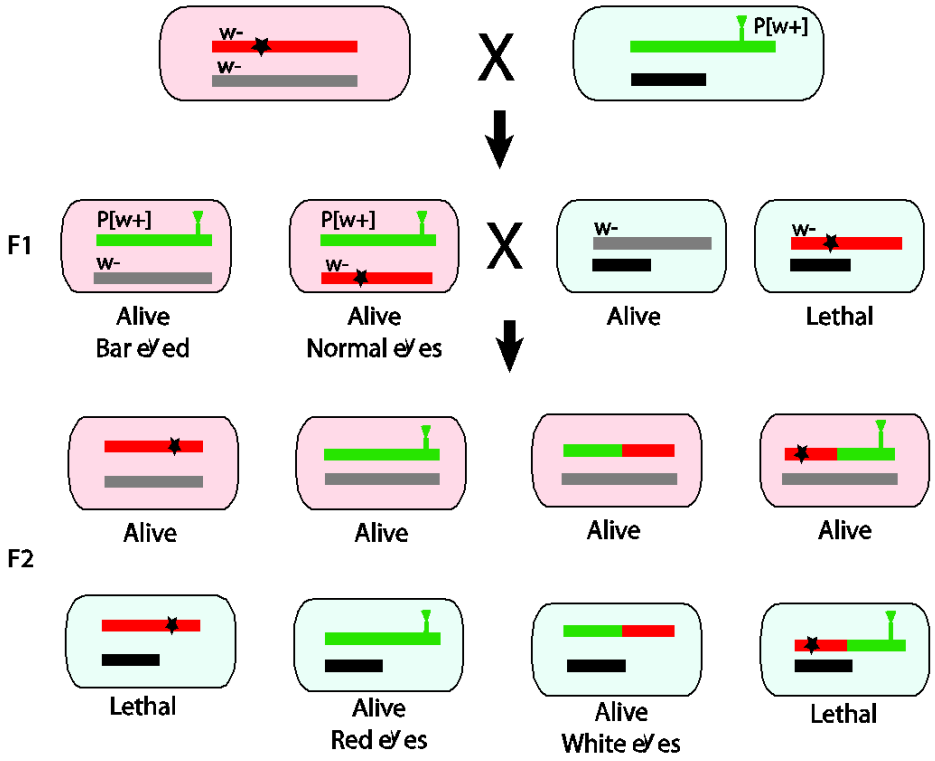

Figure 2.2: P-Element Mapping Technique- Virgin females (pink) containing the mutation (red star) in a w^- background and a balancer chromosome in a w^- background (grey) are crossed to males (blue) with a P-element containing the w^+ gene (green). The F1 progeny are sorted for females containing normal eyes and crossed to F1 progeny males. The males from the F2 progeny are scored for the number of males with red eyes (no recombination) and males with white eyes (recombination occurred). The closer the mutation is to the P-element the less likely recombination will occur.

Region	Stock	% White	Total Counted
1-0 (1A)	36539	27.4%	259
1-6 (4A)	33304	25.0%	340
1-12 (5A)	19277	16.9%	201
1-18 (6C)	26611	14.7%	285
1-24 (8A)	22596	5.35%	636
1-30 (9A)	32651	0.456%	4825
1-36 (10E)	20044	5.87%	732
1-42 (11E)	10113	8.55%	269
1-48 (12E)	19646	10.4%	229
1-54 (14D)	15830	22.5%	200
1-60 (17A)	11444	30.0%	203
1-66 (20A)	33445	20.2%	332

Table 2.1: Rough P-Element map- A rough P-element map was performed using fly lines with P-elements equally spaced across the X-chromosome. A lower percent white eyes indicates the p-element is closer to the mutated gene. A region was identified between the cytological region 8A (5.4% white eyes) and 10E (5.8% white eyes) with a hotspot at 9A where there is only 0.46% white eyes. The rough mapping only has one hotspot indicating there are not two widely separated regions that have a lethal mutation.

Region	Stock	% White	Total Counted
8B7	33459	3.53%	170
8C13	11270	2.32%	905
8E7	3345	0.361%	1663
8F1	32636	0.330%	1515
8F5	22594	0.101%	6941
8F9	30733	0.00%	1880
9A1	32591	0.255%	3532
9A2	18206	0.247%	4866
9A3	32651	0.456%	4825
9A5	18146	0.574%	3658
9B1	21869	0.949%	1791
9B5	15492	0.730%	137

Table 2.2: Fine P-Element map- A fine P-element map was performed using fly lines with P-elements equally spaced between the region found from the rough map, cytologic region 8A and 10E. A lower percent white the eyes indicates the p-element is closer to the mutated gene. A region was identified between 8E7 (0.36% white eyes) and 9A1 (0.26% white eyes) with a hotspot at 8F9. The fine mapping only has one hotspot indicating there are not two closely separated regions that have a lethal mutation. The most likely region for the mutation is around 8F9.

Since Nej is known to interact with Smad proteins, it appeared to be the most likely candidate and the corresponding region was sequenced from $mvent^{1}$ mutant larva. The *nej* gene contains 13 exons and the mRNA is 15729 bases long, with the mature transcript containing 3276 amino acids. This is longer than the mammalian CBP protein which contains 2414 amino acids. All thirteen exons were sequenced, and eleven of twelve introns were fully sequenced. Intron six was quite large and only the first two hundred base pairs on each side were sequenced. Five changes were found in *nej* exons and four changes were found in the introns

(Table 2.3). The changes in the introns were not in the splicing donor or acceptor sites and are less likely to affect Nej activity. In the exons, four of the changes were fairly conservative. However one C to T transition leads to a change of Glutamine 2844 at base 8527 to a stop codon in exon 12. This change was found in 2 overlapping high quality sequencing reads. Thus, Nej was pursued as the most likely candidate for encoding the *mvent*^{1} gene.

Location	Base Change	Amino Acid Change
Base 1129, Exon 4	A->T	T->S
Base 1198, Exon 4	C->G	P->A
Base 1236, Exon 4	Insert CAG	Add Q
Base 1260, Exon 4	Deletion	Delete Q
Bases 11976:11978, Intron 4	CAA->AGG	No changes
Base 12009, Intron 4	Delete T	No changes
Base 16248, Intron 10	A->T	No changes
Base 8527, Exon 12	C->T	Q->stop
Bases 18386, Intron 12	A->G	No changes

Table 2.3: Sequencing of *nejire*- The gene *nej* was sequenced as the most likely candidate for containing the lethal mutation. All thirteen exons were sequenced and all introns were sequenced with at least 200 base pairs on each end. Four conservative changes were found in the exons and one stop codon in exon 12. Four changes were found in the introns, but none of the changes were in splicing donor or acceptor sites. The premature stop codon is the most likely change for causing the lethal mutant phenotype.

To confirm that the premature stop codon in nej^{mvent1} caused the mutant phenotype, non-complementation and rescue experiments were performed. The nej^{mvent1} allele showed non-complementation with the nejQ7 allele (Table 2.4). In addition, the nej^{mvent1} allele was recused using the balancer for the nejQ7 allele (Table 2.4). However, the nej^{mvent1} allele did not show rescue with stock 29782 Dp(1;Y)BSC58 in the Bloomington duplication collection, which is supposed to contain *nej*. The rescue and non-complementation data confirm that the affected gene causing the lethal phenotype is from the stop codon found in *nej*.

Cross	Number non-bar eyed males	Number bar eyed males	Number non-bar eyed females	Number bar eyed females
Line 82, Cross 1	47	21	0	49
Line 82, Cross 2	41	16	0	73
Line 82, Cross 3	19	19	0	35
Line 82, Cross 4	13	13	0	19
Total	120	69	0	176
Line 54, Cross 1	17	32	0	42
Line 54, Cross 2	13	13	0	19
Line 54, Cross 3	6	8	0	14
Line 54, Cross 4	10	7	0	17
Total	46	60	0	92

Table 2.4: *nej* Non-Complementation and Rescue Data- Two separate fly lines containing the Mvent1 mutated allele (82 and 54) were crossed to *nejQ7* allele that was balanced over a duplication of *nej*. The duplication of *nej* rescued the lethal male phenotype as 120/189 males and 46/106 males were non-bar eyed for fly line 82 and 54 respectively. The nej^{mvent1} allele also showed non-complementation with the nejQ7 allele as no females that were non-bar eyed were found for either the 82 or 54 crosses. Similar data was obtained in multiple crosses for each fly line. The non-complementation and rescue data confirm that the $mvent^{1}$ lethal mutation is within the nej gene and is now referred to as nej^{mvent1}

Maternal Nejire D/V Patterning Phenotype

I next analyzed the pMad phenotype for maternal nej^{mvent1} clones. The maternal nej^{mvent1} clones have a highly variable phenotype. In pre-cephalic furrow embryos, all maternal nej^{mvent1} clones (10/10) had areas with no pMad staining in the central region along the A/P axis, which is never seen in control embryos (Figure 2.3 A, D, and G). However the severity in terms of how much pMad was missing

along the A/P axis ranged from a small region (Figure 2.3 D) to most of the A/P axis (Figure 2.3 G). pMad was always present in the anterior region of the embryo. In slightly older embryos, just after the cephalic furrow formed, the pMad phenotype for maternal nej^{mvent1} clones ranged from relatively normal in 12/27 embryos (Figure 2.3 E) to areas with absent pMad staining in the central region of the A/P axis in 15/27 embryos (Figure 2.3 H). During germ band extension, 7/15 embryos were relatively normal (Figure 2.3 F) and 8/15 embryos had significantly expanded pMad expression over the dorsal surface (Figure 2.3 I) compared to control embryos (Figure 2.3 C). Maternal Nej appears to be required for consistent pMad patterning on the dorsal surface, and its loss lead to a highly variable phenotype that is stage dependent.

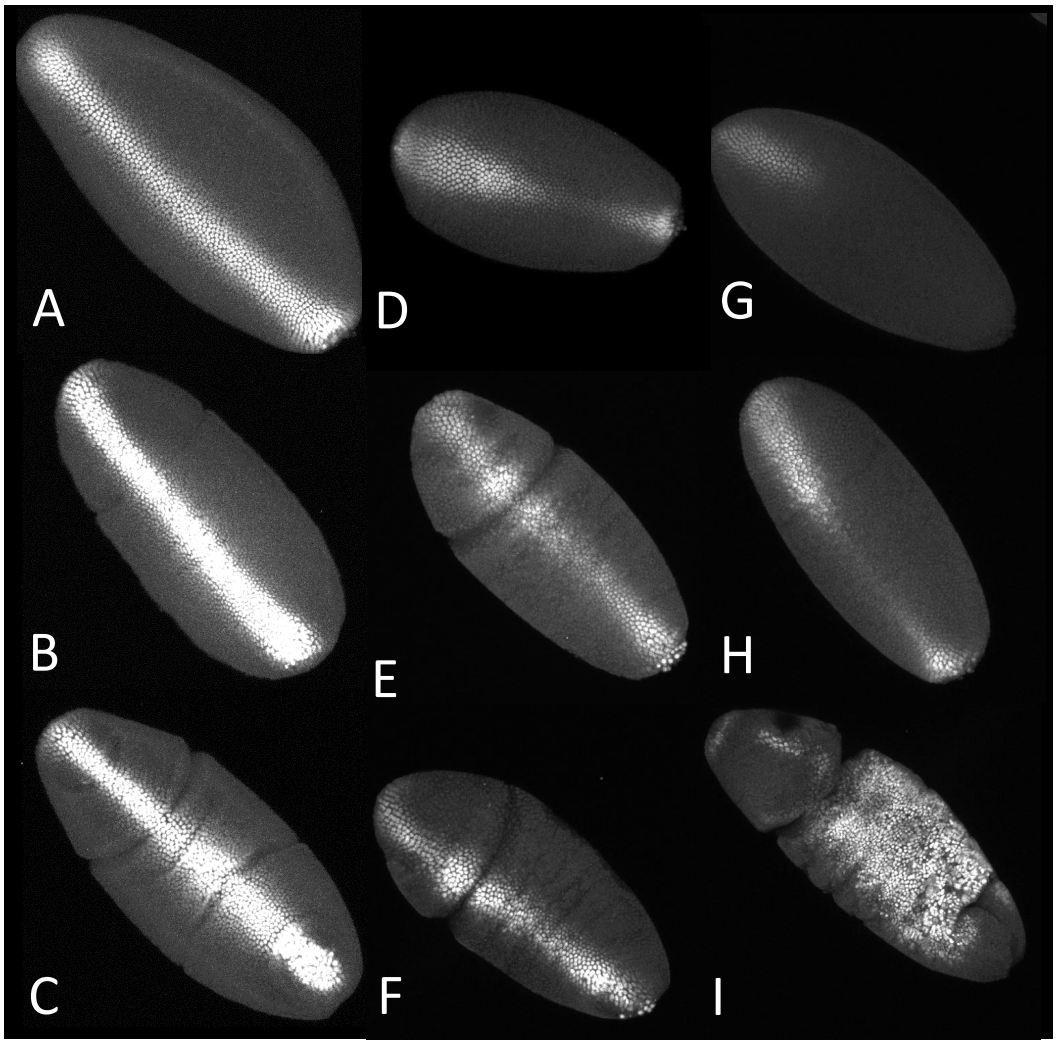

Figure 2.3: *Nejire* Maternal Clones- A-C are His-GFP control embryos and D-I are maternal nej^{mvent1} embryo clones. A, D, and G are pre-cephalic furrow embryo. B-C, E-F, and H-I are post-cephalic furrow embryos. C, F, and I are embryos starting germband extension. All embryos are oriented with the anterior region on the left and posterior region on the right. D-F are maternal nej^{mvent1} embryo clones that are more similar to control embryos. In pre-cephalic furrow embryos, 10/10 maternal nej^{mvent1} embryo clones only had regions of absent pMad staining in the central (D and G) and sometimes posterior (G) region of the A/P axis surface. In embryos right after the cephalic furrow formed maternal nej^{mvent1} clones showed a range from normal (E), 12/27 embryos, to embryos missing pMad staining in the central region of the A/P axis (H), 15/27 embryos. During germband extension, 8/15 embryos had expanded pMad signaling over the dorsal surface (F) and 7/15 embryos were fairly normal (I).

2.2.2 Cv-2 Characterization

Crossveinless-2 (Cv-2) is a membrane associated protein that has been shown to modulate BMP signaling in the wing disk. However, the Cv-2 phenotype has not been characterized in the early embryo. Here I show the Cv-2 is BMP responsive, inhibits overall BMP signaling, and leads to a smaller amnioserosa during dorsal surface patterning.

Cv-2 Expression Patterns

To identify Cv-2s role in embryonic patterning, I first performed *in situ* hybridizations for *cv-2* mRNA on *yw*, Cv-$2^{1-/-}$, a mixture of $Dpp^{+/+}$ or $Dpp^{+/-}$, and $Dpp^{-/-}$ embryos (Figure 2.4). In control embryos, *cv-2* mRNA first accumulates broadly over the central region of the dorsal surface, but is absent from the poles (Figure 2.4 A and C). At the beginning of gastrulation, the *cv-2* mRNA is seen in a graded pattern with more mRNA along the dorsal midline and absent at the poles (Figure 2.4 D and F). In $Dpp^{-/-}$ embryos, *cv-2* mRNA is absent (Figure 2.4). In the Cv-$2^{1-/-}$ point mutant, the mRNA is present and follows the same pattern as control embryos (Figure 2.4 B and E). However this is not surprising as the Cv-$2^{1-/-}$ embryo are protein missense functional nulls, so the mRNA is still produced but the mature protein is not active. Based on this evidence I conclude that Cv-2 is positively regulated by BMP signaling during dorsal surface

patterning.

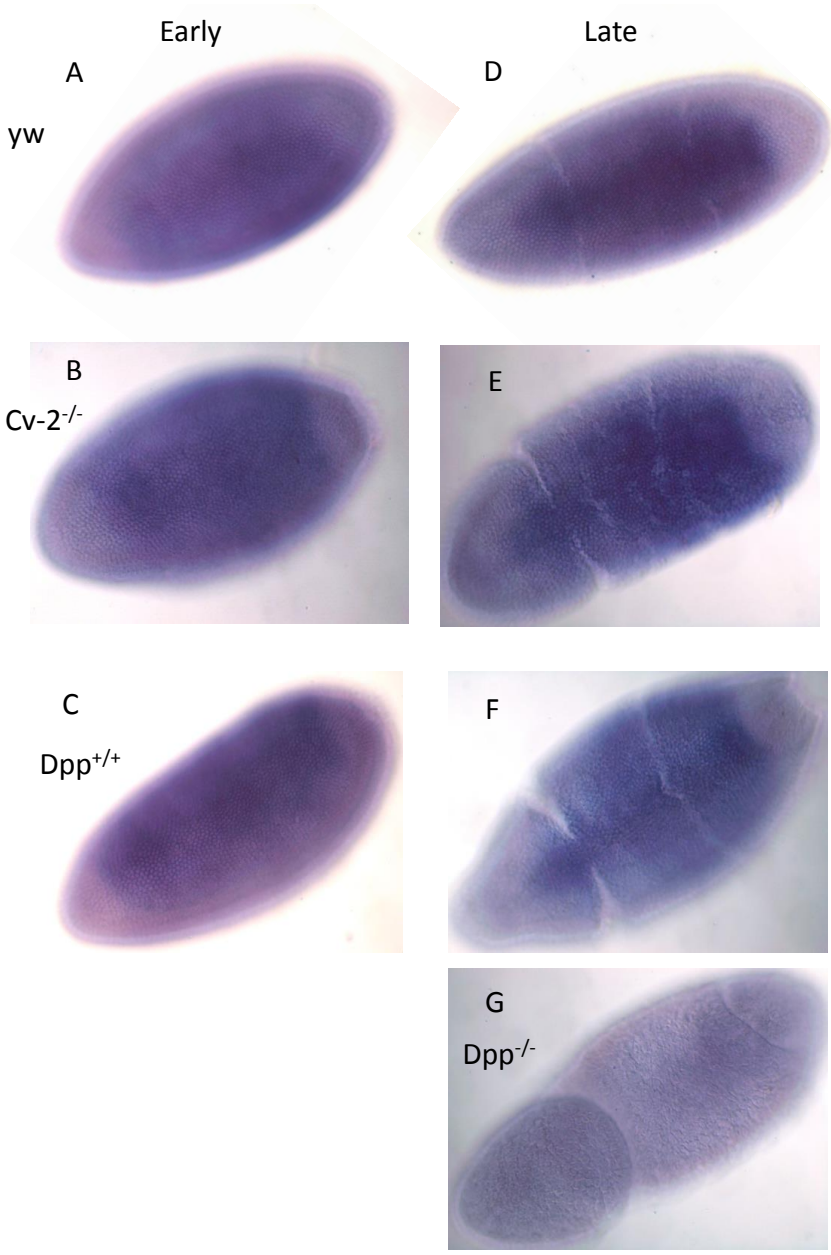

Figure 2.4: *Cv-2 In Situ* Hybridizations- *Cv-2 in situ* hybridizations for Yw (A and D), Cv-$2^{1-/-}$ (B and E), $Dpp^{+/+}$ or $Dpp^{+/-}$ (C and F), and $Dpp^{-/-}$ (G) embryos. Early pre-gastrulation embryos (A-C) show Dpp to be at low levels across the central region of the dorsal surface and absent at the poles. In later gastrulating embryos (D-G) in control embryos (D and F) *cv-2* mRNA is expressed across the dorsal surface, but is more concentrated along the dorsal midline. *cv-2* mRNA is absent in $Dpp^{-/-}$ embryos. In Cv-$2^{-/-}$ embryos, *cv-2* mRNA follows the same pattern as control embryos.

Cv-2 is an Inhibitor of BMP Signaling During DV Patterning

I next investigated how the pMad profiles on the dorsal surface evolve over time in control and Cv-$2^{1-/-}$ embryos. Both Cv-$2^{1-/-}$ and control embryos undergo contraction and intensification of pMad on the dorsal surface (Figure 2.5, 2.6). pMad starts broadly distributed over about 18 nuclei. Over time the low intensity signaling contracts by about 5 nuclei, while there is little contraction seen in the region of high signaling. In the region of high signaling, the peak intensity increases over time. Simple visual inspection between control and Cv$2^{1-/-}$ embryos suggests a difference in the width of pMad between the embryos. However it is not clear if this difference is significant indicating a need for more precise measurements. Since Cv-$2^{1-/-}$ embryos show contraction and intensification similar to control embryos, without precise quantification between Cv-$2^{1-/-}$ and wild type embryos it is difficult to determine if Cv-2 plays a role in dorsal surface patterning.

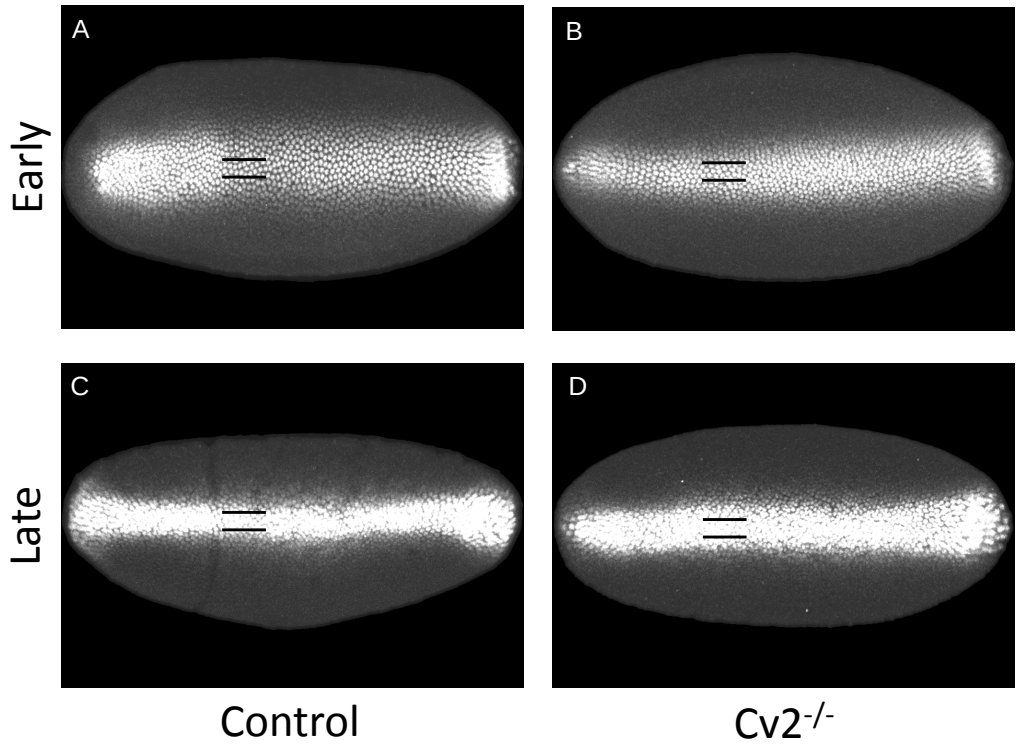

Figure 2.5: pMad Staining on the Dorsal Surface of Cv-$2^{1-/-}$ and His-GFP Control Embryos- A and B show pre-cephalic furrow embryos and C and D show embryos after the cephalic furrow is formed. A and C are His-GFP control embryos and B and D are Cv-$2^{1-/-}$ embryos. The pMad staining starts broad but contracts and intensifies along the dorsal midline for both control and Cv-$2^{1-/-}$ embryos.

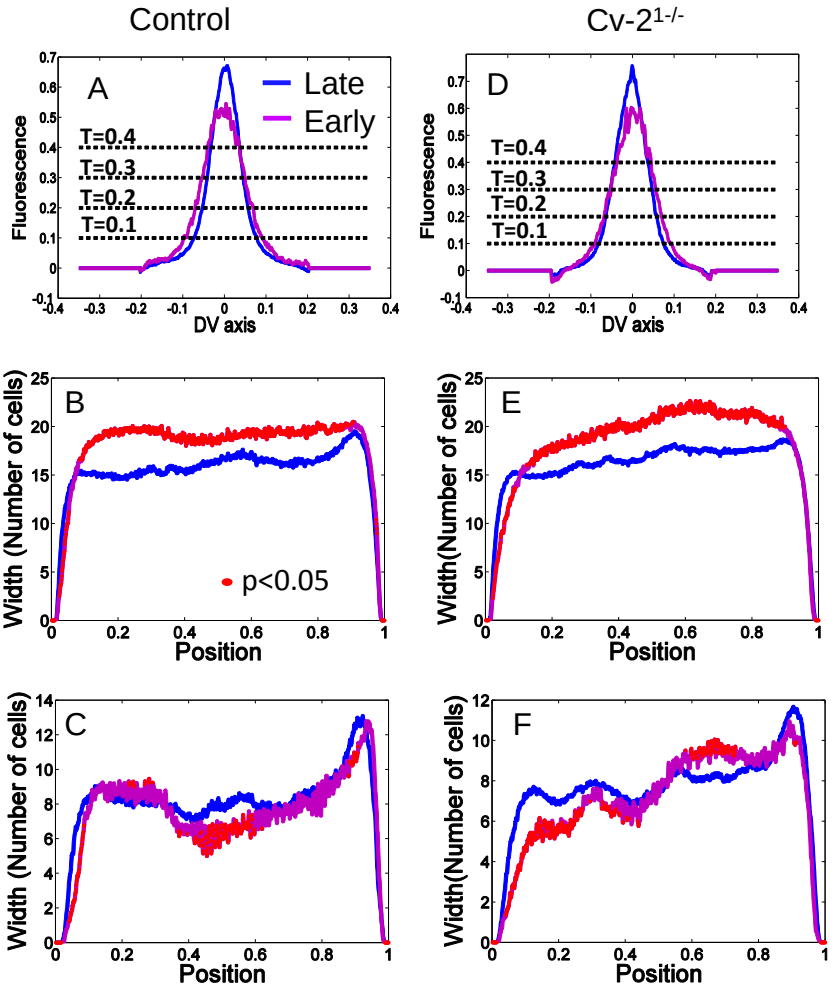

Figure 2.6: Evolution of pMad in Control and Cv-$2^{1-/-}$ Embryos- A-C are His-GFP control embryos and D-F are Cv-$2^{1-/-}$ embryos. Blue lines are post-cephalic furrow embryos and the purple lines are pre-cephalic furrow embryos. Red dots are areas of significant difference ($p<0.05$) between pre- and post-cephalic furrow embryos. A and D are profiles across the dorsal surface at the midline of the embryo. B and E are A/P profiles at the threshold T=0.1 and C and F are A/P profiles at T=0.4. The Dorsal profiles show the peak intensity increase on the dorsal midline for both Cv-$2^{1-/-}$ and control embryos. There is a contraction of the low intensity signaling (B and E), but the higher intensity signaling does not show any contraction.

The pMad phenotype for *cv-2* is very subtle, and when I used a standard antibody staining protocol, I found significant variability in the quality of staining between samples each day and between days. However, the variability of staining quality between embryos within each sample was low. When I did not normalize for the inter-tube staining variability, half the data sets showed the width of Cv-$2^{1-/-}$pMad staining compared to control embryos was larger and the other half showed it was smaller. Therefore, I tested four different protocols to find one that was able to give consistent results. I initially tried three different methods; the staining method, ratio method, and parallel method, briefly described below, that did not work to adequately control for staining variability. However, the fourth procedure, which I refer to as the mixing method, which was developed by Shavartsman and colleagues (personal communication) was used successfully.

The first method I used involved pre-staining control embryos with a marker and then mixing them with experimental embryos followed by pMad antibody staining. *yw* embryos were collected and split in half. Half of the embryos were stained with DAPI or Propidium iodide (PI) for 15 minutes, and the other half were washed in PBT. Then, the embryos were mixed and a standard antibody staining protocol for pMad was followed. DAPI and PI both diffused out of the pre-stained embryos and resulted in staining all the embryos. There was a gradient of intensity of staining, but the difference was not great enough to definitively

separate the control from the test embryos. Since the binding affinity of DAPI or PI does not appear to be high enough to prevent bleeding into test embryos, I did not pursue this method further.

The next method I used was designed to normalize for day to day staining variations by taking the ratio of the fluorescence intensity (FI) of pMad to RNA polymerase (pol). While the FI varied from day to day, I tried taking the average intensity of pMad in the embryo and compare it to the average amount of pol as an internal control. The average FI of the maximum intensity projection of the embryo was found by drawing a mask around the embryo. The average embryo FI of pMad between four different days varied from 32 to 43 and was significantly different ($p<0.05$) (Table 2.5). However the ratio of pMad:pol did not attenuate the differences and if anything amplified the day to day variability. The ratios varied from 0.47 to 0.68 and were significantly different ($p<0.05$) (Table 2.5). Based on this data, I concluded that taking the ratio of pMad:pol does not attenuate the variations in staining between test samples.

Sample	pMad	pMad:pol
Sample 1 (N=13) Avg. FI	32.8	0.68
Sample 2 (N=9) Avg. FI	43.0	0.47
Sample 3 (N=22) Avg. FI	37.3	0.52
Sample 4 (N=15) Avg. FI	33.9	0.62
Anova p-Value	$9.0 * 10^{-4}$	$6.2 * 10^{-14}$

Table 2.5: Ratio Method for Normalizing Antibody Staining Between Samples- The average FI of pMad and pol was found for each embryo and the ratio of pMad:pol was found to see if it could attenuate the day to day variability in staining. Four samples were looked at with the number of embryos (N) ranging from 9-22 per sample. An ANOVA p-value comparing the four different days found significant differences for both pMad and pMad:pol. The ratio method made the differences between the four samples worse and does not work the control for day to day variability.

Next I attempted to control for differences due to the fixation process and antibody staining by collecting and staining *yw* and Cv-$2^{1-/-}$ embryos in parallel. First, the embryos were fixed in parallel to minimize the differences due to the fixation process. Next the embryos were stained in a chamber that allowed fluid to move between the different chambers, so that both the control and test embryos were exposed to the same wash and antibody solutions. The *yw* and Cv-$2^{1-/-}$ embryo collections were each split in half and all 4 sets were fixed in parallel and stained in the chamber allowing exposure to the same solutions. This process was repeated two times. There was no significant difference between the samples within the same genotype (Table 2.6). However, the two sets of data showed opposite results for the difference between *yw* and Cv-$2^{1-/-}$ in the average FI.

This indicates that fixing in parallel is not sufficient to obtain reproducible results for the average FI between samples. When the width of the pMad positive nuclei along the A/P axis was examined for the embryos fixed together and split in half for antibody staining, there were areas of significant difference in both sets of data (Figure 2.7). While staining embryos in the same chamber reduced the variability in the width of pMad positive nuclei, there are still subtle differences.

Samples	pValue
Yw set 1 a vs b	0.15
Cv-$2^{-/-}$ set 1 a vs b	0.30
Yw set 2 a vs b	0.72
Cv-$2^{-/-}$ set 2 a vs b	0.43

Table 2.6: Average Fluorescence Intensity for Embryos Processed Using the Parallel Method- On two separate days *yw* and Cv-$2^{1-/-}$ embryos were split in half, fixed in parallel, and stained in the same chamber. The table shows the average FI for each set of data that were processed in parallel. The average FI between the samples did not show any differences for fixing in parallel and staining together.

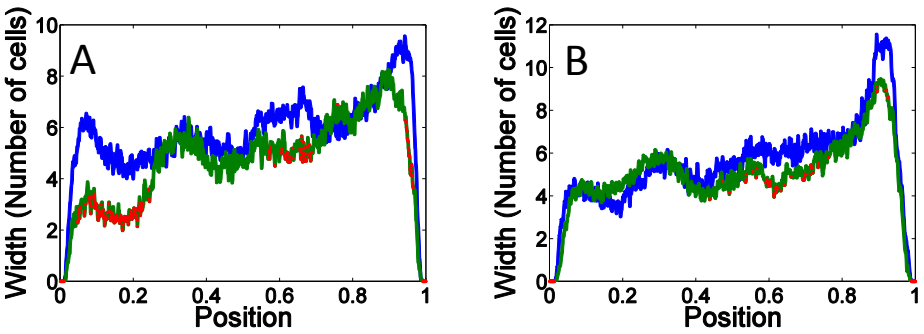

Figure 2.7: Parallel Method for Embryo Processing- On two separate days *yw* and *cv-2*$^{1-/-}$ embryos were split in half, fixed in parallel, and stained in the same chamber. A) Width of pMad positive cells at the relative position across the A/P axis for yw embryos from set 1. Blue is *yw* set 1a, green is *yw* set 1b, and red are areas of significant difference. B) Width of pMad positive cells at the relative position across the A/P axis for *cv-2*$^{1-/-}$ embryos from set 2. Blue is *cv-2* set 1a, green is *cv-2* set 1b, and red are areas of significant difference. While the average FI is not different between the samples, there are areas of difference along the A/P axis in comparing the width of the number of cells. Thus, there are still sample to sample variations that cannot be corrected by simply fixing and staining embryos using the same solutions.

The mixing method is the only method where all embryos are exposed to the same environmental variables throughout the entire process. Thus, this proved to be the most reliable method for examining subtle changes in pMad signaling profiles. In this method, control and mutant embryos are collected separately, mixed together, and then fixed and stained in the same tube from the beginning of the procedure. To distinguish control (wt) embryos from mutants, a GFP reporter

is incorporated into the wt control parents that enables the investigator to sort wt embryos from mutant on the basis of GFP fluorescence. This method was the only one in which consistent results for differences in the pattern and pMad staining intensity was observed between Cv-$2^{1-/-}$ mutant and control (Histone-GFP+ (His-GFP)) embryos. However for each batch processed, there was a difference in the average width of the pMad positive nuclei, which depended upon the intensity of the staining. However the pertinent different between the control and mutants remained the same. Thus by mixing His-GFP embryos as a control with Cv-$2^{1-/-}$ embryos I were able to get consistent results in the difference in width of signaling between the two samples.

I first studied the difference in pMad profiles in His-GFP control and Cv-$2^{1-/-}$ embryos raised at 25°C. Cv-$2^{-/-}$ embryos have a higher average FI and a wider number of total pMad positive nuclei compared to His-GFP control embryos. Both genotypes follow similar pMad profiles along the D/V axis with the pMad FI initially slowly increasing and then more rapidly increasing closer to the Dorsal midline (Figure 2.8 A-C). Along the A/P axis, the pMad intensity is lowest in the anterior region and highest in the posterior region. In the lateral region of the dorsal surface where pMad intensity is low, both Cv-$2^{1-/-}$ and His-GFP embryos have similar pMad expression profiles. On average, the width of the pMad stripe along the dorsal midline, at four different thresholds in the central

region of the embryo, for Cv-$2^{1-/-}$ mutant embryos is about 2 nuclei more than for a comparably aged His-GFP^{+} wt embryo (Figure 2.8). Cv-$2^{1-/-}$ embryos also have a higher peak FI (Figure 2.8). The width of pMad expression at the poles of the embryo is not affected by Cv-2. I also examined if the Cv-2 mutant phenotype varies depending on temperature. However, the differences in pMad profiles between mutant and control is the same pattern at 18°, 21°, and 25°C (Figure 2.9). At all temperatures the width of the pMad stripe in Cv-2 mutant embryos is 2 nuclei wider than His-GFP^{+} controls. Thus, I conclude that Cv-2 is a negative regulator of BMP signaling during dorsal surface patterning.

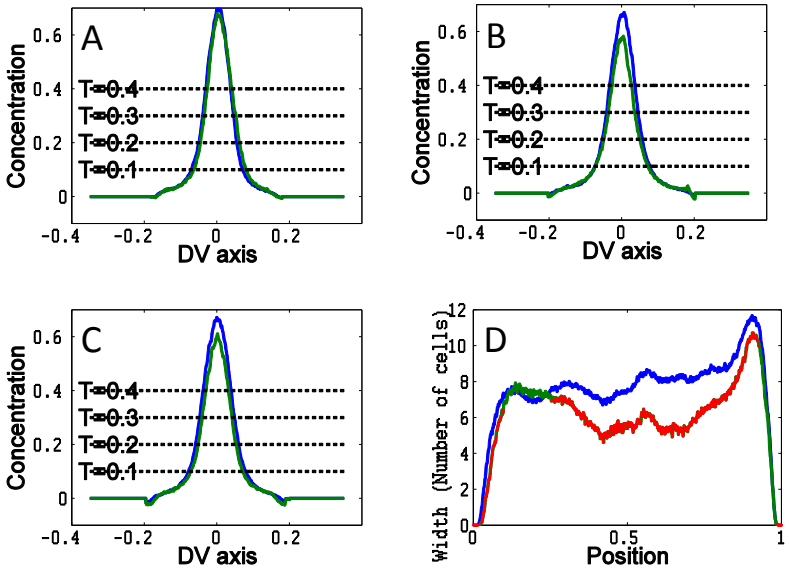

Figure 2.8: pMad Profiles at 25°C Comparing Cv-$2^{1-/-}$ (blue) and His-GFP (green)Control Embryos- A-C shows p-Mad profiles along the D-V axis with A being an anterior slice, B a central slice and C and posterior slice. At all positions along the D-V axis the Cv-2 embryos have a higher and wider p-Mad staining. D) Cv-$2^{1-/-}$ embryos (blue lines) are 2 nuclei wider than His-GFP control embryos (green). Red dots show where there is a significant difference from the dark blue line ($p<0.05$) using a students t-test. Threshold (T) taken at T=0.4.

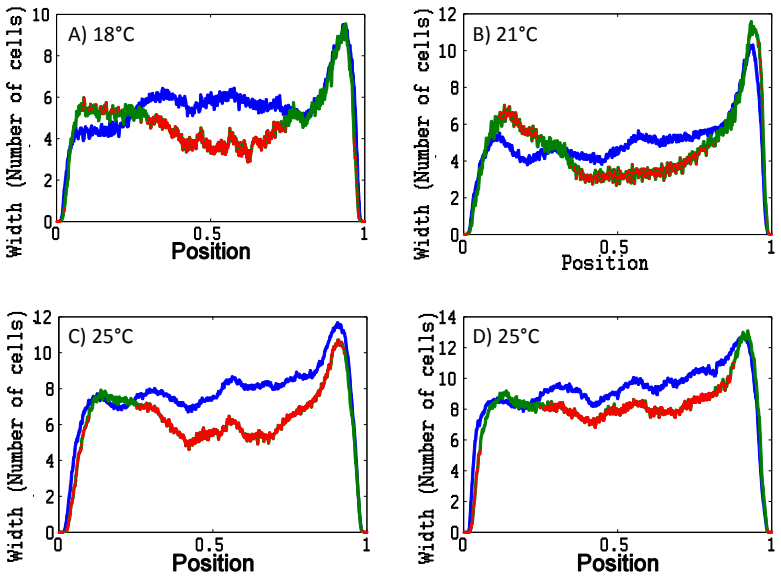

Figure 2.9: pMad Profiles Along the AP axis for Cv-$2^{1-/-}$ (blue) and His-GFP (green) Control Embryos at 18-25°C- A is at 18°C, B is at 21°C, C is at 25°C and D is at 25°C. All profiles show a 2 nuclei difference in width. There is a difference in the width of the p-Mad between samples which is most likely differences in the intensity of p-Mad staining. Red dots show where there is a significant difference from the dark blue line ($p<0.05$) using a students t-test. Threshold (T) taken at T=0.4

Cv-2 May Increase the Noise in the Width of pMad Positive Nuclei During D/V Patterning

Since Cv-2 has been proposed to reduce the noise caused by putatively low levels of Dpp in the PV space [71], I examined the average variability in the width of the pMad stripe in Cv-$2^{1-/-}$ embryos (Figure 2.10). To study the noise or variability in the width of pMad positive nuclei, I used the coefficient of variation (CV) to

measure noise levels. The coefficient of variation is the standard deviation/mean for a data set. Since the CV is computed for each data set, I was unable to obtain meaningful statistics due to not having enough replicates to determine if there is a statistical difference for the CV between His-GFP control and Cv-$2^{1-/-}$ embryos. However, there is a trend for Cv-$2^{1-/-}$ embryos to have a lower CV than His-GFP control embryos (Figure 2.10). Unlike the prediction of one current mathematical model where Cv-2 buffers noise created by fluctuations in Dpp levels, Cv-2 may actually increase the amount of noise in Dpp signaling during dorsal surface patterning.

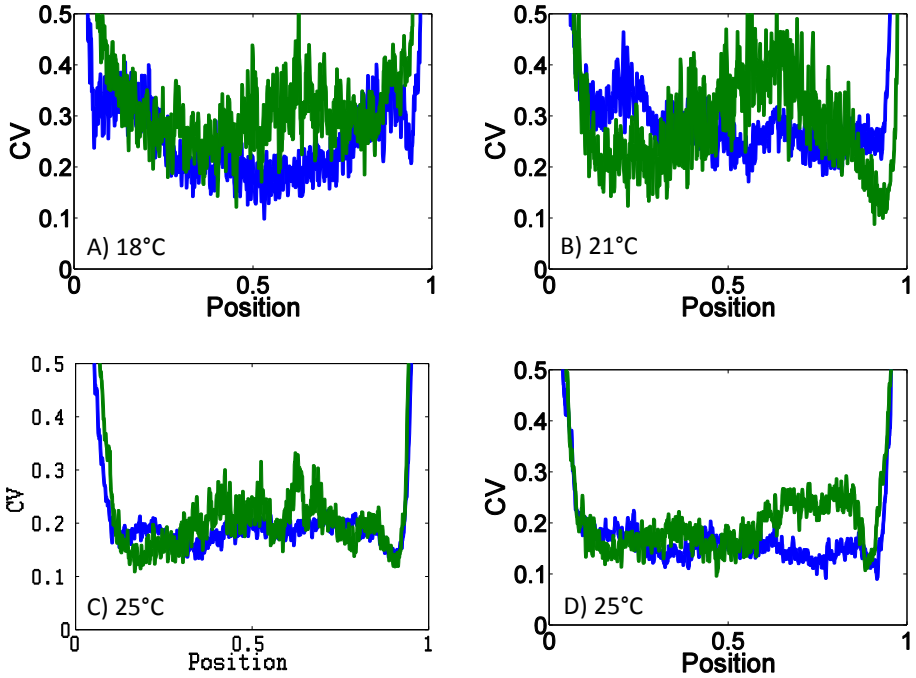

Figure 2.10: Coefficient of Variation for Width on the Dorsal Surface at 18-25°C Comparing Cv-$2^{1-/-}$ (blue) and His-GFP (green) Control Embryos- The coefficient of variation of the width of pMad positive nuclei at T=0.4 was plotted along the A/P axis for Cv-$2^{1-/-}$ (blue) and His-GFP (green) embryos at 18°C (A), 21C (B) and 25°C (C and D). At approximately 75% of the total positions along the A/P axis, Cv-2 mutants have a lower CV than control embryos.

Loss of Cv-2 Leads to a Larger Amnioserosa

The pMad positive nuclei posterior to the cephalic furrow ultimately will form amnioserosa cells. To determine if the 20-30% change in the width of the pMad nuclei ultimately affects cell fate and tissue size, later in development, the average number of amnioserosa cells was determined at the germband retraction stage by

counting the number of hindsight, a marker for the amnioserosa, positive cells (Figure 2.11). There is a 35% increase in the size of the amnioserosa of Cv-$2^{1-/-}$ embryos ($p = 2.05 * 10^{-15}$) compared to the His-GFP^{+} controls. Thus, the change in early Dpp signal reception in Cv-$2^{1-/-}$ mutant embryos has a functional consequence during development since in translates into a significant change in the final size of the amnioserosa.

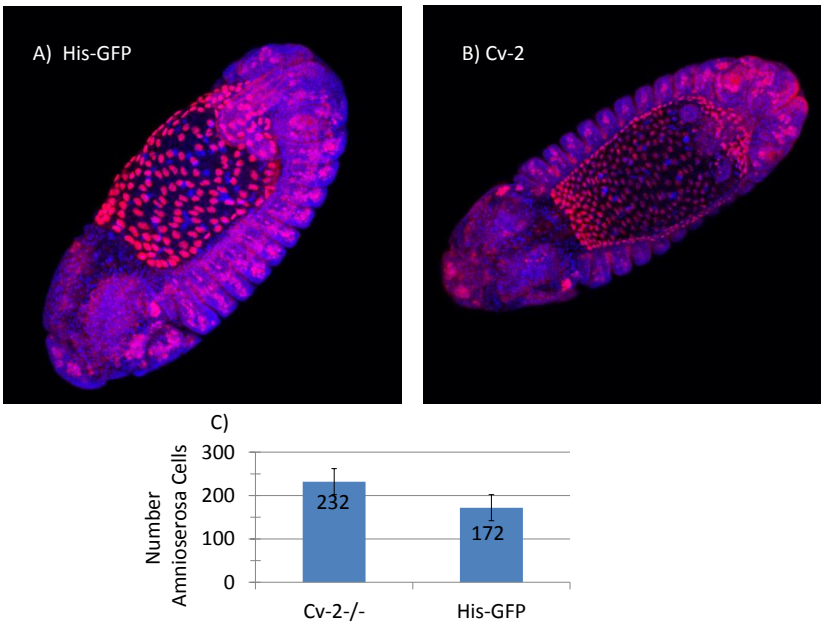

Figure 2.11: Size of the Amnioserosa in Cv-$2^{1-/-}$ and His-GFP Control Embryos- The amnioserosa of Cv-$2^{1-/-}$ (A) and His-GFP (B) embryos is shown in red. Blue shows the nuclei with DAPI staining. C) There is an average of 232 amnioserosa cells for Cv-$2^{1-/-}$ embryos and 172 amnioserosa cells for His-GFP embryos with a p-value of $2.05 * 10^{-15}$.

2.3 Discussion

I have studied two genes that are involved in the feedback control and robustness of Dpp signaling during dorsal surface patterning in the early *Drosophila* embryo. I have identified a new novel allele of *nej* with a stop codon near the C-terminus. This truncation leads to a highly variable Dpp patterning in the early *Drosophila* embryos. I have also studied the function of Cv-2 during dorsal surface patterning. Cv-2 is a BMP response gene that inhibits BMP signaling during dorsal surface patterning. Cv-$2^{1-/-}$ embryos have a slightly larger area of pMad signaling that leads to a larger amnioserosa. Surprisingly, I found that Cv-2 has no effect or may actually decrease the robustness of Dpp signaling. Thus I have identified one protein, Nej, that enhances the robustness of Dpp signaling and another protein, Cv-2, that appears to reduce robustness with respect to wild type.

2.3.1 The Role of Nej in the Robustness of Dorsal Surface Patterning

We have identified a new allele of *nej* with a stop codon in the 12th exon that is most likely causes a dominant negative phenotype (see below). Curiously, I was unable to map the mutation using the Bloomington stock collection duplication series. The end points of the duplications in the Bloomington collection have

not all been confirmed, so it may be that *nej* was not actually contained in any of the duplications that I used. Another possibility is that while *nej* coding sequences might be contained on the Bloomington duplications, some regulatory areas may be missing. In either case, the fact that the Dp(1;Y)FF1 duplication derived from the nej^{Q7} containing stock did successfully rescue the $mvent^{1}$ lethal phenotype helped confirm that $mvent^{1}$ was near the *nej* locus. We were able to further fine map the $mvent^{1}$ mutation using a P-element recombination strategy and then confirmed that $mvent^{1}$ is a *nej* allele by sequencing. This allele has a premature stop codon located near the C-terminus of the gene at the 2844th amino acid out of 3246 amino acids. This truncation removes a glutamine and alanine rich domain of Nej [103, 104, 105]. A deletion of Nej starting at amino acid 2677 produces a dominant negative mutation when assayed for activity in the *Drosophila* eye. Thus it is likely our mutation is also a dominant negative mutation. The glutamine and alanine rich region is most likely important for the activation of transcription [105]. The mammalian homologue of Nej, the CREB Binding Protein (CBP), is significantly shorter than *Drosophila* Nej, however, it too contains a glutamine rich domain [80], likely indicating conserved function for this portion of the protein in transcriptional regulation. Since the nej^{mvent1} allele does not truncate the entire glutamine rich domain, it is possible that it does not completely inhibit transcriptional activation and represents a hypomorphic

mutation. However, a dominant negative phenotype for nej^{mvent1} allele might also arise if the truncated protein is able to assemble into complexes with other transcriptional binding partners but is unable to initiate transcription. Additional genetic tests will be required to determine if nej^{mvent1} is a dominant negative or hypomorphic mutation.

The nej^{mvent1} allele most likely inhibits dorsal surface patterning through physical interactions with Mad. Previous work has shown that Nej residues 2240-2608 [80] bind to the MH2 region of Mad and loss of *nej* affect Dpp signaling in many tissues including the midgut [80], trachea [80, 106], and wing disc [80]. Evidence from the wing disc suggests that Nej functions downstream of the Dpp receptor Saxophone [80]. Previous work has also suggested a role for Nej in regulating D/V patterning. The hypomorphic nej^{1} allele leads to loss of dorsal structures and diminished Dpp target gene expression patterns with in the dorsal ectoderm, but the neurogenic ectoderm appears intact [39]. The loss of high levels of Dpp signaling in nej^{1} mutants is thought to result from the decrease in expression levels of *scw*, *tsg*, and *tld* [81] thereby prevent the Dpp gradient from forming correctly along the dorsal midline. In the early embryo the Nej acetyltransferase activity is not required for Dpp patterning [107]. It is presumed that Nej acts as a bridge between the transcription factor Mad and the transcriptional machinery [107]. Thus the nej^{mvent1} phenotype is most likely due to Nej binding to Mad

and occupying various transcriptional start sites of Dpp target genes, but being unable to properly interact with other components to initiate transcription. It is also likely the nej^{mvent1} allele affects other transcriptional activities besides those involving pMad. For example, in the early embryo *nej* is uniformly expressed [108] and also interacts with Deformed to mediate ventral surface specification [79] and Bicoid to mediate anterior-posterior patterning [109]. Additional staining of nej^{mvent1} mutant embryos with markers for other patterning processes will be required to address this issue.

Although *nej* has been previously implicated in mediating dorsal surface patterning, it is hard to directly compare my results with the previously reported data since the embryos where mounted very differently. I found loss of pMad in the central and often posterior regions of the A/P axis of nej^{mvent1} whereas in nej^{1} mutant embryos, pMad was seen in the anterior most cells, but not in posterior cells [**?**]. Thus nej^{mvent1} may be weaker than the nej^{1} allele during early Dpp embryo patterning, however I observed a stronger phenotype in the post-cephalic furrow embryos compared to the nej^{1} allele. At cellularization, nej^{1} mutant embryos were reported to have recovered normal pMad staining presumably in both males and female embryos. The nej^{mvent1} allele only showed recovery in approximately 50% of the embryos. In the other 50% of the embryos I observed significantly expanded pMad expression on the dorsal surface. While in our crosses we were

unable to differentiate between males and females, the 50/50 split suggests we may have a male / female difference. One possibility is the zygotic expression of Nej from the paternally supplied balancer chromosome rescues female pMad patterning, whereas in males that lack the X chromosome balancer, no zygotic expression of wt *nej* is possible leading to loss of dorsal structures that require high levels of BMP signaling. The eventual broad pMad staining detected at gastrulation likely reflects the second wave of BMP signaling that occurs in dorsal neuroectoderm as gastrulation progresses [44].

One intriguing possibility concerning the role for Nej is that it may help achieve robustness in early Dpp patterning. My data showed a range of severity in the abnormal pMad staining at all stages. As described, however, this variability might simply reflect hypomorphic activity for this nej allele. It is interesting to note that a range of phenotypes was also produced by the nej^{1} allele during midgut formation [78]. To truly determine if Nej contributes to robustness of early D/V patterning it will be necessary to analyze the phenotype of a true molecular null such as a complete deletion of the gene or a very early stop codon.

In conclusion, I have found a new allele of *nej* that truncates the glutamine rich domain at the C terminal end of the protein. Based on comparing our allele to other published *nej* alleles, nej^{mvent1} is either hypomorphic or a dominant negative allele either of which could explain the variable loss of dorsal patterning

through effects on Dpp signaling or the ability of pMad to properly regulate Dpp target gene transcription.

2.3.2 The Role of Cv-2 in Dorsal Surface Patterning

I have shown that *cv-2* is a BMP responsive gene that is a negative regulator of BMP signaling in dorsal surface patterning. I found that *cv-2* mRNA is completely absent in Dpp null embryos, indicating BMP expression is required for *cv-2* expression. The pattern of *cv-2* mRNA expression follows that of BMP signaling on the dorsal surface where BMP signaling starts broad but contracts and intensifies to a narrow region along the dorsal surface. Induction of *cv-2* expression in response to high BMP signaling is consistent with results in the wing disc [57] and with results on vertebrate cv-2 homologs [97, 96, 98]. Since the *cv-2* null allele is a point mutation in the gene that renders the protein inactive, it is not surprising that mRNA expression for the *cv-2* null allele was similar to that of controls, and in fact may have slightly higher amounts of mRNA than controls since I also found that the level of BMP signaling was increased in $cv\text{-}2^{1-/-}$ embryos. Thus similar to results in the wing disc and vertebrate models, *cv-2* expression requires BMP signaling.

In order to consistently and accurately characterize the $cv\text{-}2^{1-/-}$ phenotype with respect to BMP signaling, very careful controls were needed. We found that it

was necessary to control for all steps in the fixing and antibody staining protocols in order to get consistent results. In particular, the anti-pMad antibody seemed to be very sensitive to the fixation process, and without identical fixing conditions consistent results were not obtained. I was not able to get consistent results processing embryos in parallel or by staining with the same antibody solutions as has been proposed for quantitative image analysis by other groups [110, 111, 112, 113, 114]. Before identifying a staining method that yielded consistent results, my data initially showed that the *cv-2*$^{1-/-}$ phenotype was more pronounced at lower temperatures. However, I found this to be false when both fixation and antibody staining was carried out in the same tube using a mixture of control and mutant embryos. Thus it is very important to have identical embryo processing conditions when quantitating antibody staining. My results showed that the width of the signal varied greatly from 8-16 nuclei depending on the intensity of the staining and the threshold examined. My results indicate that quantification from fluorescence intensity must be done in a relative manner between carefully controlled samples as the results depend greatly upon the quality of the antibody staining.

Our results showed that both control (His-GFP) and *cv-2*$^{1-/-}$ undergo contraction and intensification of BMP signaling. On the dorsal surface, peak signaling intensifies over time and the low level signaling contracts towards the midline.

The amount of contraction that occurs over time depends upon the threshold of signaling intensity examined. For low levels of signaling we found a contraction of 5 nuclei, which is consistent with previous results [44, 40]. However, our data may actually underestimate the total amount of contraction occurring as we could not precisely stage early embryos. As a result I grouped together all data from the early time point when the contraction is proposed to be happening. For high level of signaling, we did not see any contraction, but we did see an increase in the peak intensity of the strong signaling. The inability to see any contraction in the high signaling area may be due to how we grouped the pre-cephalic furrow embryos together. Some embryos in the pre-cephalic furrow data set had already undergone a significant amount of contraction and intensification, which may have skewed the data towards intensification of pMad along the dorsal midline. Since both *cv-2*$^{1-/-}$ do undergo some contraction of pMad signal intensity, Cv-2 is not likely the sole mediator of this event.

While in *cv-2* mutant embryos contraction of pMad does occur, the amount of pMad contraction is less than wild type. There was a 2 nuclei change in the overall width of BMP signaling. While only 2 nuclei may seem like a subtle change, it corresponds to a 20-30% increase in the width of the pMad stripe depending upon where the threshold for high level signaling is drawn. The 2 nuclei change is also significant as it leads to a 35% increase in the size of the amnioserosa, which is

specified by high levels of BMP signaling. Thus Cv-2 is necessary for the full contraction of Dpp/Scw on the dorsal midline and is required for correct sizing of the amnioserosa.

It has been proposed that in order for both contraction and intensification of BMP signaling during dorsal surface pattering to occur, a positive feedback mechanism is needed [22, 52]. Cv-2 has been hypothesized to be involved in positive feedback to up-regulate BMP signaling. However, I have shown that Cv-2 functions to slightly narrow BMP signaling through a negative feedback mechanism. My data shows Cv-2 contributes to the contraction on BMP signaling through shifting the BMP profile downwards which both lowers peak signal intensity and narrows the overall signaling width. However, in *cv-2* mutant embryos some contraction and intensification of pMad signal intensity still occurs. Thus there still must be unknown factors that contribute to the contraction and intensification of pMad. Several ideas have been suggested including an inhibitor in the lateral regions of the dorsal surface [22], modulation of Dpp/Scw endocytosis rates [111], or modulation of receptor activity or levels [111, 22]. Mathematical modeling suggests that an up-regulation by a positive feedback mechanism best fits the experimental data [111]. However, there is currently no experimental evidence or new protein candidates that would favor one of these hypotheses over another. Thus, it is still an open question on how Dpp/Scw signaling both contracts and

intensifies along the dorsal surface.

Cv-2 being a negative regulator of BMP signaling is also consistent with previous modeling results. Using binding parameters derived for BMP-2, the vertebrate homologue of Dpp, interactions with to BMP receptor IA and to vertebrate Cv-2 and then performing a parameter scan employing different rates for BMP transfer between Cv-2 and the BMP type IA receptor, one model found that Cv-2 acted as a strong antagonist of BMP signaling over 75.5% of the parameter space [57]. In cell culture experiments, the effects of Cv-2 on Dpp were also found to be purely antagonistic [57]. These results are also consistent with studies employing human Cv-2 where it has been shown to be an antagonist of BMP-2 and -4, during osteoblast and chondrocyte differentiation [96].

The BMP inhibitory role of Cv-2 in Dorsal surface patterning is different from the role of Cv-2 in modulating BMP signaling in the wing disc. In this tissue, Cv-2 has a biphasic role where low levels of Cv-2 enhance BMP signaling and high levels of Cv-2 inhibit signaling [57, 76]. However, in this case Cv-2 likely interacts with both Dpp and the BMP ligand Glass Bottom Boat (Gbb) for proper crossvein patterning. Gbb has low affinity for the BMP receptor and modeling indicates it can produce multiple steady states of BMP activity with a larger parameter set than for Cv-2 interacting with Dpp alone [57]. In the chick, Cv-2 has been shown to enhance BMP-4 signaling, [98, 97]. Thus, it appears that in

certain circumstances Cv-2 enhances BMP signaling while in others it may act strictly negatively depending on the various binding partners involved. While our data shows that ultimately Cv-2 inhibits Dpp signaling during dorsal surface patterning, it is possible that it may transiently enhance Dpp signaling during the earliest stages, but then as its concentration rises it switches to a pure inhibition mode. My analysis only looked at the effect at the endpoint of the contraction process when Cv-2 levels would be the maximum, so it is possible that I may have missed a very transient time point during the earliest stages of Dpp signaling where Cv-2acts as a BMP agonist.

My data further suggests that Cv-2 either has no effect on robustness of Dpp signal or may actually make the output less robust. This conclusion is opposite from what some mathematical models predicted which is that Cv-2 should reduce noise the system [71]. The mathematical model assumed that Cv-2 was a positive regulator of BMP signaling as seen in the wing disc, but I found that this is not the case during dorsal surface patterning and that it actually a negative regulator. Thus, Cv-2 may buffer noise when it is a positive regulator and enhance noise when it is a negative regulator of signaling. If there are fluctuations in embryonic BMP signaling the negative regulation may enhance these fluctuations leading to a higher level of noise in signaling. It is not apparent how increased noise in BMP signaling might be advantageous for embryonic development.

In summary, I found that Cv-2 is a negative regulator of BMP signaling during dorsal surface patterning. In its absence, signal contraction about the midline still occurs but the peak levels of BMP signaling on the dorsal surface are increase by 20-30% leading to a large amnioserosa. The fact that contraction still occurs in the absence of CV-2 suggest that there must still be other unidentified factors that are involved in controlling the dynamics of BMP signal output on the dorsal surface.

2.4 Conclusion

I have studied two proteins that are involved regulation of BMP signaling. We have identified a new allele of *nej* that has a stop codon in the 12th exon on the gene. Loss of *nej* leads to a high degree of variation in BMP signaling output in the embryo. I also studied the role of Cv-2 in the feedback regulation of BMP signaling. Cv-2 is found to be a BMP response gene that acts as a negative feedback regulator of early embryonic BMP signaling. This inhibition leads to a smaller peak number of pMad positive nuclei on the dorsal surface and possibly to a slight loss of robustness in the average width of pMad expression domain.

2.5 Experimental Methods

2.5.1 Nejire Mapping

The Mvent^1 mutant was a gift from Armen Manoukian, Univeristy of Toronto as a possible fly line with a dorsal surface patterning defect. A stable fly line is kept as Mvent^1 / FM7. As an initial attempt to map Mvent^1, I tried using a Duplication mapping technique employing fly lines with sections of the X chromosome duplicated on the 3rd (DC duplication series) or Y (DC duplication series) chromosome from Bloomington Stock Center [101, 102]. If Mvent^1 is covered on the duplicated element, the duplication should rescue lethality. However, for unknown reasons, I was not able to map Mvent^1 using the duplication mapping technique. As an alternative to duplication mapping I turned to a P-element mapping strategy using stocks in Tables 2.1 and 2.2 from the Bloomington Stock Center. Virgin Mvent^1 females in a w^- background were crossed to flies containing a w^+ marked P-element on the X chromosome. Non-FM7 F1 Females containing the Mvent^1 chromosome and the P-element chromosome were crossed to F1 progeny males. F2 progeny males were scored for eye color, with red eyes indicating no recombination and white eyes indicating that recombination occurred. The closer the mutation is to the P-element the lower the probability of recombination. Approximately 100-7000 males were scored per fly line. Using this methodology, I mapped

Mvent^1 to within three genes located at (8F2-8F9). Based on the strong maternal phenotype, I guessed that the Mvent^1 mutation might be in *nejire*, since this is a known maternally expressed gene [39].

2.5.2 Nejire Sequencing

Genomic *mvent*^{1} DNA was extracted for 200 L1-L2 *nejire* mutant larva. The larva were ground in 1mL of G buffer (13.7 ML 50% 1.46M sucrose, 10 mL 0.5M EDTA pH8, 10mL 1M Tris pH9, 2.5mL 20% SDS in 63.8mL H_2O). Another 1mL of G buffer was added and the solution was heated to 70°C for 20 minutes. The solution was centrifuged at 5K for 10 minutes. The supernatant was extracted and 1/2 volume H_2O was added. Two phenol extractions were performed followed by, a phenol-$CHCl_3$ extraction and then one $CHCl_3$ extraction. The DNA was precipitated by addition of an equal volume of isopropanol followed by centrifugation at 10K for 10 minutes. The pellet was dried and then resuspended in 35ul of 5M NaCl. This was followed by a phenol extraction (2 times), a phenol-$CHCl_3$ extraction and a $CHCl_3$ extraction. The aqueous phase was removed after the final extraction and 2 volumes of 95% ethanol were added and the mix centrifuged at 10K for 10 minutes. The pellet was washed with 70% ethanol, dried, and resuspended in 100ul H_2O.

The *nej* gene was amplified using PCR in 5 different fragments using the

primers listed in Table 2.7. A high Fidelity PCR System (Roche) was used for PCR amplification. The 5ul of PCR product were combined with 2 ul ExoSAP-IT (Affymetrix) and heated to 37°C for 15 minutes and 80°C for 15 minutes. 3.5ul of the ExoSap solution was combined with 1 ul sequencing primer (Table 2.8) and 7.5ul H_2O. The mixture was sent to Genewiz for sequencing. The sequencing data was analyzed using MacVector. The sequence was compared to the extended gene region and transcript sequence for *nej*, and nej-RA from Flybase.

Name	Sequence	Direction	Pair
nej set1 for t2	CCTCGCCAGCCACGCCTTTT	Forward	nej set1 rev t2 and nej set1 reverse t2b
nej set1 rev t2	GCCGGCTGAGCGCCTTGAAT	Reverse	nej set1 for t2 and nej set1 forward t2b
nej set1 forward t2b	GGCATGAACACCATTGCGCAGG	Forward	nej set1 rev t2
nej set2 forward	CAAGGACAGCAGGTTGC	Forward	nej set2 reverse
nej set2 reverse	GATGCTCTCCGGCTGTC	Reverse	nej set2 forward
nej set3 forward	GCGAGAATACGAACGGC	Forward	nej set3 reverse
nej set3 reverse	GCCATCGAACATCGAGC	Reverse	nej set3 forward
nej set4 forward	CCATCTCGCTTGCACGC	Forward	nej set4 reverse
nej set4 reverse	GGCTAACTGCCACACCG	Reverse	nej set4 forward
nej set5 for t2	AACTGCCGCCTGCCATCGTG	Forward	nej set5 rev t2 and nej set5 forward t2b
nej set5 rev t2	TCCCTGCCGGTTGGTCTTCGT	Reverse	nej set5 for t2 and nej set5 forward t2b
nej set5 reverse t2b	CCTGAGTAGAAACGCCTGGCGAC	Reverse	nej set5 for t2

Table 2.7: Sequencing Primers for *Mvent*[1] DNA Fragment Amplification- The *mvent*[1] (*nej*) gene was broken into 5 overlapping fragments for DNA Amplification. The primer name, sequence, direction, and primer pair with are listed in the table.

name	Sequence
nej set1 f1 seq	GGATCCAAGTGAGTACCG
nej set1 R1 seq	GAGATATCCGCTGGAGG
nej set1 f2 seq	CCCAGATGAACGGAGCC
nej set1 f3 seq	CTGACCAACAGCGTTGG
nej set1 f4 seq	CAACAACTTCTCGCCCAG
nej set1 f5 seq	CCTGAATCCGAACAGGG
nej set 1 f6 seq /nej set2 forward	CAAGGACAGCAGGTTGC
nej set2 f1 seq	GGACCAAATGTTCTGCCG
nej set2 R1 seq	GGAATGTTGCCACCCAG
nej set2 f2 seq	GGCGACAACGAGAAAGAC
nej set2 f3 seq	GGACCACCTGGAATACTG
nej set2 f4 seq	CAGGCGACTAGCAACAG
nej set2 f5 seq	GGTACACCACTCAGCTC
nej set 2 f6 seq / nej set 3 forward	GCGAGAATACGAACGGC
nej set3 f1 seq	GAGGATGGACTCGATGG
nej set3 R1 seq	GTCACCTGCATTGGGTG
nej set3 f2 seq	GGCACTATACGCACCAAC
nej set4 f1 seq	CGATACGGTCACACTGG
nej set4 R1 seq	GAACACGTAGACGCTTGG
nej set4 f2 seq	CTGCGTACTCTGGCTGG
nej set4 f3 seq	CAGCTGGGCTACACAATG
nej set4 f4 seq	GAAGGGCCAGAAGAAGG
nej set4 f5 seq	GCGCTACCACTGTACTG
nej set 4 f6 seq / nej set 5 forward	CAAGCAGCAGCAGTCAC
nej set5 f1 seq	CGTGGCAGTTCCATCGC
nej set5 R1 seq	CCATGCGATACCTGCTG
nej set5 f2 seq	CAAGCCCGCTATGCCAAC
nej set5 f3 seq	GCAGCAGCAACAGCAAC
nej set5 f4 seq	CAACACAGGTGCCCAAC
nej set5 f5 seq	GCTCAGGTGATGGGTCC
nej s6 fa2 seq	GCGGCGGTAAGGATAAC
nej s6 ra2 seq	GTTGGTGCGTATAGTGCC
nej s7 for seq	CAGCACATCCTTGCCATACT
nej s7 rev seq	GGTTGCTGTTGCTGCTG
nej s6 rev frag seq	CCTTAGCACGTCTCGAC
nej s4 r1b	GGTTTACTCAGGAGCAAG

nej s1 r1/s1f1	CCATCTGAGTGCCCACC
nej s2	GGATGTCGATGTGGTGG
leth r1b	CTGCAGCTGCTGCAACTG
leth r2b	GACGGTGGCTTGGACTC
nej set1 for t2	CCTCGCCAGCCACGCCTTT
nej set1 forward	GTCAAAGTGCTAGGCGAC
nej set1 forwardb	AATGGCAACAATGGCATGAAC
nej set1 forward t2b	GGCATGAACACCATTGCGCAGG
nej set3 forward	GCGAGAATACGAACGGC

Table 2.8: *Mvent1* Sequencing Primers- The $mvent^{1}$ gene was sequenced using 45 sequencing primers. The primer name and sequence are included in the table.

2.5.3 Maternal Nejire Clones

Maternal germline clones for the nej^{mvent1} allele were made by crossing Mvent1FRT01/FM7-GFP; nosGal4-UASFLP/Cyo-GFP with OvoD FRT101 Bloomington Stock Center line 1813. The F1 progeny were crossed to *yw* males and the F2 progeny were collected on apple juice plates as described in section 2.5.5. The embryos were processed for pMad antibody staining as described in section 2.5.5.

2.5.4 Cv-2 *In Situ* Hybridizations

Cv-2 *in situ* hybridizations were performed to study Cv-2 mRNA expression patterns in yw: Dpp$^{hinr46-/-}$; Cv-2$^{1-/-}$, and embryos. Stable homozygous stocks of the Cv-2^{KO1} fly line [57] for performing the Cv-2 experiments could not be

made. Instead I used the Cv-$2^{1-/-}$ fly line which by most reports is a strong loss of function and was obtained as a gift from Seth Blair [115]. Dpp^{Hinr46} is an embryonic null allele and was maintained over $CyoDpp^{23}$. The Dpp null embryos were identified by their deep cephalic furrow morphology.

Cv-2 mRNA probes were made from cv-2 cDNA in pGem7+, a gift from Seth Blair. XbaI and HindIII restriction enzymes were used to linearize the cDNA. Digoxigenin-UTP (digU) labeling of the RNA probes was done using the Riboprobe kit from Promega using the T7 and SP6 polymerases. Embryos were collected as described in Section 2.5.5 and stored in 100% ethanol. Embryos were brought into 0.1% PBTween (PBTw) by 5 minute washes in 50/50 ethanol/PBTw, 30/70 ethanol/PBTw, then 100% PBTw. The embryos were fixed for 25 minutes in PBTw+5% formaldehyde, and then washed 5 times in PBTw. Embryos were incubated in PBTw+4ug/ml proteinase K (Roche) for 5 minutes. Then, the embryos were washed quickly twice with PBTw, and then four time for 2 minutes each in PBTw. The embryos were washed for 10 minutes in 50/50 PBTw / embryo hybridization solution (50% formamide, 5X SSC, 50 ug/ml heparin, 0.1% Tween-20, and 100 ug/mL salmon sperm DNA in H_2O). Then the embryos were washed in 100% embryo hybridization solution for 2 minutes at room temperature, followed by incubation in hybridization solution for 2 hours at 55°C. The *cv-2* probe was prepared by adding 5ul of digU cv-2 probe to 25ul of hybridization solution

and heated to 80°C for 5 minutes, followed by quenching on ice. The probe was added to the embryos and hybridized at 55°C for 30 hours. 5 washes were done over 3 days at 55°C in embryo hybridization solution. Embryos were brought into PBTw with four 20 minutes washes in 800/200, 600/400, 400/600, and 200/800 hybridization solution/ PBTw. Embryos were then washed 5 more times over 24 hours in PBTw. Embryos were incubated in pre-absorbed anti-Digoxigenin-AP Fab fragments (Roche) at 1:2000 overnight at 4°C. Then embryos were washed four times in PBTw over 24 hours. Embryos were washed 2 more times for 5 minutes in Alkaline phosphatase (AP) staining buffer (100mN NaCl, 50 mM $MgCl_2$, 100 mM Tris pH9.5, 0.1% Tween 20 in H_2O). 3.38ul of 100mg/mL of NBT (Roche) and 3.5ul of 50mg/mL of BCIP were added to 1 mL of AP staining buffer, and the solution was added to the embryos for 48 hours. Then the embryos were washed 3 times in PBTw and stored in 80% glycerol and 20% PBTw. Embryos were mounted on slides with the dorsal surface facing up and imaged using a Nikon Optiphot light microscope at 20X with a Namarksi lens and ProgRes Mac Capture Pro2.6 software.

2.5.5 Embryo Collections, Antibody Staining, and Imaging

Cv-$2^{1-/-}$ and *yw* or His-GFP embryos were collected at 18, 21, and 25°C on apple juice plates for histochemistry analysis. Flies were allowed to acclimate to the temperature for at least 48 hours before embryos were collected. The embryos were devitellinized with bleach for 2 minutes, fixed in 500μL heptane, 500 μL PBT, and 70 μL electron microscopy grade paraformaldehyde for 20 minutes, and then dechorionated with 3 washes of methanol. The embryos were exposed to as little methanol as possible since it decreases the quality of the pMad staining. The embryos were stored in either ethanol at -20°0C or PBT at 4°C. The quality of the staining did not change for storage in either ethanol or PBT. If the embryos were stored in ethanol, they were brought back to PBT by 10 minutes washes of 75%, 50%, and 25% ethanol in PBT. Then, the embryos were washed for 10 minutes 4 times in PBT, and were incubated overnight at 4°C in primary antibody. Antibodies used were Epitomics Phospho Smad3 (pS423/425) Rabbit Monoclonal antibody (1:500-1:1000) to visualize the amount of pMad, DAPI (1:300) to stain nuclei, Clontech Mouse monoclonal JL-8 antibody (1:1000) for GFP, and Covance RNA Polymerase II H5 Mouse Monoclonal antibody (1:1000) for polymerase antibody staining. Then, the embryos were washed 4 times in PBT for 10 minutes,

incubated in Alexa Flourophore 488 or 555 secondary antibodies for 4 hours at room temperature, and washed 4 times in PBT for 10 minutes. During the second to last wash, DAPI at 1:300 was added. The embryos were stored in 80% glycerol and 20% PBT overnight. Embryos are mounted onto slides with the dorsal surface facing up and imaged using a LSM 720 confocal microscope. Microscope settings for imaging are kept constant from day to day. Embryos are selected for imaging by looking at the nuclei for signs of the cephalic furrow starting to form to ensure that all embryos are at the same developmental stage, unless otherwise noted. A z-stack is selected that is 36 μm wide at 2 μm intervals. Images were saved in a 12bit format for image processing.

2.5.6 Controlling for Staining Variations

In order to quantitate the amount and location of BMP signaling on the dorsal surface of the *Drosophila* embryo, we used antibody staining to p-Mad, the downstream transcriptional transducer of the Dpp and Scw signals. However, I noted that the p-Mad antibody is very sensitive to the fixation process making it difficult to obtain reproducible, consistent staining. In order to develop a methodology to control for the quality of staining, we tried four different strategies: 1) use an internal control in each embryo by looking at the ratio of p-Mad to another protein (RNA polymerase subunit RPB1) that is expressed at a constant level in

all cells (Ratio Method, RM), 2) develop a method to control for variations in the antibody staining process (Staining Control, SC), 3) perform all staining and fixation in parallel (Parallel Method, PM), and 4) Develop a method to control for both the fixation and staining by mixing in wt GFP marked embryos (Mixing Method, MM).

The RM method takes the ratio of the average intensity of pMad to RNA polymerase in a maximum intensity projection of the embryo. This method assumes that the staining variability will affect all proteins consistently.

The SC method controls for staining variations, but not variations due to fixation. In the SC method, the control embryos are pre-stained with DAPI or Propidium iodide (PI) and then mixed with the experimental embryos for pMad staining. After the embryos are stained they are sorted based on being PI or DAPI positive vs negative.

The PM method attempts to control for variations in staining due to procedural error. In this method the experimental and control embryos are fixed in parallel. The embryos were placed in a device that enabled the control and experimental embryos to be fixed in parallel tubes immersed in the same fixative solutions. This method was designed to mitigate the differences in the fixation step.

The MM method controls for staining variations that arise from both the

fixation and staining. In this method, embryos expressing a Histone-GFP fusion protein (Gift of Stas Shvartsman) were mixed with experimental embryos and then fixed and stained within the same tube. After the embryos were imaged, the control GFP marked embryos were identified by GFP fluorescence. Only embryos from the same tube are compared for each experimental condition.

2.5.7 pMad Image Analysis

Two methods were used to compare the amount of p-Mad staining. The first method (Average Method, AM) used an approximation of the total amount of pMad, which is found by drawing a mask around a maximum intensity projection of the embryo and finding the average intensity using the LSM 720 imaging software. This method gives a fast approximation of the total pMad content and the maximum intensity of the pMad. However this method does not give any positional information. This method was used for developing the protocol for studying the changes in pMad staining.

To compare the width of all the pMad positive nuclei, first a population data set was obtained for each experimental condition. A Matlab program (described in [111]) was used to extract the width of p-Mad positive stripe from confocal images. Briefly, the program realigns the embryos so their A/P axis is horizontally aligned. The embryos are rescaled to an interval of $[0, 1]$. Next, the embryos are rotated

around the AP axis so the dorsal stripe is vertically aligned. A mask is applied to cover the width of the nuclei where there is pMad staining. A population level data set is created from the masks for the average and standard deviation of pMad signaling across the embryo's length. A student's t-test with $p<0.05$ is tested across the AP axis for areas of significant difference between the 2 populations being tested. A $p<0.00005$ was also tested and similar results were found. The fluorescence intensity from a 12 bit image across the DV axis at relative A/P positions of 0.25%, 0.5%, and 0.75% embryo length were also compared.

The code from [111] was modified to look at the coefficient of variation (CV) in the width of pMad positive nuclei across the AP axis between different population sets. The CV for the width of the pMad across the AP axis was found by taking the standard deviation/mean for the width of pMad positive nuclei. A student's t-test with $p<0.05$ was applied.

2.5.8 Analysis of Downstream Effects for Loss of Cv-2

The nuclei with high levels of p-Mad signaling posterior to the cephalic furrow form amnioserosa cells [38]. To determine if the changes in the width of the p-Mad stripe affects the number of amnioserosa cells formed, 12-24 hour embryo collections on apple juice plates at 25°C of Cv-$2^{1-/-}$ and His-GFP control embryos were processed and imaged as described in Section 2.5.5 using a anti-Hindsight

(HNT) antibody (1:20), a specific marker for amnioserosa cells [116, 117]. The mouse monocolonal ant-HNT 27B7 IG9 supernatant was obtained from the Developmental Studies Hybridoma Bank funded by NICHD and maintained by The University of Iowa, Department of Biology, Iowa City, Iowa 52242. The number of nuclei positive for Hindsight were counted from 24 imaged embryos from both wt and *cv-2* mutants. A student's t-test with $p<0.05$ was used to test significance between the two populations.

Chapter 3

Single Cell Stochastic Model of BMP Signaling

3.1 Introduction

During embryonic development, an embryo must correctly position, specify, and grow tissues that will form the adult body. To do this an embryo must make numerous cell fate decisions in a setting where there can be fluctuations or noise in its environmental surroundings, protein levels, or genome expression. Cells can either exploit the fluctuations or have processes that filter or dampen these fluctuations. For *Drosophila melanogaster* how the embryo copes with noise is especially important since it develops externally from its mother. During *Drosophila*

early embryonic development, tissues are patterned in a concentration dependent manner through morphogen gradients. In some cases, the gradient involves a signaling molecule located external to the plasma membrane. In this case, nuclei must interpret the external concentration of morphogen via a signal transduction cascade to specify the correct genome expression. One example involves dorsal surface patterning, by Bone Morphogenic Protein (BMP) type factors that are members of the larger Transforming Growth Factor-beta superfamily. BMPs form a morphogen gradient on the dorsal surface to help specify at least two cell fates, amnioserosa and dorsal ectoderm. Experimental evidence from cell culture suggests the active signaling levels for free BMP ligand may be in the picomolar range. If this is true in vivo then it suggests stochasticity may play a role in interpretation of BMP gradients. However, the intracellular output of BMP signaling, pMad, forms sharp and reproducible boundaries suggesting that there is little noise in the system. In this chapter, I examine how noise propagates through the BMP signaling pathway and what steps in the pathway may either enhance or filter out noise.

The *Drosophila* BMP ligands, Decapentapolegic (Dpp), and Screw (Scw) form a heterodimeric morphogen that specifies the dorsal surface of the Drosophila embryo. High levels of Dpp/Scw specify amnioserosa, and low to moderate levels of Dpp/Scw or Dpp homodimers specify dorsal ectoderm in the dorsalmost 40

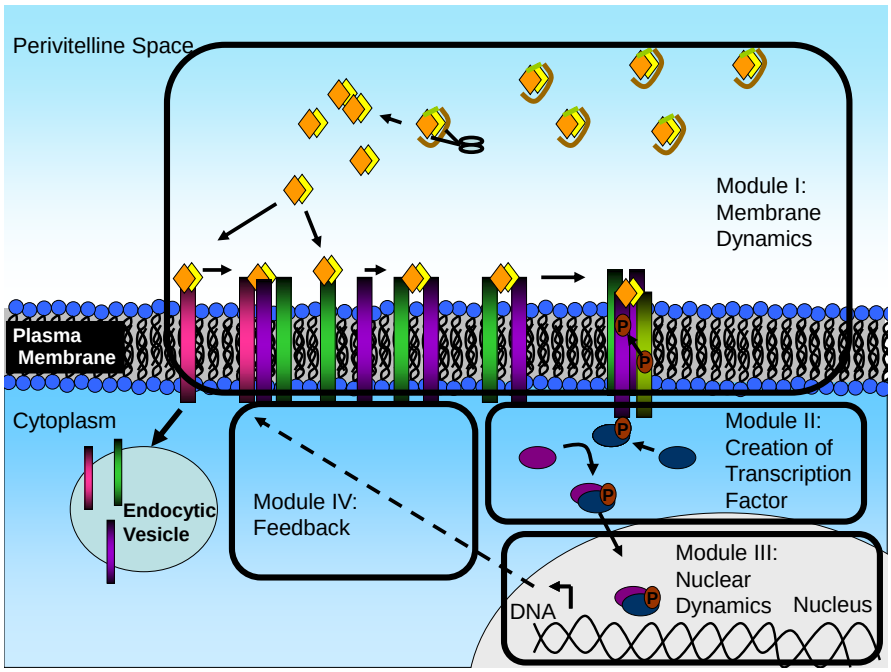

Figure 3.1: Model of BMP signaling in the early *Drosophila* embryo- Module I: BMP ligand is transported and released by extracellular modulators in the PV space. The BMP ligand binds to its receptor to activate it. The active receptor phosphorylates Mad in the cytoplasm. These reactions can occur on the plasma membrane or in an endocytic vesicle. Module II: Two pMad molecules combine with Medea to form an active transcription factor and are transported to the nucleus. Module III: The active transcription factor binds to DNA to activate transcription. Module IV: Proteins can be produced that can feedback to modulate the BMP signaling pathway.

BMP signaling during early *Drosophila* development can be broken into four general modules: membrane dynamics to create an active signaling complex, creation of the active transcription factor, nuclear dynamics to create mRNA, and feedback for upregulating and / or downregulating BMP signaling (Figure 3.1). On the membrane, BMP signals through a heterodimer of two type I receptors

and a dimer of a type II receptor [22, 23, 24, 118]. Endocytosis of the bound receptors is an important step in creating a strong sustained response to BMP signaling [119]. The active receptor signaling complex phosphorylates the intracellular transcription factor Mad to p-Mad [28]. Two p-Mad molecules combine with the co-factor Medea and accumulate in the nucleus to regulate transcription [29]. In the absence of the BMP signal, the Mad, pMad, and Medea proteins can all shuttle between the nucleus and cytoplasm fairly rapidly. In contrast the pMad/Medea complex is also be transported into the nucleus, but only monomeric unphosphorylated Mad or Medea can be exported [120]. This differential translocation leads to the accumulation of the pMad/Medea complex in the nucleus, where it binds DNA, regulates transcription and controls feedback reactions.

The first mathematical models for DV patterning could not explain the simultaneous contraction and intensification of BMP signaling on the dorsal surface. Wang and Ferguson proposed that a positive feedback loop which increases the amount of BMP signaling in a local area could account for both the contraction and intensification of signaling [22], and mathematical models have confirmed that such a mechanisms could work [52]. However, the mechanistic details remain obscure, in part because the protein creating the positive feedback has not been identified. One hypothesis envisions the use of a BMP Surface Binding Protein (SBP), as an exchange factor. In this model the SBP has a relatively high affinity

for both the ligand and receptors such that it can capture and transfer the ligand to its signaling receptor. In imaginal wing disc development Crossveinless-2 (Cv-2) has been shown to be such a molecule. It is up-regulated by BMP signaling, binds ligand and the type I receptor, and stimulates crossvein formation. During this process, Cv-2 both focuses the BMP signaling output and enhances its signal. Since Cv-2 is expressed in the early embryo, it was a good candidate to also be a component of the feedback mechanism that sharpens the BMP gradient at this stage. However in chapter 2, I showed that Cv-2 is actually a negative regulator of BMP signaling during dorsal surface pattering. Thus, Cv-2 has different functions in regulating BMP signaling at different developmental stages, but the nature of the mechanism responsible for how the contraction and intensification of BMP signaling takes place in the embryo remains an open question.

Most models for how BMP signaling affects DV patterning have been analyzed using deterministic mathematical methods. Some models have studied the BMP transport process in the PV space, which has suggested that one or more molecules is missing to explain how the BMP gradient is formed [70, 47]. Based on these models, positive feedback has been proposed as a mechanism to produce contraction and intensification of the BMP signal around the dorsal midline [52]. The intracellular dynamics have also been studied to analyze how nuclear / cytoplasmic shuttling system can lead to nuclear accumulation of pMad [121].

Another set of intracellular models have addressed how endocytosis leads to a strong sustained response from BMP signaling [122, 123, 120]. However if the concentration of BMP molecules is low, stochastic effects may impact signaling and, presumably, mechanisms must exist to compensate for noise in the system. While the amount of Dpp in the PV space has not been quantified, we can make rough estimates of the average amount of Dpp per nucleus. In cell culture, the dynamic range for Dpp signaling is $10^{-10} - 10^{-9}$M [50]. The amount of PV fluid is approximately 500pL. In the early embryo there are approximately 3000 dorsal nuclei. Thus, the average number of molecules per nucleus is 8 molecules/nucleus (Equation 3.1).

$$10^{-10}\frac{moles}{L} \cdot 500 * 10^{-12}L \cdot 6.02 * 10^{23}\frac{molecules}{mole}/3000nuclei = 8molecules \quad (3.1)$$

However, the actual number of Dpp molecules may be higher at the dorsal midline and lower in areas away from the midline. Fluctuations in actual numbers in areas with a lower concentration of molecules may be very important in determining where the boundary between high and low signaling is located. Thus we choose to study how these fluctuations may influence the overall BMP signaling network using a stochastic model.

One study of BMP signaling used stochastic models to examine the dynamics

of BMP reactions at the membrane [71]. This model assumed that during dorsal surface patterning, Cv-2 is a primarily a positive regulator of BMP signaling. However experimental evidence from Chapter 2 suggests that Cv-2 is actually a negative regulator at this stage. This difference in regulation may affect how noise propagates through the signaling network. In addition, the stochastic model proposed that Cv-2 may have a role in filtering out noise. However experimental evidence suggests that noise at the level of pMad is either not affected or may be noisier with Cv-2. This model also assumed that the intracellular dynamics are not stochastic. There are a large number of Mad and Medea molecules in the cytoplasm [121], which may help attenuate noise in the cytoplasm. However, this depends upon the phosphorylation rate of Mad. The intracellular dynamics have not been studied in detail with stochastic models. While there may be noise attenuation in the cytoplasm, the transcriptional gene activation is a stochastic process where there are very few DNA binding sites for the transcription factors. This can lead to transcriptional bursting of mRNA molecules, which may also lead to protein bursting. This may have a large influence on the temporal evolution of the signaling network output and possible noise attenuation. Thus a more detailed stochastic model studying the intracellular dynamics of BMP signaling is warranted.

We developed a 3-D single cell stochastic model to characterize the downstream

biological network. By conducting a detailed scale analysis of reaction frequencies and stochastic simulations of the biological system, we seek to understand how reactions of different time scales affect the propagation of fluctuations in the network. We hypothesize that endocytosis, large numbers of Mad molecules, trimer formation of the Mad/coMad complex, nuclear transport, and feedback of a co-receptor all decrease the amount of noise in the signaling network. This noise may arise from the low levels of free signaling molecules in the PV space, slow phosphorylation of Mad in the cytoplasm, or translation of mRNA molecules from DNA in the nucleus. We also propose that the mechanisms of endocytosis, trimer formation, and nuclear transport may be ways to integrate the low levels of BMP signaling over time to create a sustained signal. Our model employs a prototypical BMP signaling network system, and our conclusions may carry over to other signaling networks.

3.2 Models

3.2.1 3D Stochastic Model

The single cell model consists of three different domains: the PV space, the cytoplasm, and the nucleus. BMP (B) diffusion, production and degradation occur in the PV space. Near the embryo membrane, the reactions are the insertion

of receptors (R) at a constant rate, the secretion of Cv-2 (C) after cytoplasmic translation, endocytosis and exocytosis of receptors, Cv-2, bound receptor (BR), BMP bound to Cv-2 (BC) and BMP bound to Cv-2 and its receptor (BCR), and the phosphorylation of the cytoplasmic Mad by BR. We use the endocytosis and exocytosis mechanism described by[124], in which internalized BR can phosphorylate Mad, and BMP will disassociate from its receptor and Cv-2 when BR, BCR and BC are recycled. Without any quantitative information about intracellular degradation, we assume the intracellular degradation of BR, BCR, BC, Cv-2 and R occurs at the same rate as it does in the PV space. The binding reactions between BMP, R and Cv-2 as in [52] are assumed to occur throughout the PV space.

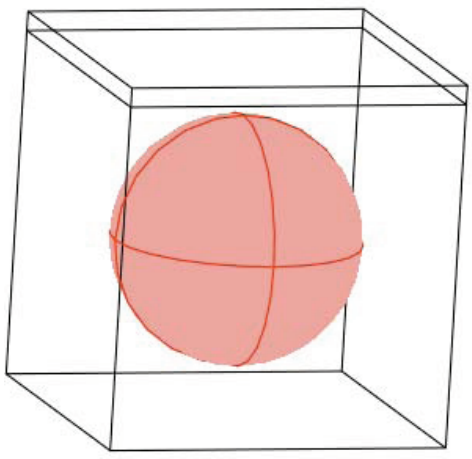

Figure 3.2: Single Cell System Geometry- The PV space is a rectangle over the cytoplasm. The cytoplasm is a box with a sphere (red) for the nucleus in its center.

In the cytoplasm, we use the structure of the Smad2 pathway as determine by studies in human cell lines. Through transgenic experiments, human Smad2 was found to function in the same way as Mad in Drosophila, and Smad4 works in the same way as Medea [125]. Without signaling, the Smad2 protein shuttles between the nucleus and cytoplasm. During signaling, the occupied receptor phosphorylates Smad2, which facilitates formation of a Smad/Smad4 and Smad2/Smad2 complexes. The exact structures of the Smad oligomers have not been fully determined. Both types of complexes can be transported into the nucleus, while dephosphorylated Smad is the only molecule that is exported in the monomeric form [121, 126]. The differential transport kinetics leads to the accumulation of pSmad2/pSmad2/Smad4 and pSmad2/Smad2/pSmad2 complexes in the nucleus, where they can bind to DNA, regulate transcription and control feedback reactions. Therefore, the reactions in the cytoplasm are the phosphorylation of Mad, the association and dissociation reactions between pMad and Medea, the synthesis of Cv-2 from mRNA translation, the degradation of mRNA, and the intracellular degradation of BR, BCR, BC and Cv-2. For simplicity, we denote pMad/Medea as pMMe and pMad/pMad as pMad2. Near the nuclear membrane, the reactions are the nuclear export and import of Mad, pMad, and Medea, the unidirectional import of pMad2 and pMMe, and the nuclear export of mRNA.

It has been suggested that the transcription factors are actually not dimers

(Smad2/Smad2 or Smad2/Smad4) but are hetero-trimers consisting of two pSmad2's and one Smad4 [127]. Moreover, our estimation in the following section shows the amount of Mad and Medea are likely much larger than is necessary for pMad and pMad/Madea to activate the downstream gene expressions. So we use the trimer as the transcription factor.

The reactions in the nucleus are the dephosphorylation of pMad, the association and dissociation reactions between pMad and Medea, the binding and unbinding reactions between the transcription factors and the promoter site, and the production of mRNA. During transcription, we divide the production of mRNA into two steps: 1) RNA polymerase (RNAp) binds to the DNA sequence to form an elongation complex, RNAt; 2) RNAt proceeds to become mRNA. Depending on the status of the promoter site, the formation rate of RNAt switches between a basal rate and an enhanced rate, while RNAt always proceeds at the same rate.

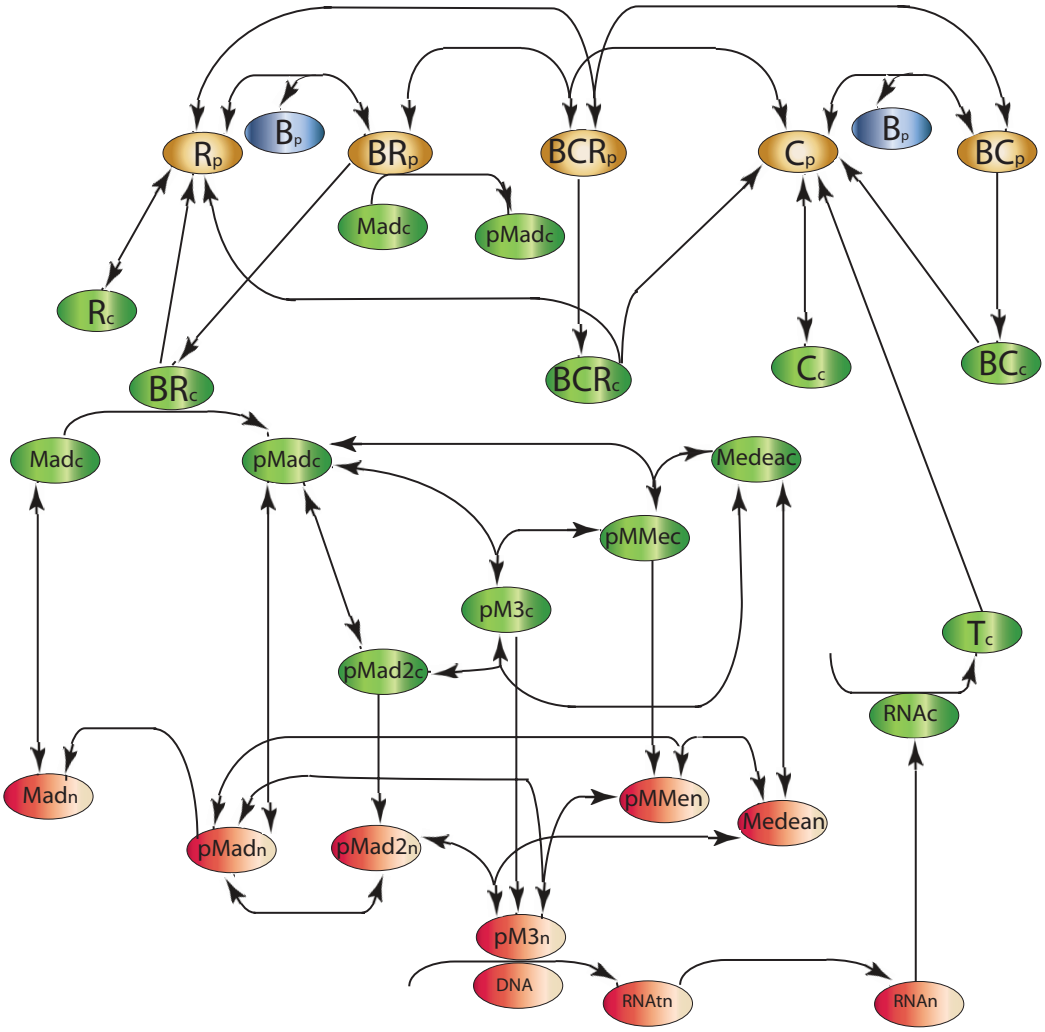

Figure 3.3: Reaction network-Blue and Yellow are reactions in the PV space. Green is reactions in the cytoplasm. Red is reactions in the nucleus

The reaction network is shown in Figure 3.3. In addition, we make the following assumptions:

1. Only the species that can be produced undergo degradation. Therefore, BMP, R, Cv-2, BR, BC, BCR and mRNA undergo degradation, and the total amount of Mad and Medea in all forms is constant.

2. Proteins synthesized from mRNA translation can be transported actively and rapidly to their end-destination. So we approximate the transport of proteins synthesized from mRNA translation either as fast cytoplasmic diffusion with a large flux into the PV space or as direct random insertion into the PV space.

3. All species except DNA and proteins synthesized from mRNA translation diffuse. DNA is kept at the center of the nuclear sphere.

Initially, the concentration of each species is set to zero except the following ones:

1. The concentrations of the receptors in the PV space and the cytoplasm are 160nM in order to be consistent with the endocytosis and exocytosis rates [52, 124];

2. The concentrations of the cytoplasmic Mad and Medea are the concentrations from [121], i.e., the concentrations of the cytoplasmic Mad and Medea are 15.1nM and 12.7nM respectively;

3. The concentrations of the nuclear Mad and Medea are the concentrations from [121], i.e., the concentrations of the nuclear Mad and Medea are 7.125nM and 12.7nM respectively.

The deterministic equations of the system can be written as below. The general form for each reaction is

$$\frac{\partial X}{\partial t} = D_X \Delta[X_i] + R(X) \tag{3.2}$$

where $\frac{\partial X}{\partial t}$ is the rate of change of X with respect to both position and time, $D_X \Delta[X_i]$ is diffusion of X in the ith compartment, and $R(X)$ are the reactions involving X. Without specification, the boundary conditions are Neumann boundary condition. The following equations describe the evolution of the molecules in the PV space:

$$\begin{aligned}
\frac{\partial [B_p]}{\partial t} &= D_{Bp}\Delta[B_p] + s_B - k_4[B_p][C_p] + k_{-4}[BC_p] - k_5[B_p][R_p] \\
&\quad + k_{-5}[BR_p] - d_{Bp}[B_p] \qquad (3.3a) \\
\frac{\partial [C_p]}{\partial t} &= D_{Cp}\Delta[C_p] - k_4[B_p][C_p] + k_{-4}[BC_p] - k_7[BR_p][C_p] \\
&\quad + k_{-7}[BCR_p] - d_{Cp}[C_p] \qquad (3.3b) \\
\frac{\partial [R_p]}{\partial t} &= D_{Rp}\Delta[R_p] + s_R(x,y,z) - k_5[B_p][R_p] + k_{-5}[BR_p] - k_6[BC_p][R_p]
\end{aligned}$$

$$+ k_{-6}[BCR_p] - d_{Rp}[R_p] \tag{3.3c}$$

$$\frac{\partial[BC_p]}{\partial t} = D_{BCp}\Delta[BC_p] + k_4[B_p][C_p] - k_{-4}[BC_p] - k_6[BC_p][R_p]$$

$$+ k_{-6}[BCR_p] - d_{BCp}[BC_p] \tag{3.3d}$$

$$\frac{\partial[BR_p]}{\partial t} = D_{BRp}\Delta[BR_p] + k_5[B_p][R_p] - k_{-5}[BR_p] - k_7[BR_p][C_p]$$

$$+ k_{-7}[BCR_p] - d_{BRp}[BR_p] \tag{3.3e}$$

$$\frac{\partial[BCR_p]}{\partial t} = D_{BCRp}\Delta[BCR_p] + k_6[BC_p][R_p] - k_{-6}[BCR_p] + k_7[BR_p][C_p]$$

$$- k_{-7}[BCR_p] - d_{BCRp}[BCR_p] \tag{3.3f}$$

Near the cytoplasmic membrane the following fluxes occur:

$$-D_{Cc}\frac{\partial[C_c]}{\partial z} = -k_{ex}[C_c] + k_{en}[Cp], \tag{3.4a}$$

$$-D_{Cp}\frac{\partial[C_p]}{\partial z} = -k_{en}[C_p] + k_{ex}[BC_c] + k_{ex}[BCR_c] + k_{ex}[C_c] + k_{se}[T_c], \tag{3.4b}$$

$$-D_{Tc}\frac{\partial[T_c]}{\partial z} = -k_{se}[T_c], \tag{3.4c}$$

$$-D_{Rc}\frac{\partial[R_c]}{\partial z} = -k_{ex}[R_c] + k_{en}[Rp], \tag{3.4d}$$

$$-D_{Rp}\frac{\partial[R_p]}{\partial z} = -k_{en}[R_p] + k_{ex}[BR_c] + k_{ex}[BCR_c] + k_{ex}[R_c], \tag{3.4e}$$

$$-D_{BCc}\frac{\partial[BC_c]}{\partial z} = -k_{ex}[BC_c] + k_{en}[BCp], \tag{3.4f}$$

$$-D_{BCp}\frac{\partial[BC_p]}{\partial z} = -k_{en}[BC_p], \tag{3.4g}$$

$$-D_{BRc}\frac{\partial[BR_c]}{\partial z} = -k_{ex}[BR_c] + k_{en}[BRp], \tag{3.4h}$$

$$-D_{BRp}\frac{\partial[BR_p]}{\partial z} = -k_{en}[BR_p], \tag{3.4i}$$

$$-D_{BCRc}\frac{\partial[BCR_c]}{\partial z} = -k_{ex}[BCR_c] + k_{en}[BCRp], \tag{3.4j}$$

$$-D_{BCRp}\frac{\partial[BCR_p]}{\partial z} = -k_{en}[BCR_p]. \tag{3.4k}$$

The following reactions describe how the molecules evolve in the cytoplasm:

$$\frac{\partial[Mad_c]}{\partial t} = D_{Madc}\Delta[Mad_c] - k_{phos}\left([BR_c] + \delta(z-z_0)[BR_p]\right)[Mad_c] \tag{3.5a}$$

$$\begin{aligned}\frac{\partial[pMad_c]}{\partial t} &= D_{pMadc}\Delta[pMad_c] + k_{phos}\left([BR_c] + \delta(z-z_0)[BR_p]\right)[Mad_c] \\ &\quad - k_8[pMad_c]^2 + k_{-8}[pMad2_c] \\ &\quad - k_8[pMad_c][Medea_c] + k_{-8}[pMMe_c] \\ &\quad - k_8[pMad_c][pMMe_c] + k_{-8}[pM3_c]\end{aligned} \tag{3.5b}$$

$$\begin{aligned}\frac{\partial[Medea_c]}{\partial t} &= D_{Medeac}\Delta[Medea_c] \\ &\quad - k_8[pMad_c][Medea_c] + k_{-8}[pMMe_c] \\ &\quad - k_8[pMad2_c][Medea_c] + k_{-8}[pM3_c]\end{aligned} \tag{3.5c}$$

$$\begin{aligned}\frac{\partial[pMad2_c]}{\partial t} &= D_{pMad2c}\Delta[pMad2_c] + k_8[pMad_c]^2 - k_{-8}[pMad2_c] \\ &\quad - k_8[pMad2_c][Medea_c] + k_{-8}[pM3_c]\end{aligned} \tag{3.5d}$$

$$\begin{aligned}\frac{\partial[pMMe_c]}{\partial t} &= D_{pMMec}\Delta[pMMe_c] \\ &\quad + k_8[pMad_c][Medea_c] - k_{-8}[pMMe_c]\end{aligned}$$

$$- k_8[pMMec][pMad_c] + k_{-8}[pM3_c] \tag{3.5e}$$

$$\frac{\partial[pM3_c]}{\partial t} = D_{pM3c}\Delta[pM3_c] \tag{3.5f}$$

$$+ k_8[pMad2_c][Medea_c] - k_{-8}[pM3_c]$$

$$+ k_8[pMMe_c][pMad_c] - k_{-8}[pM3_c] \tag{3.5g}$$

$$\frac{\partial[T_c]}{\partial t} = D_{Tc}\Delta[T_c] + k_{Tpro}[RNA_c] \tag{3.5h}$$

$$\frac{\partial[RNA_c]}{\partial t} = D_{RNAc}\Delta[RNA_c] - d_{RNAc}[RNA_c] \tag{3.5i}$$

$$\frac{\partial[C_c]}{\partial t} = D_{Cc}\Delta[C_c] - d_{Cc}[C_c] \tag{3.5j}$$

$$\frac{\partial[R_c]}{\partial t} = D_{Rc}\Delta[R_c] - d_{Rc}[R_c] \tag{3.5k}$$

$$\frac{\partial[BC_c]}{\partial t} = D_{BCc}\Delta[BC_c] - d_{BCc}[BC_c] \tag{3.5l}$$

$$\frac{\partial[BR_c]}{\partial t} = D_{BRc}\Delta[BR_c] - d_{BRc}[BR_c] \tag{3.5m}$$

$$\frac{\partial[BCR_c]}{\partial t} = D_{BCRc}\Delta[BCR_c] - d_{BCRc}[BCR_c] \tag{3.5n}$$

The following equations describe the fluxes across the nuclear membrane:

$$-D_{Madc}\frac{\partial[Mad_c]}{\partial n} = -k_{in}[Mad_c] + k_{out}[Mad_n], \tag{3.6a}$$

$$-D_{Madn}\frac{\partial[Mad_n]}{\partial n} = k_{in}[Mad_c] - k_{out}[Mad_n] \tag{3.6b}$$

$$-D_{pMadc}\frac{\partial[pMad_c]}{\partial n} = -k_{in}[pMad_c] + k_{out}[pMad_n], \tag{3.6c}$$

$$-D_{pMadn}\frac{\partial[pMad_n]}{\partial n} = k_{in}[pMad_c] - k_{out}[pMad_n], \tag{3.6d}$$

$$-D_{pMadc}\frac{\partial[Medea_c]}{\partial n} = -k_{in}[Medea_c] + k_{mout}[Medea_n], \tag{3.6e}$$

$$-D_{Medean}\frac{\partial[Medea_n]}{\partial n} = k_{in}[Medea_c] - k_{mout}[Medea_n], \tag{3.6f}$$

$$-D_{pMad2c}\frac{\partial[pMad2_c]}{\partial n} = -k_{din}[pMad2_c], \tag{3.6g}$$

$$-D_{pMad2n}\frac{\partial[pMad2_n]}{\partial n} = k_{din}[pMad2_c], \tag{3.6h}$$

$$-D_{pMMec}\frac{\partial[pMMe_c]}{\partial n} = -k_{din}[pMMe_c], \tag{3.6i}$$

$$-D_{pMMen}\frac{\partial[pMMe_n]}{\partial n} = k_{din}[pMMe_c], \tag{3.6j}$$

$$-D_{pM3c}\frac{\partial[pM3_c]}{\partial n} = -k_{din}[pM3_c], \tag{3.6k}$$

$$-D_{pM3n}\frac{\partial[pM3_n]}{\partial n} = k_{din}[pM3_c], \tag{3.6l}$$

$$-D_{RNA_c}\frac{\partial[RNA_c]}{\partial n} = k_{rout}[RNA_n], \tag{3.6m}$$

$$-D_{RNA_n}\frac{\partial[RNA_n]}{\partial n} = -k_{rout}[RNA_n]. \tag{3.6n}$$

The following equations describe the evolution of the molecules in the nucleus:

$$\frac{\partial[Mad_n]}{\partial t} = D_{Madn}\Delta[Mad_n] + k_{dephos}[pMad_n] \tag{3.7a}$$

$$\begin{aligned}\frac{\partial[pMad_n]}{\partial t} &= D_{pMadn}\Delta[pMad_n] - k_{dephos}[pMad_n] \\ &\quad - k_8[pMad_n]^2 + k_{-8}[pMad2_n] \\ &\quad - k_8[pMad_n][Medea_c] + k_{-8}[pMMe_n]\end{aligned} \tag{3.7b}$$

$$- k_8[pMad_n][pMMe_n] + k_{-8}[pM3_n] \tag{3.7c}$$

$$\frac{\partial[Medea_n]}{\partial t} = D_{Medean}\Delta[Medea_n]$$

$$- k_8[pMad_n][Medea_n] + k_{-8}[pMMe_n]$$

$$- k_8[pMad2_n][Medea_n] + k_{-8}[pM3_n] \tag{3.7d}$$

$$\frac{\partial[pMad2_n]}{\partial t} = D_{pMad2n}\Delta[pMad2_n] + k_8[pMad_n]^2 - k_{-8}[pMad2_n]$$

$$- k_8[pMad2_n][Medea_n] + k_{-8}[pM3_n] \tag{3.7e}$$

$$\frac{\partial[pMMe_n]}{\partial t} = D_{pMMen}\Delta[pMMe_n]$$

$$+ k_8[pMad_n[Medea] - k_{-8}[pMMe_n]$$

$$- k_8[pMMe_n][pMad_n] + k_{-8}[pM3_n] \tag{3.7f}$$

$$\frac{\partial[pM3_n]}{\partial t} = D_{pM3n}\Delta[pM3_n] \tag{3.7g}$$

$$+ k_8[pMad2_n][Medea_n] - k_{-8}[pM3_n]$$

$$+ k_8[pMMe_n][pMad_c] - k_{-8}[pM3_n] \tag{3.7h}$$

$$\frac{\partial[DNA_n]}{\partial t} = -k_9[DNA_n][pM3_n] + k_{-9}[NDNA_n] \tag{3.7i}$$

$$\frac{\partial[NDNA_n]}{\partial t} = k_9[DNA_n][pM3_n] - k_{-9}[NDNA_n] \tag{3.7j}$$

$$\frac{\partial[RNAt_n]}{\partial t} = k_{bT}[DNA_n] + k_{eT}[NDNA_n] - k_T[RNAt_n] \tag{3.7k}$$

$$\frac{\partial[RNA_n]}{\partial t} = D_{RNAn}\Delta[RNA_n] + k_T[RNAt_n] \tag{3.7l}$$

3.2.2 Computation for 3D Stochastic Model

The simulation is done using Urdme version 1.1 [128]. Urdme is an open source 3-dimensional stochastic simulation software package. The model geometry is built and discretized in Comsol Multiphysics (Figure 3.4). The 3-D system is discretized into 445 tetrahedrons with the maximal length less than $3\mu m$. Then model geometry is exported and brought into Matlab. In Matlab the stochastic simulation is run using the mesh generated from Comsol Multiphysics.

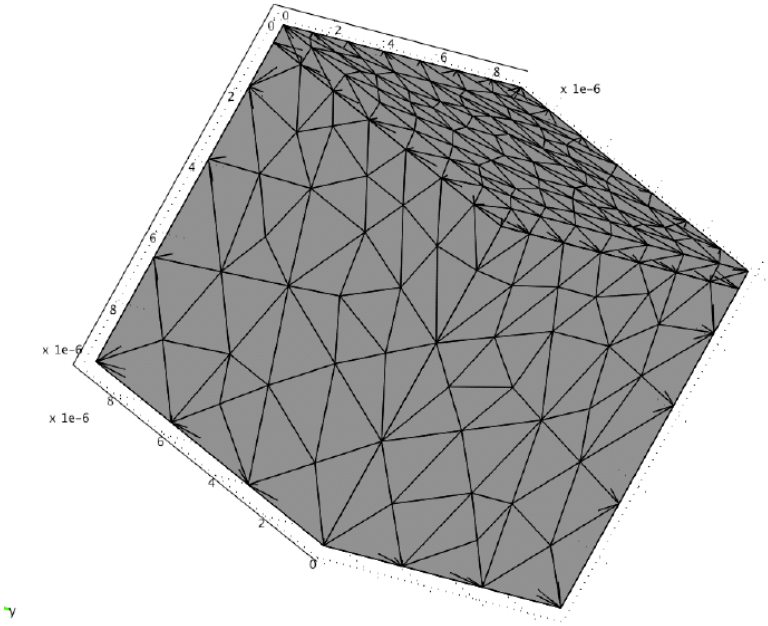

Figure 3.4: Discretization of the Single Cell Stochastic Model in Comsol Multiphysics- The model was discretized into 445 tetrahedrons in Comsol Multiphysics.

The reaction and diffusion rates are defined in the same way as the conventional

spatial Gillespie simulation method. Moreover, the reaction rates are chosen based on the discretization of the deterministic model. For example, in a tetrahedron with length h and volume V, the deterministic governing of C_p is as follows:

$$\frac{\partial[C_p]}{\partial t} = D_{Cp}\Delta[C_p] - k_4[B_p][C_p] + k_{-4}[BC_p] - k_7[BR_p][C_p] + k_{-7}[BCR_p] - d_{Cp}[C_p],$$

and the reactions with Cp involved happen with the rates in Table 3.1.

Reaction	Rates in stochastic simulation	Terms in the deterministic model
$B_p + C_p \xrightarrow{k_4} BC_p$	$(k_4[\#B_p][\#C_p])/(V\mathcal{N}_\mathcal{A})$	$-k_4[B_p][C_p]$
$BC_p \xrightarrow{k_{-4}} C_p + B_p$	$k_{-4}[\#BC_p]$	$k_{-4}[BC_p]$
$BR_p + C_p \xrightarrow{k_7} BCR_p$	$(k_7[\#BR_p][\#C_p])/(V\mathcal{N}_\mathcal{A})$	$-k_7[BR_p][C_p]$
$BCR_p \xrightarrow{k_{-7}} C_p + BR_p$	$(k_{-7}[\#BCR_p])$	$k_{-7}[BCR_p]$
Diffusion	$[\#C] * D_{Cp}/h^2$	$D_{Cp}\Delta[C_p]$

Table 3.1: Relation Between the Stochastic and Deterministic Reaction Rates- The relation between the Deterministic and Stochastic reaction and diffusion rates are described for all reactions involving C in the PV space h and V are the length of volume of the tetrahedron where the reaction is occurring. $\mathcal{N}_\mathcal{A}$ is Avagadro's number.

If the tetrahedron is near the cytoplasm membrane, the transport of C_p is

controlled by the following flux equation in the deterministic model.

$$-D_{Cp}\frac{\partial[C_p]}{\partial z} = -k_{en}[C_p] + k_{ex}[BC_c] + k_{ex}[BCR_c] + k_{ex}[C_c] + k_{se}[T_c].$$

In stochastic simulation, the transport reactions occur as described in Table 3.2.

Reaction	Rates in stochastic simulation	Terms in the deterministic model
$C_p \xrightarrow{k_{en}} C_c$	$(k_{en}[\#C_p])/(h)$	$-k_{en}[C_p]$
$BC_c \xrightarrow{k_{ex}} C_p$	$(k_{ex}[\#BC_c])/(h)$	$k_{ex}[BC_c]$
$BCR_c \xrightarrow{k_{ex}} C_p$	$(k_{ex}[\#BCR_c])/(h)$	$k_{ex}[BCR_c]$
$C_c \xrightarrow{k_{ex}} C_p$	$(k_{ex}[\#C_c])/(h)$	$k_{ex}[C_c]$
$T_c \xrightarrow{k_{ex}} C_p$	$(k_{ex}[\#T_c])/(h)$	$k_{ex}[T_c]$

Table 3.2: Relation Between the Transport Reactions in the Deterministic and Stochastic Simulation- The relation for the transport rates across the plasma membrane for all reactions involving C between the deterministic and stochastic models. h is the length of the tetrahedron where the flux is occurring. The transport rates are modified for all other parameters in the same way.

Table 3.3 describes the abbreviations used in the stochastic and deterministic models.

Symbol	Description
*p	Species in the PV space
*c	Species in the Cytoplasm
*n	Species in the nucleus
B	BMP
C	Surface bound protein
R	Receptor
BR	BMP bound to its Receptor
BC	BMP bound to C
BCR	Complex ofBMP bound to C and R
Mad	Mad
$pMad$	Phosphorylated Mad
$pMad2$	The homodimer of pMad
Me	Medea
$pMMe$	The heterodimer of pMad and Medea
$pM3$	The trimer of two pMads and one Medea
T	C produced from translation
DNA	Free DNA sequence
$NDNA$	DNA occupied by trimer
RNA	mRNA
$RNAt$	Polymerase formed during transcription

Table 3.3: Species Used in the Single Cell Stochastic Model

Table 3.4 describes the reaction rates used in the single cell stochastic model. The reaction rates were taken from experimental estimations whenever possible. Otherwise reaction rates were taken from other mathematical models or estimated. The same approach was applied for finding diffusion coefficients. The diffusion coefficients used in the model are described in Table 3.5.

Reactions	Rate constants	References
	Receptor Intereactions	
$B_p + C_p \underset{k_{-4}}{\overset{k_4}{\rightleftharpoons}} BC_p$	$k_4 = 1\frac{1}{nM*min}, k_{-4} = 2\frac{1}{min}$	[52]
$B_p + R_p \underset{k_{-5}}{\overset{k_5}{\rightleftharpoons}} BR_p$	$k_5 = 2.4 * 10^{-2}\frac{1}{nM*min}, k_{-5} = 4\frac{1}{min}$	[52]
$BC_p + R_p \underset{k_{-6}}{\overset{k_6}{\rightleftharpoons}} BCR_p$	$k_6 = 5 * 10^{-1}\frac{1}{nM*min}, k_{-6} = 10\frac{1}{min}$	[52]
$BR_p + C_p \underset{k_{-7}}{\overset{k_7}{\rightleftharpoons}} BCR_p$	$k_7 = 1.3 * 10^{-1}\frac{1}{nM*min}, k_{-7} = 10\frac{1}{min}$	[52]
	Endocytosis	
$C_p \xrightarrow{k_{en}} C_c$, $R_p \xrightarrow{k_{en}} R_c$ $BC_p \xrightarrow{k_{en}} BC_c$, $BR_p \xrightarrow{k_{en}} BR_c$ $BCR_p \xrightarrow{k_{en}} BCR_c$	$k_{en} = 3.3 * 10^{-2}\frac{\mu m}{min}$	[129]
	Excytosis	
$C_c \xrightarrow{k_{ex}} C_p$, $R_c \xrightarrow{k_{ex}} R_p$ $BC_c \xrightarrow{k_{ex}} C_p$, $BR_c \xrightarrow{k_{ex}} R_p$ $BCR_c \xrightarrow{k_{ex}} R_p + C_p$	$k_{ex} = 3.3 * 10^{-3}\frac{\mu m}{min}$	[129]
	Secretion	
$T_c \xrightarrow{k_{se}} C_p$	$k_{se} = 3\frac{\mu m}{min}$	Estimated
	Cytoplasmic Intereactions	
$Mad_c \xrightarrow{k_{phos}\cdot[BR_c]} pMad_c$ $Mad_c \xrightarrow{k_{phos}\cdot[BR_p]} pMad_c$	$k_{phos} = 2.4 * 10^{-2}\frac{1}{nM*min}$	[121]
$2pMad_c \underset{k_{-8}}{\overset{k_8}{\rightleftharpoons}} pMad2_c$	$k_8 = 1.1 * 10^{-1}\frac{1}{nM*min}$, $k_{-8} = 1\frac{1}{min}$	[121]
$pMad_c + Medea_c \underset{k_{-8}}{\overset{k_8}{\rightleftharpoons}} pMMe_c$		
$pMad2_c + Medea_c \underset{k_{-8}}{\overset{k_8}{\rightleftharpoons}} pM3_c$		
$pMMe_c + pMad_c \underset{k_{-8}}{\overset{k_8}{\rightleftharpoons}} pM3_c$		
$\varnothing \xrightarrow{k_{Tpro}\cdot[RNA_c]} T_c$	$k_{Tpro} = 2.4 * 10^2\frac{nM}{min}$	[130]
	Nuclear/Cytoplamic Transport	

$Mad_c \xrightarrow{k_{in}} Mad_n$	$k_{in} = 4.5 * 10^{-1} \frac{\mu m}{min}$	[121]
$pMad_c \xrightarrow{k_{in}} pMad_n$		
$Medea_c \xrightarrow{k_{in}} Medea_n$		
$pMad2_c \xrightarrow{k_{din}} pMad2_n$	$k_{din} = 2.7 \frac{\mu m}{min}$	[121]
$pMMe_c \xrightarrow{k_{din}} pMMe_n$		
$pM3_c \xrightarrow{k_{din}} pM3_n$		
$Mad_n \xrightarrow{k_{out}} Mad_c$	$k_{out} = 1 \frac{\mu m}{min}$	[121]
$pMad_n \xrightarrow{k_{out}} pMad_c$		
$Medea_n \xrightarrow{k_{mout}} Medea_c$	$k_{mout} = 4.5 * 10^{-1} \frac{\mu m}{min}$	[121]
$RNA_n \xrightarrow{k_{rout}} RNA_c$	$k_{rout} = 100 \frac{\mu m}{min}$	Estimated
	Nuclear Reactions	
$pMad_n \xrightarrow{k_{dephos}} Mad_n$	$k_{dephos} = 3.96 * 10^{-1} \frac{1}{min}$	[121]
$2pMad_n \underset{k_{-8}}{\overset{k_8}{\rightleftharpoons}} pMad2_n$	$k_8 = 1.1 * 10^{-1} \frac{1}{nM*min}$, $k_{-8} = 1 \frac{1}{min}$	[121]
$pMad_n + Medea_n \underset{k_{-8}}{\overset{k_8}{\rightleftharpoons}} pMMe_n$		
$pMad2_n + Medea_n \underset{k_{-8}}{\overset{k_8}{\rightleftharpoons}} pM3_n$		
$pMMe_n + pMad_n \underset{k_{-8}}{\overset{k_8}{\rightleftharpoons}} pM3_n$		
$pM3_n + DNA_n \underset{k_{-9}}{\overset{k_9}{\rightleftharpoons}} NDNA_n$	$k_9 = 600 \frac{1}{nM*min}$, $k_{-9} = 67 \frac{1}{min}$	[131]
$\varnothing \xrightarrow{k_{bT} \cdot [DNA_n]} RNAt_n$	$k_{bT} = 6 \frac{1}{min}$	[130]
$\varnothing \xrightarrow{k_{eT} \cdot [NDNA_n]} RNAt_n$	$k_{eT} = 180 \frac{1}{min}$	[130]
$RNAt_n \xrightarrow{k_T} RNA_n$	$k_T = 10 \frac{1}{min}$	Estimated
	Reactions not on the figure	
$\varnothing \xrightarrow{s_B} B_p$	$s_B = 1 \frac{nM}{min}$	Estimated
$B \xrightarrow{d_{Bp}} \varnothing$	$d_{Bp} = 3.3 * 10^{-2} \frac{1}{min}$	[52]
$\varnothing \xrightarrow{s_R} R_p$	$s_R = 5 * 10^{-4} \frac{nM}{min}$	Estimated
$R_p \xrightarrow{d_{Rp}} \varnothing$, $R_c \xrightarrow{d_{Rc}} \varnothing$	$d_{Rp} = d_{Rc} = 5 * 10^{-4} \frac{1}{min}$	[52]
$C_p \xrightarrow{d_{Cp}} \varnothing$, $C_c \xrightarrow{d_{Cc}} \varnothing$	$d_{Cp} = d_{Cc} = 1.67 * 10^{-4} \frac{1}{min}$	[52]
$BR_p \xrightarrow{d_{BRp}} \varnothing$, $BR_c \xrightarrow{d_{BRc}} \varnothing$	$d_{BRp} = d_{BRc} = 1.67 * 10^{-4} \frac{1}{min}$	[52]
$BC_p \xrightarrow{d_{BCp}} \varnothing$, $BC_c \xrightarrow{d_{BCc}} \varnothing$	$d_{BCp} = d_{BCc} = 1.67 * 10^{-4} \frac{1}{min}$	[52]

$BCR_p \xrightarrow{d_{BCRp}} \varnothing$, $BCR_c \xrightarrow{d_{BCRc}} \varnothing$	$d_{BCRp} = d_{BCRc} = 1.67 * 10^{-4} \frac{1}{min}$	[52]
$RNA_c \xrightarrow{d_{RNAc}} \varnothing$	$d_{RNAc} = 6.6 \frac{1}{min}$	[132]

Table 3.4: Reaction Rates Used in the Single Cell Stochastic Model- The table lists the base set of reactions used in the model. All reaction rates can be assumed to be the same as in the table unless noted otherwise in the text. Reaction rates were taken from experimental estimation whenever possible. If no experimental data was available, reaction rates were taken from other mathematical models, and if those were not available the rates were estimated.

Species	Diffusion Coefficients	References
	PV space	
B_p	$D_{Bp} = 73\mu m^2/s$	[52]
C_p	$D_{Cp} = 1.7\mu m^2/s$	Estimated
R_p	$D_{Rp} = 1.3\mu m^2/s$	Estimated
BC_p	$D_{BCp} = 1.5\mu m^2/s$	Estimated
BR_p	$D_{BRp} = 1.2\mu m^2/s$	Estimated
BCR_p	$D_{BCRp} = 1.1\mu m^2/s$	Estimated
	Cytoplasm	
Mad_c	$D_{Madc} = 16\mu m^2/s$	Estimated
$pMad_c$	$D_{pMadc} = 16\mu m^2/s$	Estimated
$Medea_c$	$D_{Medeac} = 14\mu m^2/s$	Estimated
$pMad2_c$	$D_{pMad2c} = 13\mu m^2/s$	Estimated
$pMMe_c$	$D_{pMMec} = 12\mu m^2/s$	Estimated
$pM3_c$	$D_{pM3c} = 10.5\mu m^2/s$	Estimated
T_c	$D_{Tc} = 100\mu m^2/s$	Estimated
RNA_c	$D_{RNAc} = 0.03\mu m^2/s$	[133, 134]
C_c	$D_{Cc} = 12\mu m^2/s$	Estimated
R_c	$D_{Rc} = 9.5\mu m^2/s$	Estimated
BC_c	$D_{BCc} = 10\mu m^2/s$	Estimated
BR_c	$D_{BRc} = 8.8\mu m^2/s$	Estimated
BCR_c	$D_{BCRc} = 7.8\mu m^2/s$	Estimated
	Nucleus	
Mad_n	$D_{Madn} = 16\mu m^2/s$	Estimated
$pMad_n$	$D_{pMadn} = 16\mu m^2/s$	Estimated
$Medea_n$	$D_{Medean} = 14\mu m^2/s$	Estimated
$pMad2_n$	$D_{pMad2n} = 13\mu m^2/s$	Estimated
$pMMe_n$	$D_{pMMen} = 12\mu m^2/s$	Estimated
$pM3_n$	$D_{pM3n} = 10.5\mu m^2/s$	Estimated
RNA_n	$D_{RNAn} = 0.03\mu m^2/s$	[133, 134]

Table 3.5: Diffusion Coefficients Used in the Single Cell Stochastic Model- The table lists the base set for diffusion coefficients used in the model. All diffusion coefficients can be assumed to be the same as in the table unless noted otherwise in the text. Diffusion coefficients were taken from experimental estimation whenever possible. If no experimental data was available diffusion coefficients where taken from other mathematical models, and if those were not available the diffusion coefficients were estimated.

3.2.3 Simplified Model

I created a simplified model of BMP signaling. Table 3.6 describes the reactions in the model and the reaction rates that are modified from the full stochastic model. Reactions involving R were made into pseudo-first order reaction rates by multiplying the rate constant by 160nM for the concentration of R. In the simplified model we adjusted the C production rate to be on the same order of magnitude as BR. All species in the system start at zero at $t = 0$. The reactions for B, BR, and C all take place in the PV space of volume $V_1 = 40.5\mu m^3$. The reaction for pMad takes place in the nucleus of volume $V_3 = 268\mu m^3$. The reaction for mRNA takes place in the cytoplasm with volume $V_2 = 461\mu m^3$. The simulations are solved using the Gillespie algorithm with a code modified from [135] and were run in Matlab. The output of the mean number of molecules and the CV of the parameter scan was averaged over the last 10 simulation points after the system reached steady state. 50 simulations were run for each parameter set.

Reactions	Rate constants
$\varnothing \xrightarrow{k_1} B$	$k_1 = 10\frac{nM}{min}$
$B \xrightarrow{k_2} BR$	$k_2 = 3.84\frac{1}{min}$
$BR \xrightarrow{k_3} BR + pMad$	$k_3 = 1.22\frac{1}{min}$
$pMad \xrightarrow{k_4} pMad + mRNA$	$k_4 = 0.6\frac{1}{min}$
$mRNA \xrightarrow{k_5} mRNA + C$	$k_5 = 0.24\frac{1}{min}$
$B + C \xrightarrow{k_6} BC$	$k_6 = 1\frac{1}{nMmin}$
$BC \xrightarrow{k_{-6}} B + C$	$k_{-6} = 2\frac{1}{min}$
$BC \xrightarrow{k_7} BR + C$	$k_7 = 80\frac{1}{min}$
$BR + C \xrightarrow{k_{-7}} BC$	$k_{-7} = 10\frac{1}{nMmin}$
$B \xrightarrow{k_{d1}} \varnothing$	$k_{d1} = 0.033\frac{1}{min}$
$BR \xrightarrow{k_{d2}} \varnothing$	$k_{d2} = 0.033\frac{1}{min}$
$pMad \xrightarrow{k_{d3}} \varnothing$	$k_{d3} = 0.396\frac{1}{min}$
$mRNA \xrightarrow{k_{d4}} \varnothing$	$k_{d4} = 6.6\frac{1}{min}$
$C \xrightarrow{k_{d2}} \varnothing$	$k_{d2} = 0.033\frac{1}{min}$
$BC \xrightarrow{k_{d2}} \varnothing$	$k_{d2} = 0.033\frac{1}{min}$

Table 3.6: Reactions in Simplified Stochastic Model

3.3 Results

3.3.1 Time Scales of Reactions

In this section we compare time scales of different reaction steps to understand the temporal scale of signal evolution. We first estimate the maximal numbers of molecules of different species based on literature, and then use them to estimate

reaction frequencies. We find that the major rate limiting steps are phosphorylation of Mad and the nucleocytoplasmic transport of mRNA.

We first estimate the maximal number of molecules of each species in the PV space, cytoplasm and nucleus in order to understand possible areas of stochasticity. For free BMP, the estimated concentration from previous models on the dorsal surface at maximal signaling is around 5nM [52]. The PV space above one nucleus is approximately approximately $9\mu m \times 0.5\mu m \times 9\mu m$. The maximal number of BMP molecules in the PV space based upon the Umulis model is

$$5 * 10^{-9} M \times 6.02 \times 10^{23} \frac{molecules}{mol} \times 9\mu m \times 9\mu m \times 0.5\mu m * \frac{10^{-15} L}{\mu m^3} = 122. \quad (3.8)$$

This is an order of magnitude higher than estimates from cell culture. However the estimates from cell cultures are an average over all dorsal nuclei and do not take into account any transport of molecules towards the dorsal midline. Even taking transport of molecules into account, the level of free BMP is within a stochastic range.

For simplicity of modeling it is assumed that receptors are distributed in the whole PV space as in [52]. Therefore the maximal number of receptors in the PV

space is

$$160 * 10^{-9} M \times 6.02 \times 10^{23} \frac{molecules}{mol} \times 9\mu m \times 9\mu m \times 0.5\mu m * \frac{10^{-15} L}{\mu m^3} = 3900, \quad (3.9)$$

where the concentration of receptors $160nM$ is taken from [52]. Similarly, the maximal numbers of molecules of other species can be estimated. Table 3.7 shows the maximal number of molecules of species in the PV space, cytoplasm, and nucleus. We denote BMP as B, receptors are as R and a surface binding molecule similar to Cv-2 as C. In addition, to differentiate molecules in different locations, we use *p, *c and *n to denote the species in the PV space, the cytoplasm and the nucleus respectively. For example, Bp represents B in the PV space and Bc represents B in the cytoplasm. The total amount of receptors and Cp molecules is much larger than the amount of Bp. This may allow Cp and the receptors to bind Bp more effectively and possibly attenuate fluctuations in Bp. The number of molecules in the system varies by several orders of magnitude. The species with large numbers of molecules may be able to attenuate the noise in B and BR where there are significantly less molecules.

Variable	Description	Number of Molecules	Reference
B	BMP ligand	122 molecules	[52, 50]
BR	Bound Receptor	730 molecules	[52]
R	BMP receptors	3900 molecules	[52]
C	Surface Binding Protein	8400 molecules	[52]
Mad	Mad	$22,300$	[52]
$Medea$	Medea	$22,300$	[52]

Table 3.7: Maximum Estimated Number of Molecules- We estimate the maximal number of molecules in the system predicted from previous models of BMP signaling. There is a wide range of estimated number of molecules in the system. The level of free B molecules suggests that reactions involving B may be stochastic.

We next investigated the likelihood a reaction will occur in the system. To estimate reaction frequencies, we calculated the maximal propensity function of each reaction, which gives the largest probability of the occurrence of the reaction per unit time. In particular, we calculate the propensity function by Eq. (3.10)

$$X_1 \times X_2 \times rate \times V \times 6.02 \times 10^{23}, \tag{3.10}$$

where X_1 and X_2 are the concentrations of the reactant species in a bimolecular reaction ($X_2 = 1$ for a unimolecular reaction), $rate$ is the reaction rate constant, and V is the volume of the respective cuboid. X_1 and X_2 are chosen as the maximal concentrations of the reactant species in the cuboid. Table 3.8 summaries the propensity functions of selected reactions. There is a two orders of magnitude difference between the slowest and fastest reactions in the PV space. Forming

active signaling complexes by B binding to R is very slow, but the formation of active signaling complexes through binding to C is very likely, leading to almost all active signaling complexes forming through C. In the intracellular space, the major rate limiting step appears to be the phosphorylation of Mad to pMad. This is somewhat surprising because based on the maximal number of molecules analysis, since the number of Mad molecules is very high, which would suggest that it should not be a slow step. However the estimated phosphorylation rate is very slow, making the overall likelihood that the reaction occurs low. Since we calculated the maximal reaction propensities, the actual propensity of an individual reaction as the system evolves may be much slower. Thus some of the reactions estimated to be more likely to occur may initially occur less frequently until the maximal concentration of reactants is reached. The reaction propensity analysis suggests that the binding of B to its receptor, the phosphorylation of Mad, and the disassociation of the transcription factors are slow steps in the system.

Reaction	Species 1 (Max Conc)	Species 2 (Max Conc)	Rate	Propensity Function
$B + C \rightarrow BC$	B $(5nM)$	C $(200nM)$	$1.66 * 10^7 \frac{1}{M*sec}$	$405 \frac{1}{sec}$
$BC \rightarrow B + C$	BC $(30nM)$		$0.33 \frac{1}{sec}$	$241 \frac{1}{sec}$
$BC + R \rightarrow BCR$	BCR $(30nM)$	R $(160nM)$	$8.33 * 10^6 \frac{1}{M*sec}$	$975 \frac{1}{sec}$
$BCR \rightarrow BC + R$	BCR $(80nM)$		$0.17 \frac{1}{sec}$	$332 \frac{1}{sec}$
$BR + C \rightarrow BCR$	BR $(30nM)$	C $(200nM)$	$2.17 * 10^6 \frac{1}{M*sec}$	$317 \frac{1}{sec}$
$BCR \rightarrow BR + C$	BCR $(80nM)$		$0.17 \frac{1}{sec}$	$332 \frac{1}{sec}$
$B + R \rightarrow BR$	B $(5nM)$	R $(160nM)$	$4.00 * 10^5 \frac{1}{M*sec}$	$8 \frac{1}{sec}$
$BR \rightarrow B + R$	BR $(30nM)$		$0.067 \frac{1}{sec}$	$490 \frac{1}{sec}$
$BR + Mad \rightarrow pMad$	BR $(30nM)$	Mad $(50.8nM)$	$4 * 10^5 \frac{1}{M*sec}$	$15 \frac{1}{sec}$
$BCR + Mad \rightarrow pMad$	BCR $(80nM)$	Mad $(50.8nM)$	$4 * 10^5 \frac{1}{M*sec}$	$40 \frac{1}{sec}$
$pMad + pMad \rightarrow pMad2$	$pMad$ $(50.8nM)$	$pMad$ $(50.8nM)$	$1.8 * 10^6 \frac{1}{M*sec}$	$113 \frac{1}{sec}$
$pMad + Me \rightarrow pMMe$	$pMad$ $(50.8nM)$	Me $(50.8nM)$	$1.8 * 10^6 \frac{1}{M*sec}$	$113 \frac{1}{sec}$
$pMad2 \rightarrow 2pMad$	$pMad2$ $(25.4nM)$		$0.016 \frac{1}{sec}$	$10 \frac{1}{sec}$
$pMMe \rightarrow pMad + Me$	$pMMe$ $(50.8nM)$		$0.016 \frac{1}{sec}$	$20 \frac{1}{sec}$
$pMad \rightarrow Mad$	$pMad$ $(50.8nM)$		$0.0066 \frac{1}{sec}$	$8 \frac{1}{sec}$

Table 3.8: Propensity Function for Selected Reactions- We calculated the maximum likelihood a reaction will occur based on maximum concentrations of molecules from previous published models. For reactions that are not listed, concentration estimates are not available. The rate limiting steps appear to be the binding of B to R, the phosphorylation of Mad to pMad, and the disassociation of the pMad complexes. The fastest reactions are reactions involving the molecule C.

We also studied the maximal propensity for transport of molecules across the plasma and nuclear membrane. The maximal propensity function for membrane transport is calculated by Eq. (3.11)

$$X_1 \times rate \times V \times 6.02 \times 10^{23} \tag{3.11}$$

where X_1 is the maximal concentration of the respective species, $rate$ is the transport rate constant, and V is the volume of the compartment where the transport starts. For the membrane transport propensity analysis we assume all molecules are evenly distributed in their respective compartments in the PV space, cytoplasm, or nucleus. Therefore, we use the total number of molecules in the compartment in Eq. (3.11). Table 3.9 summarizes the propensity functions for transport across membranes. Transport across the plasma membrane represents endocytosis and transport across the nuclear membrane is nuclear-cytoplasmic

shuttling. The transport propensities are several orders of magnitude slower than the molecular reaction propensities. Transport of molecules across membranes may be rate limiting steps in the BMP signaling pathway.

Species	Concentration	Rate	Propensity Function
	Transport Across Plasma Membrane		
BR	BR $(30nM)$	$3.33 * 10^{-4} \frac{1}{sec}$	$0.244 \frac{1}{sec}$
B	B $(5nM)$	$3.33 * 10^{-4} \frac{1}{sec}$	$0.0406 \frac{1}{sec}$
C	C $(200nM)$	$3.33 * 10^{-4} \frac{1}{sec}$	$1.62 \frac{1}{sec}$
BCR	BCR $(80nM)$	$3.33 * 10^{-4} \frac{1}{sec}$	$0.650 \frac{1}{sec}$
R	R $(160nM)$	$3.33 * 10^{-4} \frac{1}{sec}$	$1.30 \frac{1}{sec}$
	Transport Across Nuclear Membrane		
Mad_c	Mad $(50.8nM)$	$5.16 * 10^{-3} \frac{1}{sec}$	$0.0728 \frac{1}{sec}$
Mad_n	Mad $(50.8nM)$	$0.29 \frac{1}{sec}$	$2.38 \frac{1}{sec}$
$pMad_c$	$pMad$ $(50.8nM)$	$5.16 * 10^{-3} \frac{1}{sec}$	$0.0728 \frac{1}{sec}$
$pMad_n$	$pMad$ $(50.8nM)$	$0.29 \frac{1}{sec}$	$2.38 \frac{1}{sec}$
$pMad2_c$	$pMad2$ $(25.4nM)$	$0.0294 \frac{1}{sec}$	$0.207 \frac{1}{sec}$
$pMMe_n$	$pMMe$ $(50.8nM)$	$0.0294 \frac{1}{sec}$	$0.415 \frac{1}{sec}$
Me_c	Me $(50.8nM)$	$0.00516 \frac{1}{sec}$	$0.0728 \frac{1}{sec}$
Me_n	Me $(50.8nM)$	$0.00305 \frac{1}{sec}$	$0.02502 \frac{1}{sec}$

Table 3.9: Propensity Function for Transport Across Membranes- We estimate the maximal propensity for molecules to move across the plasma or nuclear membrane. The propensity for transport across membranes is much smaller than the propensity for molecular reactions.

Finally we estimate the time scale for a molecule to diffuse throughout the PV

space, cytoplasm, or nucleus. The time scale is estimated by Eq (3.12)

$$\frac{L^2}{D} \tag{3.12}$$

where D is the diffusion coefficient, and L is the maximum length of the PV space, cytoplasm, or nucleus. Table 3.10 summarizes the time scales for selected molecules in their respective compartments. The diffusion of mRNA is several orders of magnitude slower than all other diffusion processes. Therefore, the transport of mRNA can also be a limiting step in the signal evolution. However with the exception of mRNA, the diffusion rates are fast and diffusion is not a rate limiting step in the interaction of molecules in the system.

Species	Diffusion	L^2/D Constant
B	$7.3 * 10^{-11} \frac{m^2}{sec}$	$1.1s$
R	$1.3 * 10^{-12} \frac{m^2}{sec}$	$62.3s$
$pMad_c$	$1.6 * 10^{-11} \frac{m^2}{sec}$	$5.06s$
$mRNA_c$	$3.0 * 10^{-14} \frac{m^2}{sec}$	$2700s$
$pMad_n$	$1.6 * 10^{-11} \frac{m^2}{sec}$	$4s$
$mRNA_n$	$3.0 * 10^{-14} \frac{m^2}{sec}$	$2130s$

Table 3.10: Diffusion Time Scale Analysis- The length scales for diffusion of selected molecules in the BMP signaling pathway was estimated. Overall the diffusion rate is fairly fast with the exception of mRNA. The overall diffusion of mRNA is a slow step and may affect its transport from the nucleus to the cytoplasm.

The BMP signaling pathway is a multi-scale network, which allows us to reduce

the system for stochastic simulations. Since the diffusion time of Mad and Medea is much less than the time of phosphorylation and nuclear transport, we can assume that Mad and Medea are always well mixed in the nucleus and cytoplasm. By making this assumption, we can reduce the simulation time by half to one third. Since the phosphorylation of Mad is much slower than other reactions that implies there may be a small number of pMad molecules with large fluctuations in the cytoplasm. Furthermore, the nucleocytoplasmic transport of mRNA is much slower than other reactions and diffusion processes, which may introduce noise in the feedback process of BMP signaling. The concentration and time-scale analysis indicates there are species with low numbers of molecules and several slow steps in the reaction system, which suggests that stochasticity may play a role in the BMP signaling pathway.

3.3.2 3-D Single Cell Stochastic Model

Temporal Evolution of the System

We simulate the biochemical system presented in Section **??** using the base parameter set found in table 3.4. Figure 3.5 shows the evolution of the system for one realization and Figure 3.6 shows the mean and coefficient of variation (CV) of selected molecules in different domains of the stochastic system. The coefficient

of variation is defined as the standard deviation/mean and is a way to measure noise in the system. A larger CV indicates more noise is present. The system has some noise as the trajectories in Figure 3.5 are not smooth. B represents free BMP molecules. BR is the active signaling complex where B is bound to its receptor. C represents a co-receptor, Cv-2, for B. pMad is the phosphorylated Mad molecule which arises from Mad interacting with BR. The pMad molecules can form a dimer, pMad2; a complex with Medea, pMMe; or a trimer of 2 pMads and one Medea, pM3. The active transcription factor pM3 can bind to the DNA promoter site to turn on transcription. When this occurs the DNA promoter sites goes from unoccupied (1) to bound (0). RNA is produced and diffuses to the cytoplasm where translation produces Cv-2. Cv-2 starts at zero in the system and is produced at a low basal rate that is significantly increased from activation of the BMP signaling cascade. This series of molecular interactions captures the main elements in the canonical BMP signaling pathway.

The receptor dynamics follow different trajectories for the mean amount of molecules and the CV for the respective species in the PV space and cytoplasm (Figure 3.6). The level of free BMP slowly decreases to almost zero as the system evolves since all the BMP produced immediately binds to either Cv-2 or BR (Figure 3.6 A). While the overall CV for BMP is fairly low, the CV increases as the system evolves because of the low mean (Figure 3.6 A). BR increases in the PV

space until the amount of Cv-2 produced starts to dramatically increase around 40 minutes (Figure 3.6 B). Cv-2 acts as an inhibitor of signaling by sequestering and competing for BMP. When the amount of BR starts to decrease the CV of BR starts to increase (Figure 3.6 B). However, for the endocytosed BR the levels are still increasing at 60 minutes (Figure 3.6 C). Endocytosis appears to slightly reduce the CV of cytoplasmic BR to less than the CV BR in the PV space at 60 minutes (Figure 3.6 G). BR starts to decrease as Cv-2 increases since Cv-2 has a stronger affinity for BMP. With the base parameter set, Cv-2 appears to be acting negatively to decrease the overall amount of BR and BMP in the single cell system. The addition of Cv-2 also increases the CV of BMP and BR in the PV space, but endocytosed BR is protected from the inhibition. Thus endocytosis may help create a stronger response to BMP signaling by protecting BR from inhibition by Cv-2.

Although the means of the number of molecules for pMad, pMad2, pMMe and pM3 are relatively small (less than 100), their CV's are not large (Figure 3.6 G-L). While the propensity analysis predicted that the phosphorylation of Mad was a major rate limiting step, there is only a very small increase in the CV of BR compared to pMad (Figure 3.6 G). This may be due to the large amount of Mad and Medea molecules attenuating the stochastic fluctuations. Even though there are more BR molecules in the PV space than the cytoplasm, the amount

and CV of pMad follows the trajectory of BRc. The degradation rate of pMad is very slow, so the accumulation of pMad over time may help to attenuate the fluctuations and inhibition of BR in the PV space. The active transcription factor, pM3, is formed primarily through pMad combining with Medea and then another pMad molecule combining with pMMec (Figure 3.5). This is not surprising as the amount of Medea is high throughout the simulation, but there are very few pMad molecules. It takes about 30 minutes before the first transcription factor is formed, and almost as fast as that happens it binds to the promoter site (Figure 3.6 D). The noise in the transcription factor formation is one of the noisiest steps in the model (Figure 3.6 H and J). However the noise does decrease after each pMad species is formed. The nuclear accumulation of pMad decreases the noise of the transcription factor as the CV of pM3 is higher in the cytoplasm than the nucleus (Figure 3.6 J). The noise in the transcription factor, pM3, binding to the promoter site increases steadily after transcription is initiated around 30 minutes (Figure 3.6 K). This slow response is somewhat surprising and may be due to the slow phosphorylation rate. Initially the level of RNA starts at 0 and starts to slowly increase due to a low basal level of transcription. Then, around 40 minutes the levels of RNA start to dramatically increase, and do not reach a steady state by 60 minutes (Figure 3.6 E). The noise in RNA levels in the nucleus or cytoplasm is fairly constant during the entire simulation (Figure 3.6 L). While there is noise

in the RNA levels, there is much less noise in Cv-2 due to the high production rate (Figure 3.6 L). When Cv-2 starts to inhibit the overall levels of signaling, there is an increase in the CV of Cv-2. Thus, using best estimates from the literature for the intracellular kinetics, our model suggests there is noise in the downstream signaling network with the noisiest step being transcription factor formation.

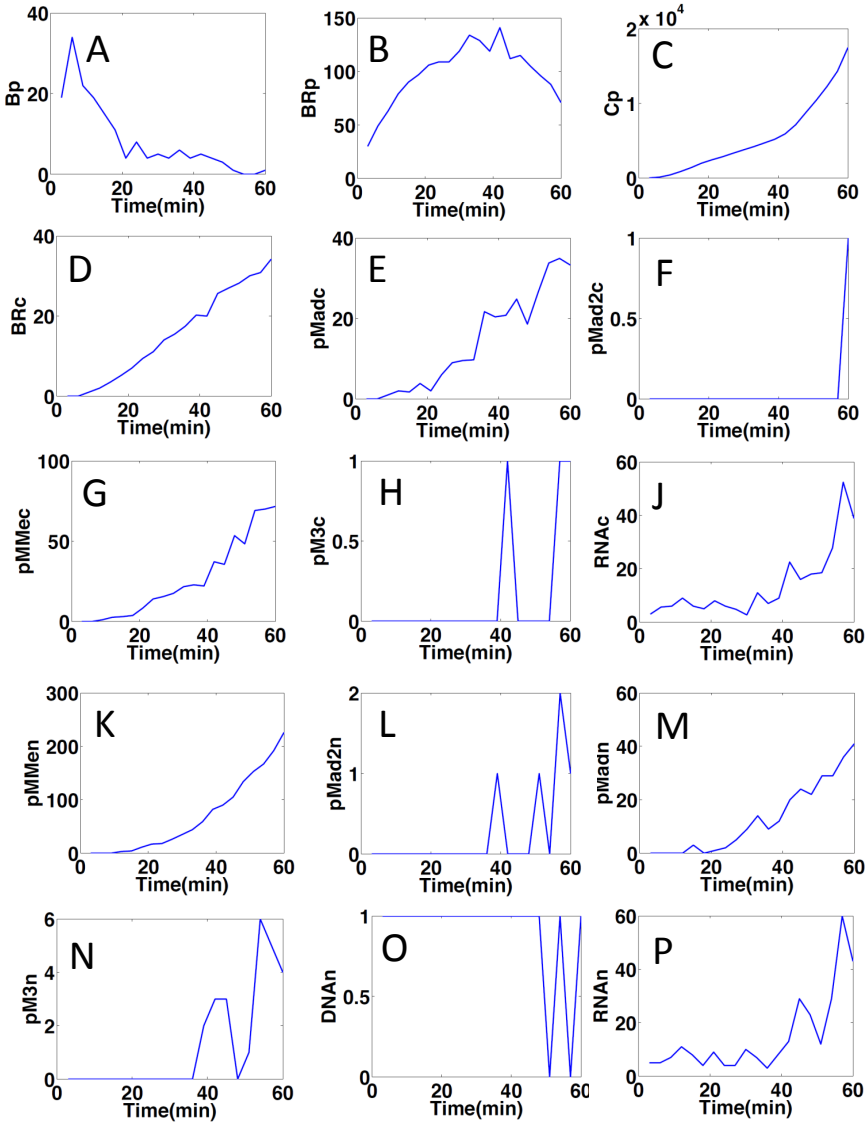

Figure 3.5: One Stochastic Realization of BMP Signaling with Slow Endocytosis- One realization of the system with the slow endocytosis/exocytosis rates$k_{en} = 3.3 \times 10^{-2} \mu m/min$ and $k_{ex} = 3 \times 10^{-3} \mu m/min$. The blue line represents the number of molecules for each respective species, except for DNA where 1 represents the DNA promoter site is free and 0 represents the transcription factor pM3 is bound to the DNA.

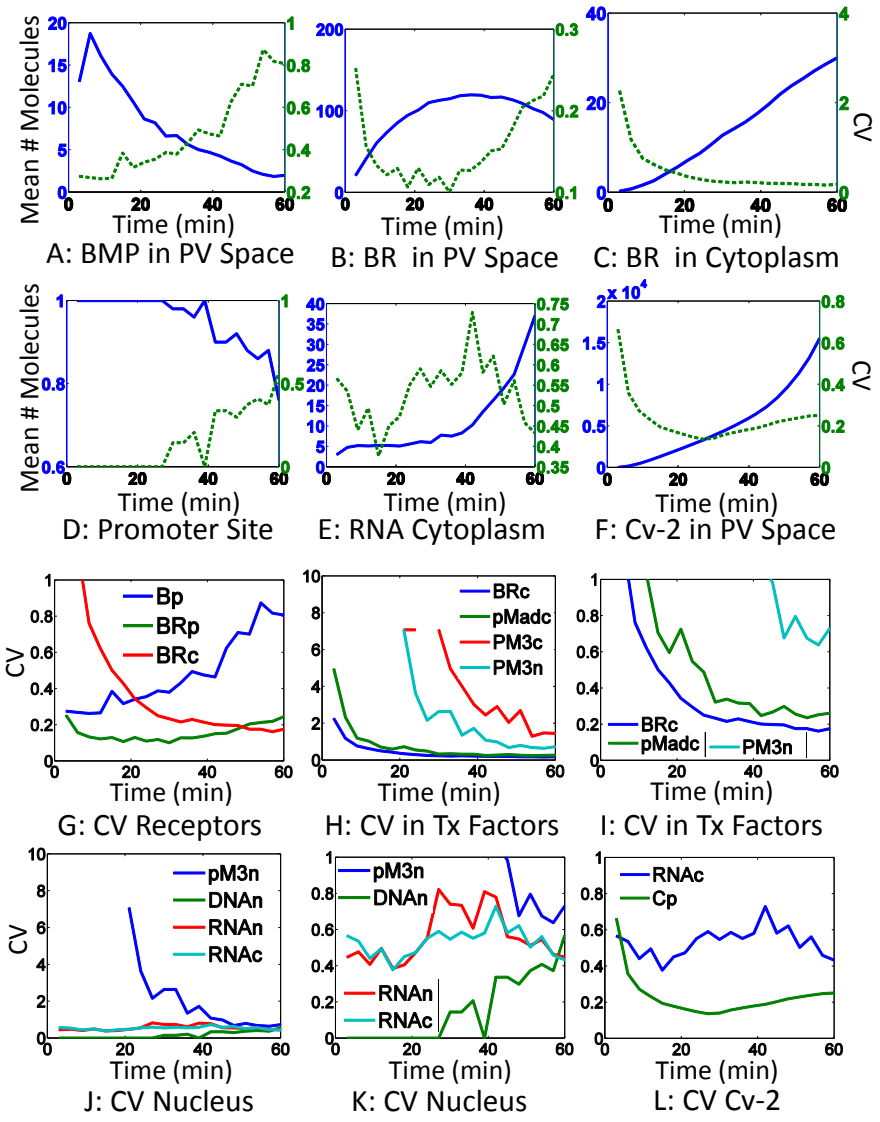

Figure 3.6: Mean Number of Molecules and the Coefficient of Variation for the System with Slow Endocytosis-The temporal evolution of the number of molecules of different species in the system with the slow endocytosis/exocytosis rates $k_{en} = 3.3 \times 10^{-2} \mu m/min$ and $k_{ex} = 3 \times 10^{-3} \mu m/min$. A-F) The blue line represents the number of molecules for each respective species, except for DNA where 1 represents the DNA promoter site is free and 0 represents the transcription factor pM3 is bound to the DNA. The green line represents the CV for each respective species. G-L) The CV between different species is compared. The results are generated from 50 realizations of the stochastic system.

Signal Responses to Different Levels of BMP

Since different positions along the D/V axis are exposed to different levels of BMP in the BMP morphogen gradient, we studied the stochastic dynamics of the system at different production rates of BMP. Figure 3.7 shows the mean and CV of number of molecules of key species for different production rates of BMP. When C starts to be produced it transiently increases the noise level in the downstream network. However, as the system equilibrates to the negative feedback of Cv-2, the levels of noise decreases. The time at which this occurs is sooner with stronger signaling. Thus by 60 minutes areas with higher signaling have less noise, whereas areas with lower signaling have higher levels of noise in mRNA and Cv-2. The simulations with larger levels of Cv-2 have higher levels of noise in free BMP and bound receptor in the PV space (Figure 3.7 G-I). However the endocytosed bound receptor has very low noise and endocytosis may help to buffer out the noise in the PV space. Interestingly, the amount of buffering from endocytosis is similar for all BMP production rates. Thus depending upon the position along the DV axis, there are different levels of signaling leading to possibly higher levels of noise in free BMP in high signaling domains but lower levels of noise in the overall amount of signaling as measured by mRNA levels.

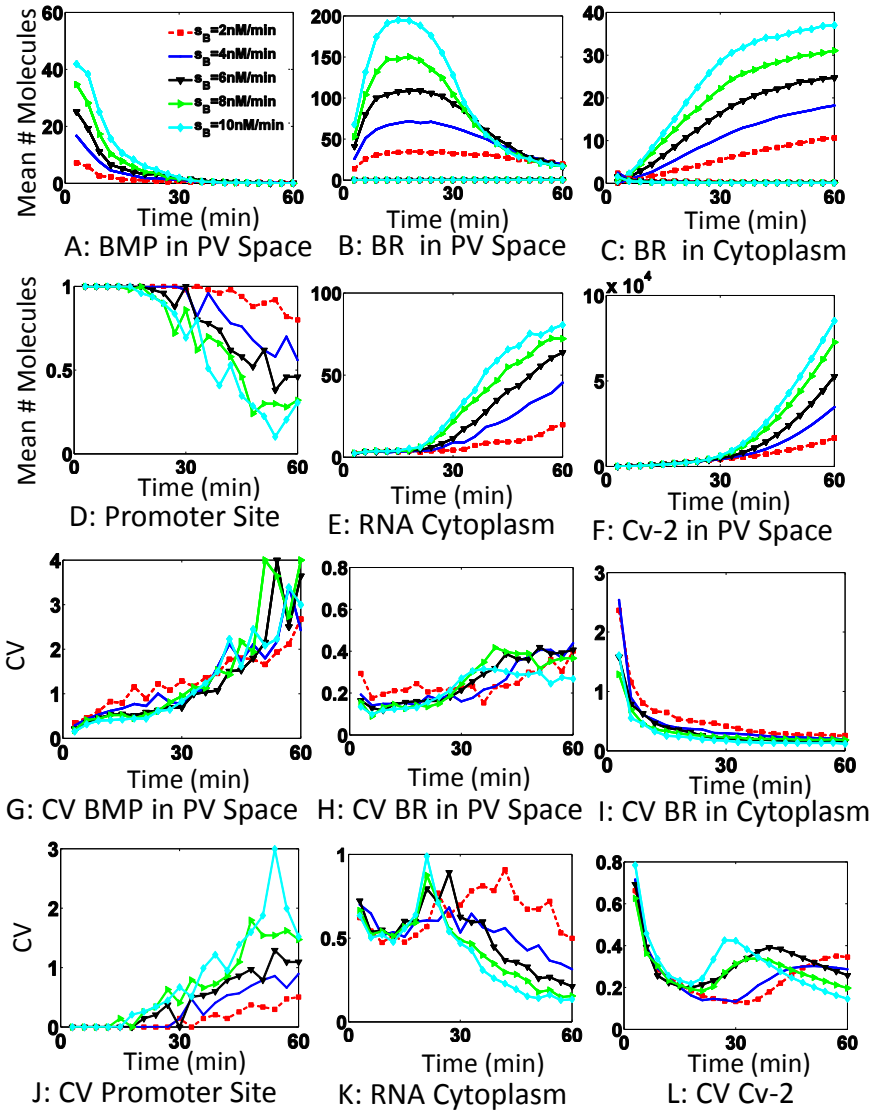

Figure 3.7: The Mean and CV of Selected Species at Different Production Rates of BMP- Here I use the slow endocytosis/exocytosis rates ken=3.3x10-2um/min and kex=3x10-3um/min. The red, dark blue, black, green, and light blue lines represents the number of molecules for each respective species, except for DNA where 1 represents the DNA promoter site is free and 0 represents the transcription factor pM3 is bound to the DNA. The red, dark blue, black, green, and light blue represent B production rates of 2, 4, 5, 6, and 10 nM/min respectively. The results are generated from 50 realizations of the stochastic system.

The Role of Slow Endocytosis/Exocytosis in Signaling

Since the endocytosis rates measured for TGF-β signaling [129] are much lower than rates measured for other signaling pathways such as the Epidermal Growth Factor pathway [136], we studied how the system would respond with faster endocytosis and receptor recycling rates. At a low level of BMP the levels of the stochastic fluctuations in RNA and proteins, measured by CV, stay constant over time in the system with slow endocytosis/exocytosis. However, they decrease in the system with fast endocytosis/exocytosis. Figures 3.6 and 3.8 show the mean and CV of the number of total molecules of key species in different domains of the stochastic system with different endocytosis and exocytosis rates. In both figures the temporal evolution of pMad in the cytoplasm follows the temporal evolution of BMP-bound receptors in the cytoplasm, which implies that endocytosis is important for signaling. In addition, although the ratio of the endocytosis and exocytosis rates in two settings are the same, pMad increases faster in the system with faster endocytosis/exocytosis promoting the feedback loop (Figure 3.8). As a result the CV of RNA begins to decrease after 30 minutes, which is when the feedback loop takes effect (Figure 3.8 E), while in the system with slow endocytosis/exocytosis rates the CV of RNA stays constant (Figure 3.6 E). Thus the rate of endocytosis may have a large effect on regulating the strength of

signaling.

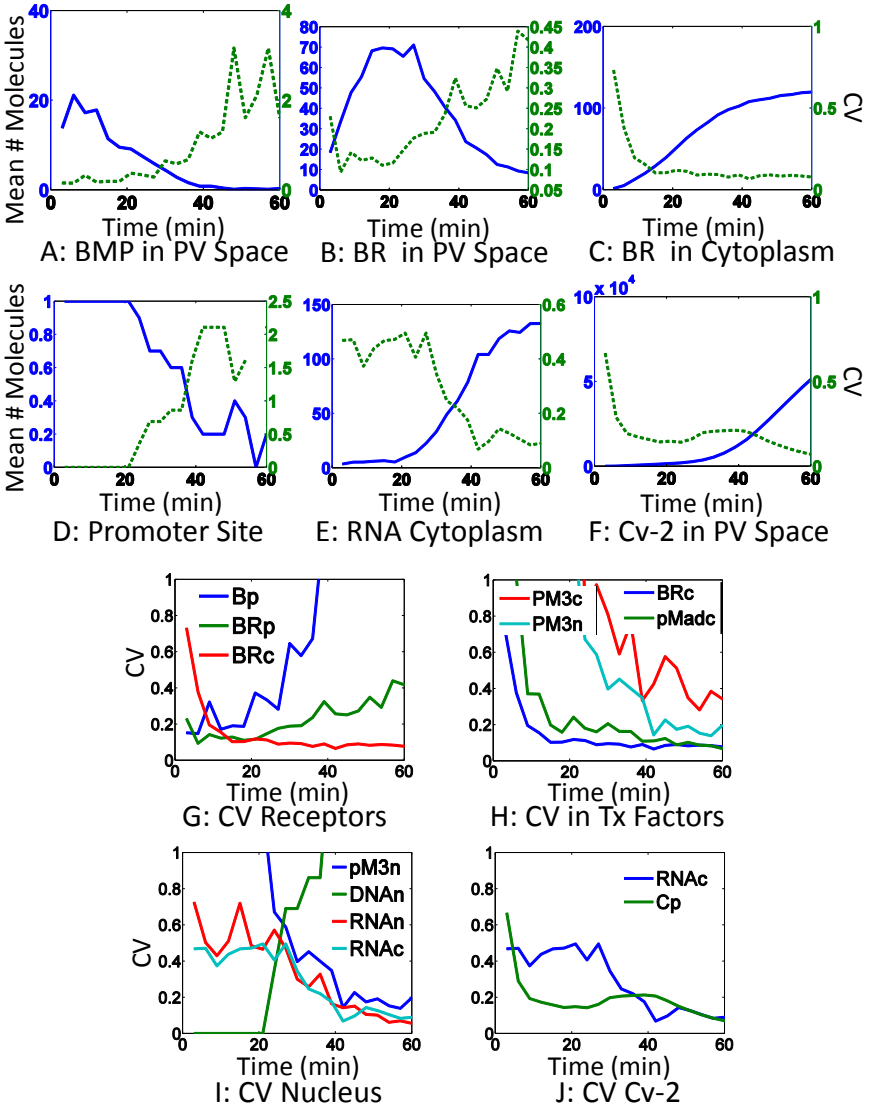

Figure 3.8: Mean and CV of Species in the 3D Stochastic Model with Fast Endocytosis- The molecular temporal evolution of different species in the system with the fast endocytosis/exocytosis rates $k_{en} = 3.3 \times 10^{-1} \mu m/min$ and $k_{ex} = 3 \times 10^{-2} \mu m/min$. A-F) The blue line represents the number of molecules for each respective species, except for DNA where 1 represents the DNA promoter site is free and 0 represents the transcription factor pM3 is bound to the DNA. The green line represents the CV for each respective species. G-J) Comparison of the CV between species. The results are generated from 10 realizations of the stochastic system.

Influence of Phosphorylation Rate on Evolution of 3D Stochastic Model

Since the propensity analysis showed that the phosphorylation rate may be a rate limiting step in the model, we studied how the model changes with increasing the phosphorylation ration by 10 and 100 times (Figures 3.9 and 3.10). An increase in the phosphorylation rate lead to an earlier and lower peak of bound receptor in the PV space (Figures 3.9 and 3.10 B) since Cv-2 was produced at both higher levels and an earlier time point. The level of cytoplasmic BR also decreased as the phosphorylation rate increased (Figures 3.9 and 3.10 C). The level of noise of free BMP and bound receptor in the cytoplasm increased, while noise of bound receptor in the cytoplasm was unchanged (Figures 3.9 and 3.10 G). Despite having lower levels of bound receptor the time at which the promoter site turned on significantly decreased (Figures 3.9 and 3.10 D). There was also a large decrease in the noise of transcription factors in the cytoplasm and nucleus (Figures 3.9 and 3.10 H and I). The nuclear accumulation of the transcription factor no longer decreased the noise in nuclear transcription factor compared to the cytoplasmic transcription factor (Figures 3.9 and 3.10 H). The level of mRNA and Cv-2 produced also significantly increased as the phosphorylation rate decreased (Figures 3.9 and 3.10 E and F). Thus the levels of molecules in the system and the overall noise were greatly affected by phosphorylation rate.

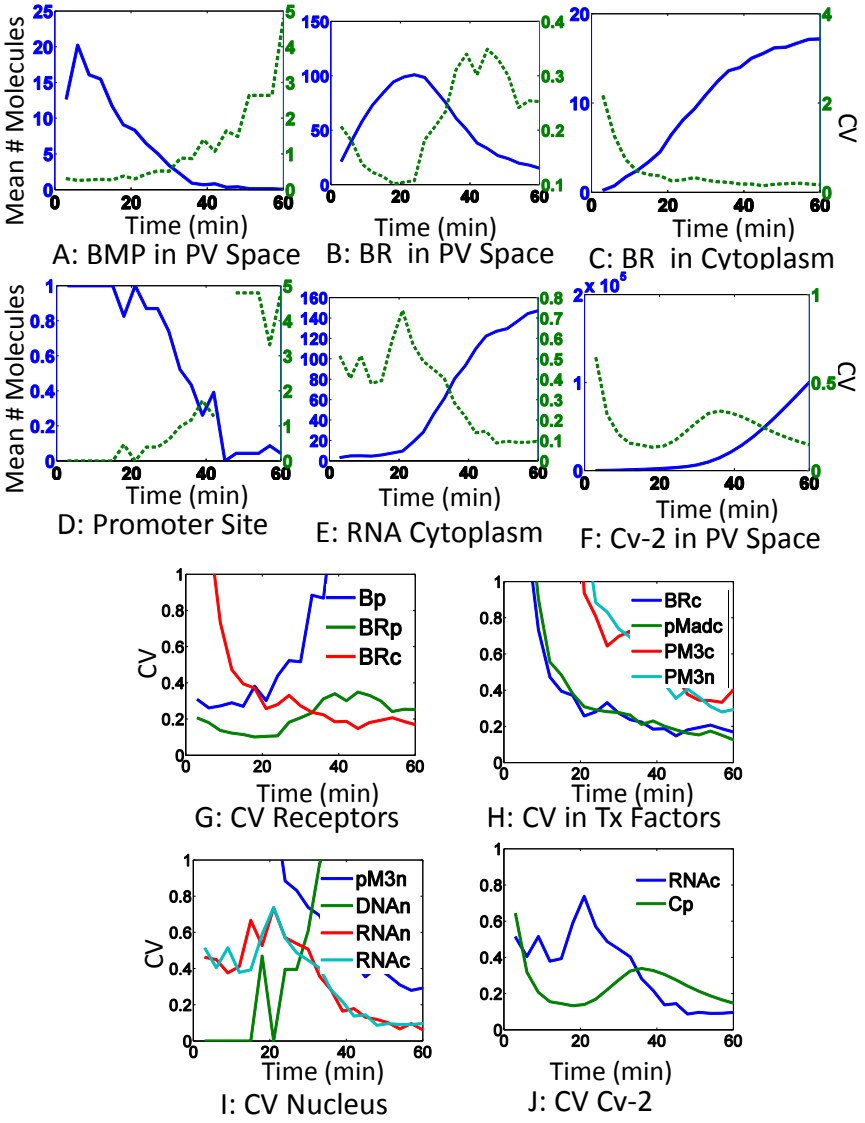

Figure 3.9: Mean and CV of Species in the 3D Stochastic Model with 10 Times Base Phosphorylation Rate- The molecular temporal evolution of different species in the system with the base parameters and no Cv-2 in the model. A-F) The blue line represents the number of molecules for each respective species, except for DNA where 1 represents the DNA promoter site is free and 0 represents the transcription factor pM3 is bound to the DNA. The green line represents the CV for each respective species. G-J) Comparison of the CV for different species in the model. The results are generated from 19 realizations of the stochastic system.

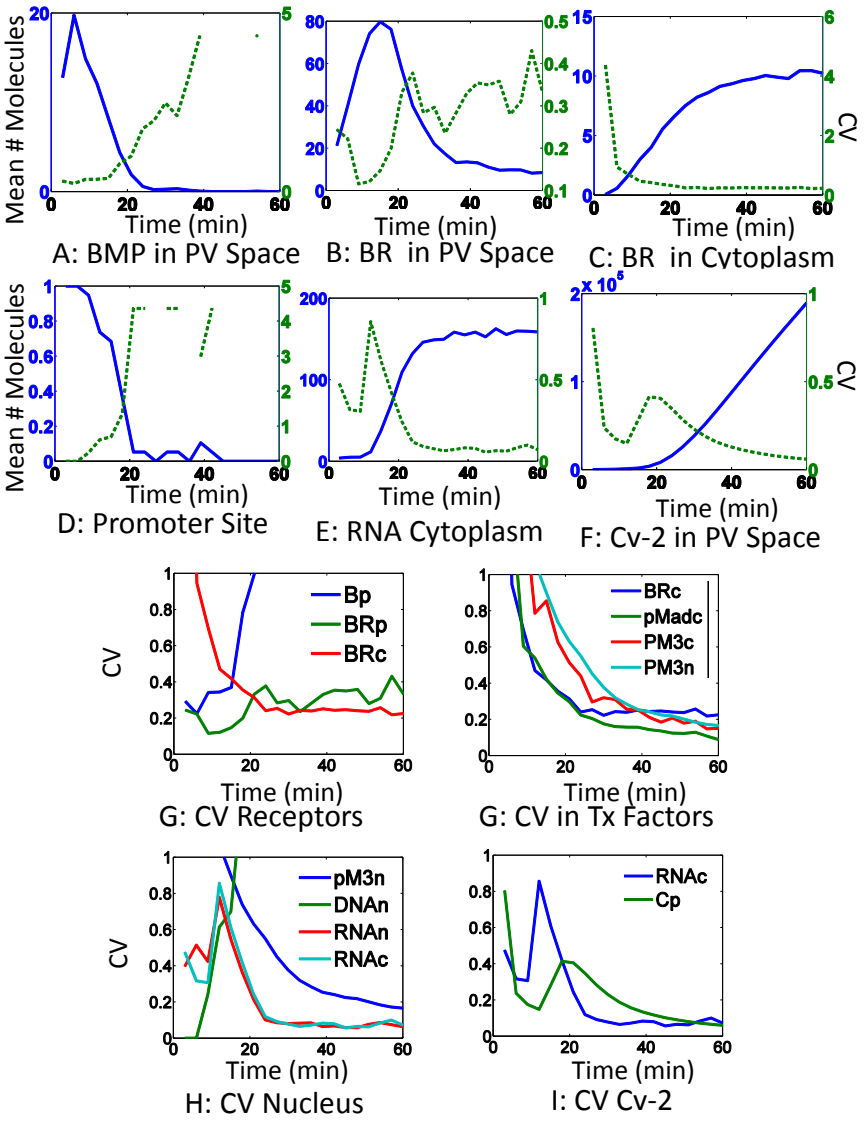

Figure 3.10: Mean and CV of Species in the 3D Stochastic Model with 100 Times Base Phosphorylation Rate- The molecular temporal evolution of different species in the system with the base parameters and no Cv-2 in the model. A-F) The blue line represents the number of molecules for each respective species, except for DNA where 1 represents the DNA promoter site is free and 0 represents the transcription factor pM3 is bound to the DNA. The green line represents the CV for each respective species. G-J) Comparison of the CV for different species in the model. The results are generated from 19 realizations of the stochastic system.

Cv-2 Knockout in 3D Stochastic Model

To compare our model with the experimental results for the Cv-2 knock out, we studied how the model was effected when Cv-2 was not allowed to be produced from mRNA (Figure 3.11). There was a large increase in the level of both free BMP and BR in the PV space and cytoplasm (Figure 3.11 A and B). However the time at which the promoter site first become occupied was similar (Figure 3.11 D). In agreement with experimental results from chapter 2, there was a slight decrease in the noise of the transcription factor in the nucleus, but there was no change in the noise in RNA levels (Figure 3.11 I). Thus our model has similar behavior to the experimental results where an increase in signaling and a decrease in noise of the transcription factor is seen when Cv-2 is knocked out of the model.

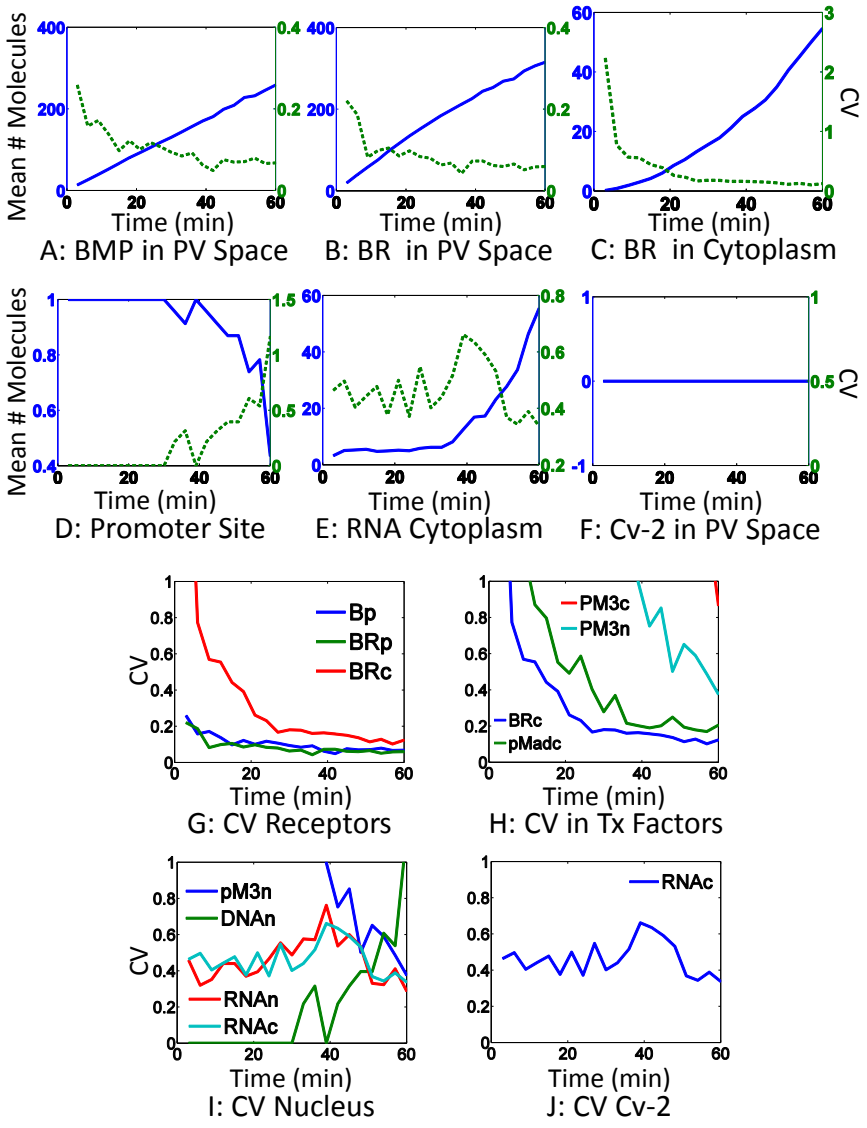

Figure 3.11: Mean and CV of Species in the 3D Stochastic Model with no Cv-2- The molecular temporal evolution of different species in the system with the base parameters and no Cv-2 in the model. A-F) The blue line represents the number of molecules for each respective species, except for DNA where 1 represents the DNA promoter site is free and 0 represents the transcription factor pM3 is bound to the DNA. The green line represents the CV for each respective species. G-J) Comparison of the CV for different species in the model. The results are generated from 50 realizations of the stochastic system.

3.3.3 Noise Propagation in a Simplified Model of BMP Signaling

A simplified model of the BMP signaling network was made to better understand how noise propagates through the signaling network and how a Cv-2 like molecule influences the noise propagation (Figure 3.12). The simplified network is a linear chain of reactions with a nonlinear feedback step using the dynamics of Cv-2. The model consists of B which is produced at a constant rate. B can go to BR directly or through a co-receptor Cv-2. BR catalyzes the production of pMad. pMad then catalyzes the production of mRNA. The mRNA catalyzes the production of C. C can bind with B to form BC, which can then pass B to BR. We assume the receptors are in excess in this model. We will let the reactions of B, BR, C, and BC occur in Volume V_1, reactions for mRNA occur in volume V_2, and pMad occur in volume V_3. We will analyze this model stochastically to see how noise propagates through this signaling network.

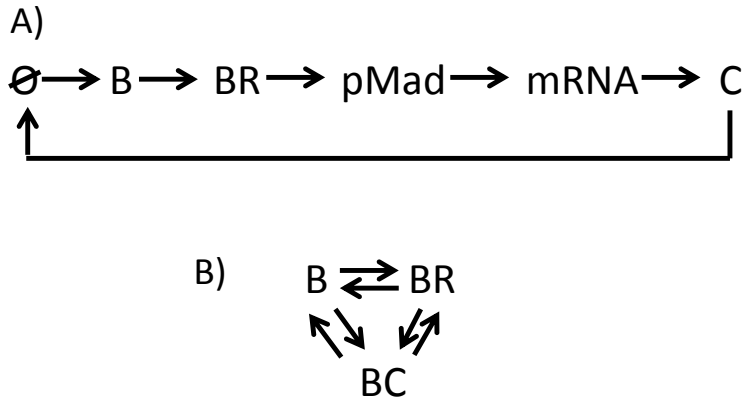

Figure 3.12: Diagram of Simplified Model for BMP Signaling- A) A simplified model of BMP signaling with C either enhancing or inhibiting the rate of B going to BR. B) C interacts reversibly with both B and BR as proposed for the mechanism of Cv-2.

We first analyzed the model with no feedback. The model reaches a steady state very rapidly. Most of the free B molecules react to become BR. BR catalyzes the formation of pMad, which then catalyzes the formation of mRNA. mRNA creates C, but C does not react with B or BR in this model. The noisiest molecule is B, which has a CV of 0.79. All other species have a very low CV, with the CV of mRNA being slightly higher than B, BR, or C. While this simple linear model is not that interesting, it provides a foundation for comparing the results when feedback is added into the model.

The interaction of BC to BR is not well understood, so we performed a parameter scan by changing the K_d and the rate of the individual reactions for the same K_d for BR to BC. As the K_d increases, the average number of molecules for

different species in the system gets closer to the case where there is no inhibition. For very large K_ds the CV of B is significantly larger than when there is no inhibition, but for all other species the CV is similar to the case of no inhibition. For smaller K_d values there is a larger amount of free B and a smaller B CV. Whereas the opposite is true for all other species. We tracked if the BC species was formed from B or BR. Except for when the K_d was 2, 20, or 200 and k_{-7} was 0.001, most of BC was formed from BR. Within the same K_d value, the on and off rates also make a difference on the levels of molecules. However, there are different trends in how the means change depending upon the magnitude of the K_d. Thus, in order to know how the system evolves it is important to know not only the K_d value but also the on and off rates.

Parameter Change	Kd	B	BR	C	BCb	BCr	BC	pMad	mRNA
no feedback	N/A	1.5	101.67	210.42	-	-	-	315.32	28.9
$k_7 = 0.002$, $k_{-7} = 0.1$	0.02	4.04	32.21	2.88	8.13	57.55	65.68	100.2	8.79
$k_7 = 0.2$, $k_{-7} = 10$	0.02	4.6	31.98	0.14	0.12	66.78	66.91	98.82	8.73
$k_7 = 0.02$, $k_{-7} = 0.1$	0.2	3.92	32.57	3.06	8.22	58.43	66.65	100.21	9.09
$k_7 = 0.2$, $k_{-7} = 1$	0.2	4.31	31.39	0.59	1.07	64.16	65.23	97.37	8.79
$k_7 = 0.002$, $k_{-7} = 0.001$	2	1.33	47.7	43.03	39.84	12.73	52.57	145.03	13.21
$k_7 = 0.02$, $k_{-7} = 0.01$	2	2.6	38.66	15.78	24.86	35.89	60.75	118.96	10.66
$k_7 = 0.2$, $k_{-7} = 0.1$	2	3.67	34.26	4.93	6.64	57.5	64.13	105.49	9.57
$k_7 = 2$, $k_{-7} = 1$	2	3.97	32.42	2.87	0.82	64.79	65.51	100.48	9.22
$k_7 = 20$, $k_{-7} = 10$	2	3.88	32.53	2.79	0.06	63.3	63.36	101.11	9.03
$k_7 = 0.02$, $k_{-7} = 0.001$	20	1.38	48.38	47.5	37.3	13.63	50.94	149.62	13.62
$k_7 = 0.2$, $k_{-7} = 0.01$	20	2.1	41.93	26.67	18.49	38.99	57.47	129.83	11.79
$k_7 = 2$, $k_{-7} = 0.1$	20	2.2	39.96	21.24	3.35	56.12	59.47	122.83	10.92
$k_7 = 0.2$, $k_{-7} = 0.001$	200	0.7	60.87	84.66	22.7	17.33	40.03	186.78	16.86
$k_7 = 20$, $k_{-7} = 0.1$	200	0.75	61.23	85.11	0.45	39.64	40.09	189.93	17.11
$k_7 = 40$, $k_{-7} = 0.1$	400	0.5	70.5	113.92	0.21	29.71	29.92	217.35	19.48
$k_7 = 100$, $k_{-7} = 0.1$	1000	0.41	82.97	150.25	0.06	19.05	19.11	256.94	23.65
$k_7 = 200$, $k_{-7} = 0.1$	2000	0.3	90.77	171.84	0.03	11.83	11.86	280.45	25.31
$k_7 = 40$, $k_{-7} = 0.001$	40000	0.2	101.28	203.93	0.12	0.81	0.93	311.73	28.18
$k_7 = 100$, $k_{-7} = 0.001$	100000	0.2	102.52	205.47	0.05	0.32	0.37	316.67	29.24
$k_7 = 200$, $k_{-7} = 0.001$	200000	0.2	100.64	204.22	0.02	0.15	0.17	309.71	27.79

Table 3.11: Mean Number of Molecules for Species in the Simplified Model for a Parameter Scan of BR to BC-A parameter scan for the interaction between BR and BC was performed. The K_d is for BR to BC. k_7 is the rate of $BR- > BR + C$ and k_{-7} is the rate $BR + C- > BR$. The simulation was run for 60 minutes and the results of the last 10 seconds were averaged. Each parameter set is from 50 simulations.

Parameter Change	Kd	B	BR	C	BCr	BCb	BC	pMad	mRNA
no feedback	N/A	0.79	0.09	0.1	N/A	N/A	N/A	0.11	0.21
$k_7 = 0.002$, $k_{-7} = 0.1$	0.02	0.51	0.2	0.58	0.14	0.42	0.13	0.2	0.38
$k_7 = 0.2$, $k_{-7} = 10$	0.02	0.44	0.2	2.57	0.13	3.28	0.13	0.2	0.39
$k_7 = 0.02$, $k_{-7} = 0.1$	0.02	0.51	0.18	0.59	0.13	0.39	0.13	0.19	0.39
$k_7 = 0.2$, $k_{-7} = 1$	0.2	0.5	0.2	1.34	0.13	1.02	0.13	0.19	0.39
$k_7 = 0.002$, $k_{-7} = 0.001$	2	0.85	0.15	0.14	0.3	0.16	0.15	0.15	0.31
$k_7 = 0.02$, $k_{-7} = 0.01$	2	0.58	0.16	0.23	0.17	0.21	0.13	0.17	0.35
$k_7 = 0.2$, $k_{-7} = 0.1$	2	0.5	0.19	0.45	0.13	0.44	0.13	0.18	0.37
$k_7 = 2$, $k_{-7} = 1$	2	0.5	0.19	0.59	0.13	1.16	0.13	0.19	0.36
$k_7 = 20$, $k_{-7} = 10$	2	0.52	0.21	0.62	0.14	N/A	0.14	0.21	0.4
$k_7 = 0.02$, $k_{-7} = 0.001$	20	0.82	0.13	0.13	0.16	0.25	0.14	0.15	0.31
$k_7 = 0.2$, $k_{-7} = 0.01$	20	0.7	0.15	0.2	0.16	0.25	0.13	0.15	0.41
$k_7 = 2$, $k_{-7} = 0.1$	20	0.7	0.16	0.23	0.14	0.56	0.14	0.15	.33
$k_7 = 0.2$, $k_{-7} = 0.001$	200	1.17	0.12	0.11	0.24	0.22	0.17	0.13	0.28
$k_7 = 20$, $k_{-7} = 0.1$	200	1.19	0.12	0.11	0.16	1.46	0.15	0.11	0.27
$k_7 = 40$, $k_{-7} = 0.1$	400	1.51	0.11	0.1	0.19	2.2	0.19	0.11	0.25
$k_7 = 100$, $k_{-7} = 0.1$	1000	1.57	0.1	0.1	0.25	4.54	0.25	0.11	0.22
$k_7 = 200$, $k_{-7} = 0.1$	2000	1.81	0.094	0.093	N/A	0.29	0.29	0.1	0.22
$k_7 = 40$, $k_{-7} = 0.001$	40000	0.81	0.1	0.1	3.07	1.14	1.06	0.12	0.23
$k_7 = 100$, $k_{-7} = 0.001$	200000	2.29	0.09	0.09	N/A	1.81	1.66	0.1	0.21
$k_7 = 200$, $k_{-7} = 0.001$	200000	2.41	0.09	0.08	N/A	2.77	2.62	0.1	0.21

Table 3.12: CV for Molecules for Species in the Simplified Model for a Parameter Scan of BR to BC- A parameter scan for the interaction between BR and BC was performed. The K_d is for BR to BC. k_7 is the rate of $BR- > BR+C$ and k_{-7} is the rate $BR+C- > BR$. The simulation was run for 60 minutes and the results of the last 10 seconds were averaged. Each parameter set is from 50 simulations.

We also performed a parameter scan where each reaction rate in the simplified model was increased and decreased by 10 fold. When the rate of B to BR was decreased, all downstream species also decreased. When the rate of BR to pMad was decreased all species in downstream steps decreased, and BR increased due to less inhibition by C. Similar results were found for decreasing the rate at successively lower points in the signaling network. The opposite occurred for increasing BR. When the rate of BC to B+C was decreased there was slightly less signaling in the network. Increasing the rate of BC to B+C had a very small effect on the amount of signaling, but a large effect on increasing the levels of free B. Changing the rates from B to BR and B to BC had the smallest effects on the network. Interestingly, the level of free B was a very poor indicator of the total level of signaling in the network. Thus both the levels of free B and amount of signaling as measured by BR or pMad are very sensitive to the network parameters and there is a very poor correlation between levels of free B and the amount of signaling.

There were no clear trends in how CV changed when the reaction rates in the simplified model was increased or decreased by 10 fold. Decreasing the rate of B to BR had little effect on the CV of the species except for free B and BC formed from B which decreased by approximately half. Whereas, increasing the rate of B to BC doubled the noise in B and tripled the noise in BC formed from B interacting with C. When the rates downstream of BR were decreased, the CV

of BR decreased and when the rates increased the CV increased. However for the CV of B increased for both a decrease or an increase in rates downstream of BR. The CV of pMad was unchanged by increasing the rate of pMad production, but was increased when the production rates of mRNA or C increased. In all three cases for pMad the level of BR and BC were similar. Thus the noise level for different species varied greatly with the overall parameter rates and it is not easy to predict how the CV will change for different species upon changing kinetic rates.

Parameter Change	B	BR	C	BCb	BCr	BC	pMad	mRNA
no feedback	1.5	101.67	210.42	-	-	-	315.32	28.9
Base Case	3.97	32.42	2.87	0.82	64.79	65.51	100.48	9.22
B->BR 0.1X	18.14	28.62	2.86	3.39	52.34	55.73	87.98	7.85
B->BR 10X	0.43	34.26	3	0.12	66.55	66.67	105.56	9.55
BR->pMad 0.1X	2.09	81.33	0.49	0.06	16.4	16.46	24.78	2.3
BR->pMad 10X	3.11	5.95	23.49	4.69	88.3	92.98	177.13	15.69
pMad->mRNA 0.1X	2.15	81.74	0.36	0.05	16.34	16.34	251.35	2.26
pMad->mRNA 10X	3.05	5.9	23.95	4.74	87.1	91.84	17.54	16.14
mRNA->C 0.1X	2.26	84.12	0.27	0.05	16.34	16.41	257.67	23.72
mRNA->C 10X	2.94	5.9	23.89	4.79	88.39	93.18	17.58	1.61
B+C->BC 0.1X	4.34	33.89	2.7	0.09	63.19	63.28	103.4	9.49
B+C->BC 10X	0.43	34.4	2.57	7.31	60.30	67.61	105.21	9.59
BC->B+C 0.1X	1.33	34.13	2.57	0.23	66.33	66.56	106.02	9.91
BC->B+C 10X	22.42	27.12	4.71	5.17	46.23	51.4	83.18	7.61

Table 3.13: Parameter Scan for the Mean Number of Molecules for Species in the Simplified Model- A parameter scan for the production rates of the molecules in simplified model was performed. The simulation was run for 60 minutes and the results of the last 10 seconds were averaged. Each parameter set is from 50 simulations.

Parameter Change	B	BR	C	BCb	BCr	BC	pMad	mRNA
no feedback	0.79	0.09	0.1	-	-	-	0.11	0.21
Base Case	0.5	0.19	0.59	1.16	0.13	0.13	0.19	0.36
B->BR 0.1X	0.24	0.19	0.61	0.55	0.15	0.14	0.18	0.39
B->BR 10X	1.55	0.19	0.58	3.07	0.12	0.12	0.19	0.36
BR->pMad 0.1X	0.69	0.11	1.28	4.56	0.27	0.27	0.23	0.72
BR->pMad 10X	0.59	0.43	0.22	0.1	0.48	0.1	0.2	0.32
pMad->mRNA 0.1X	0.67	0.11	1.57	4.83	0.28	0.28	0.12	0.67
pMad->mRNA 10X	0.57	0.43	0.25	0.47	0.1	0.1	0.29	0.39
mRNA->C 0.1X	0.64	0.13	1.91	N/A	0.24	0.24	0.15	0.24
mRNA->C 10X	0.57	0.44	0.3	0.48	0.12	0.12	0.33	0.81
B+C->BC 0.1X	0.49	0.19	0.64	3.69	0.13	0.13	0.18	0.37
B+C->BC 10X	1.52	0.18	0.65	0.37	0.14	0.13	0.19	0.37
BC->B+C 0.1X	0.86	0.18	0.62	2.1	0.12	0.12	0.18	0.36
BC->B+C 10X	0.19	0.24	0.51	1.33	0.18	0.13	0.22	0.4

Table 3.14: Parameter Scan for the CV of Molecules for Species in the Simplified Model- A parameter scan for the production rates of the molecules in simplified model was performed. The simulation was run for 60 minutes and the results of the last 10 seconds were averaged. Each parameter set is from 50 simulations.

Discussion Analysis of signaling output in cell culture suggests that the numbers of BMP molecules in vivo during dorsal patterning may be in the range of 10-100 molecules / nucleus [50] indicating stochasticity may be important. We have created a stochastic model that integrates BMP signaling on the plasma membrane with the intracellular dynamics of transcription factor formation, transcription, translation, and a positive feedback mechanism where the product of translation feeds back to influence the dynamics on the plasma membrane. This model draws upon four different deterministic models: a positive feedback model in which BMP signaling to induce a contraction and intensification of BMP signaling on the dorsal surface on the plasma membrane [52], a model using exocytosis and endocytosis of membrane receptors [120], a nuclear shuttle transport system model that leads to nuclear accumulation of pMad [121], and a new model of transcription and translation. The levels of BR, B and C in our single cell model are consistent with the previous spatial deterministic models in [52]. While there are models that have integrated the full TGF-β signaling network together [122, 123, 120], they have not included feedback that regulates the signaling pathway, nor have they been studied in detail with stochastic models. Our 3-Dimensional spatial stochastic model allows us to study in detail mechanisms of noise propagation throughout the BMP signaling network.

Frequency analysis of reactions and diffusion in the system show that it has

multi-scale organization. The phosphorylation of Mad to pMad and transport across the nucleus are possible rate limiting steps, and diffusion of BMP, MAD, and Medea is relatively fast. As a result, all the species except DNA and RNA's are well mixed in the simulation results. Due to the slow phosphorylation of Mad, the fluctuations of pMadc are much larger than the fluctuations of their upstream product BRc. The slow phosphorylation step leads to the transcription factor formation being the noisiest step in the overall model. While w3 used the phosphorylation estimated from fitting a model to experimental data in [121], it was not directly measured. When the phosphorylation rate was increased, there was a significant decrease in the noise in transcription factor formation and a significant reduction in the time when transcription was initiated. Since this is a rate limiting step in our model it may be worth more closely studying the phosphorylation rate experimentally. Similar to phosphorylation, slow transport across the nuclear membrane could lead to large fluctuations of transcription factors. However, nuclear accumulation of the transcription factors may reduce the fluctuations and cancel the amplifying effect of slow transport. Overall the nuclear accumulation reduced fluctuations in active transcription factor in the cytoplasm. Thus another role for the nuclear accumulation may be noise filtering. While there are rate limiting steps such as phosphorylation and BMP receptor binding, there are downstream steps that function to filter out some of the noise.

Positive feedback provided by a co-receptor that sequesters the BMP ligand and helps to transfer it to the receptor has been suggested as a key factor in allowing for a bistable signaling system, where for the same amount of free BMP there can be two different steady states for gene transcription. We used a very rough approximation of the signaling dynamics in the PV space by varying the levels of BMP produced. In the single cell system, we found very different dynamics for a surface binding molecule than the Umulis model [52]. In our model, the surface binding protein only served to sequester and inhibit the total amount of BMP signaling. When Cv-2 was removed from the model, there were higher levels of signaling and less noise in the nuclear transcription factor. However, these results are consistent with the experimental observations highlighted in chapter 2 as well as several other in vivo experimental systems where Cv-2 serves as an inhibitor [96, 97, 98, 99, 89, 92]. In cell culture, Cv-2 was also shown to more often be an inhibitor than an activator of BMP-2, which is the vertebrate homologue of Dpp [57]. In our system when Cv-2 feeds back to inhibit signaling, it transiently increases the total level of noise in the system. This result is consistent with the experimental work in Chapter 2 where the Cv-2 null embryos had a trend of slightly higher noise in the width of nuclear pMad staining. Thus our model is consistent with experimental results that Cv-2 can enhance the overall noise in the system through inhibiting signaling. It would be interesting to extend my

model to study how noise propagates when Cv-2 is an activator of BMP signaling.

In our single cell system there is no competition for signaling molecules, which makes it hard to show the two steady states for one level of BMP, but differences in the timing of gene activation can be observed. In order to study if the model is capable of producing multiple steady states, it would need to be extended to multiple cells. Karim et al. studied a stochastic model of BMP signaling with Cv-2 over a field of cells and found Cv-2 can help sharpen the boundaries [71]. In their model they did not include the downstream network components or endocytosis, which our model suggests may be important in creating a sustained BMP signaling and filtering noise. In addition, while they indicated that there are parameter regimes where Cv-2 increases noise, they did not study it in detail. A careful study of how the system responds under negative feedback, which is observed during dorsal surface patterning, may be warranted. However to extend our system to multiple cells, some of the downstream steps may need to be simplified as it may be too computationally expensive to simulate all the details for multiple cells. While our model hints at being able to create different levels of signaling based on different concentrations of BMP, more work is needed to see if it can produce boundaries between high and low signaling levels.

Our model implemented endocytosis in a more detailed manner than previous models, allowing for signaling in the cytoplasm and recycling of receptors. When

endocytosis is high, there is cytoplasmic accumulation of receptors and BMP bound receptors and most of the active signal came from the endocytosed bound receptors. Since BR cannot dissociate in the cytoplasm and B will be removed from the system once cytoplasmic BR, BCR and BC get exocytosed; exocytosis and endocytosis can either enhance signaling through increasing BR or inhibit signaling by removing B. In our model the enhanced endocytosis rates led to much stronger signaling. This is consistent with previous mathematical models that have suggested that endocytosis is necessary for sustained response to TGF-beta signaling [123, 120]. The accumulation of BMP receptors cytoplasmically also reduces noise in BMP signaling on the plasma membrane. This reduction of noise is very important for the precision of signaling in the system, since the fluctuations in the downstream phosphorylation of pMad are large. Therefore, endocytosis and exocytosis may be a key mechanism in modulating the levels of BMP signaling, helping allow for different thresholds of gene expression to be reached, and attenuating fluctuations in the signal transduction pathway.

The simplified model allowed for a more expanded parameter scan to study how Cv-2 affects noise propagation in a signaling network. In the simplified model, Cv-2 was an inhibitor of signaling. The levels of free BMP were greatly affected by changing different parameters. However there were not clear trends for how the level of free BMP changed. Thus, free levels of BMP may not be the best estimate

for the amount of signaling that is occurring. In areas with higher signaling and higher levels of Cv-2, there may be less free BMP. Instead it may be better to directly study the levels of bound receptor or pMad. The model was sensitive to the K_d for going between bound receptor and BMP bound to Cv-2 and the individual reaction rates. Thus it is important to know the time scale of the reaction between Cv-2 bound with BMP and the BMP receptor. The simplified model indicates it may be important to more closely study the reaction rates during D/V patterning in order to better understand how Cv-2 modulates the signaling network.

In summary, the BMP signaling system is very robust and appears to have evolved many different methods to reduce noise that arises for either low numbers of molecules or slow steps in the signaling process. Due to the different time scales of reactions and transport, the CV is larger at slow reaction steps and small at fast ones. In the PV space, the large number of receptors can help reduce the noise from only a few free BMP molecules. For the exocytosis and endocytosis mechanism, the accumulation of the cytoplasmic BR can cancel the large fluctuations in pMad caused by slow phosphorylation of Mad. Due to the one-directional transport mechanisms, the nuclear accumulation of transcription factors can reduce the fluctuations caused by slow transport across the nuclear membrane. Thus while there are noisy steps due to low production rates of BMP

and slow phosphorylation, there are multiple steps in the signaling pathway to help filter the noise.

Chapter 4

Conclusion and Discussion

In this thesis I have studied robustness and feedback control of BMP signaling during dorsal surface patterning in Drosophila melanogaster. BMP signaling is an important signaling pathway that is used throughout development for embryonic axis specification, organogenesis, and apoptosis. In order to better understand regulation of the BMP signaling pathway I have studied how it influences patterning of the embryonic dorsal surface through three projects. Using molecular biology and genetics I have studied the role of Crossveinless-2 and Nejire in the feedback control of BMP signaling. Using the experimental results for Crossveinless-2 I have collaborated with Dr. Likun Zheng to develop a 3-D stochastic model of BMP signaling for a single cellular compartment during dorsal surface patterning. A stochastic model of BMP signaling is necessary since the free levels of BMP

have been proposed to be less than 100 molecules per nucleus, which would indicate that stochasticity or noise may be present during dorsal surface patterning. The 3-D stochastic model has allowed us to study how noise propagates through the BMP signaling network during early embryogenesis. These projects help us to better understand the feedback control of BMP signaling.

I have identified a new allele of *nej* that contains a stop codon in the 12th exon of the gene. The stop codon truncates part of the highly enriched glutamine domain that is important for transcriptional activation. Based on comparisons to other *nej* alleles I believe this is a dominant negative allele. It most likely functions to bind other transcription factors, but prevents or greatly decreases the levels of transcriptional activation. Maternal loss of this new novel allele leads to a loss of robust patterning of BMP signaling on the dorsal surface. In the pre-cephalic furrow embryo there was loss of BMP signaling in the central region along the A/P axis. All embryos had some staining in the anterior region, but a few had staining in the posterior region. Half of the embryos recovered to relatively normal patterning, and the other half had a variable loss of BMP signaling in the central and posterior regions. During gastrulation half of the embryos were fairly normal and the other half had significant expansion of BMP signaling. Thus our data suggests there may be zygotic rescue of patterning just before gastrulation and we plan on following up on this in the future. We have not studied phenotype for

zygotic loss of the allele, and I plan to do so in the future. The maternal phenotype of the allele is highly variable indicating *nej* may be required for consistent and robust patterning of the dorsal surface.

I have found *cv-2* is a BMP response element that is a negative regulator of BMP signaling during dorsal surface patterning. This result is different from the role of Cv-2 during BMP signaling in the wing disc crossvein formation where it serves as an activator of BMP signaling [57]. However results from the homologue of Cv-2 in vertebrates indicate that the role Cv-2 plays may be highly context dependent. The negative inhibition of BMP signaling lowers the overall peak signaling of the gradient. In Cv-2 null embryos the intracellular signal of BMP receptor activation, pMad, is wider by 20-30%. This change in patterning is significant since it leads to a larger amnioserosa later in embryonic development. While Cv-2 appears to contribute to sharpening of the BMP gradient during dorsal surface patterning, this comes at a cost of a slight decrease in robustness. Thus Cv-2 is in a negative feedback loop in the BMP signaling pathway and contributes to helping with contraction of the BMP gradient during dorsal surface patterning.

An open question is how the BMP gradient during dorsal surface patterning both contracts and intensifies around the dorsal midline. Mathematical modeling has suggested that a positive feedback loop could explain the simultaneous contraction and intensification of BMP signaling, and Cv-2 was proposed to be a

molecule that was in the positive feedback loop [52]. However my experimental results do not support this hypothesis. While Cv-2 does contribute to the overall contraction of the gradient, it is insufficient for completely explaining the contraction and intensification. Thus there are most likely one or more molecules that are involved in a feedback loop to sharpen the BMP morphogen gradient. These unknown molecules may act synergistically with Cv-2, thus it may be necessary to knock out more than one protein in the early embryo to lose both the contraction and intensification of BMP signaling.

Through working with the *cv-2*$^{1-/-}$ allele, I have noticed that Cv-2 null flies may be hyperactive compared to *yw* controls. It would be interesting to test activity levels of the *cv-2*^{1} flies to see if this increase in activity is statistically significant. ModEncode Data from flybase shows that Cv-2 is expressed in the central nervous system throughout development and in the adult fly. During vertebrate development, Cv-2 is involved in neural crest cell migration [97]. Some of the derivatives of neural crest cell migration are cranial and sensory neurons and glia [137]. In addition BMP signaling is important for neural tube patterning [138]. One study in vertebrates has proposed that the duration of BMP signal is important for dorsal neuronal subtype identity [139]. Thus it is plausible that Cv-2 is involved in regulating BMP activity for proper formation or activity of the nervous system in *Drosophila*.

The levels of free BMP have been proposed to be in a stochastic range. To study how noise may affect the robustness of BMP signaling I have created a 3-D stochastic model of BMP signaling in collaboration with Dr.Likun Zheng. This model has allowed us to study how noise propagates through the signaling network. My experimental results indicated that Cv-2 may have increased the noise of BMP signaling during dorsal surface patterning. The stochastic model showed an increase of noise in the system when Cv-2 started to inhibit the BMP signaling pathway in the PV space through competition for the BMP ligand, which is in agreement with experimental results. Our stochastic model indicated that endocytosis may be important for both creating a stronger response to BMP receptor binding and reducing noise in BMP signaling. We also found that the slow phosphorylation step created noise in transcription factor formation. The phosphorylation rate we used was estimated from a mathematical model that was fit to experimental data. Thus, it may be interesting to confirm this rate with further experiments since it is a critical noise propagation step in our model. I also found that nuclear accumulation of the transcription factor was a mechanism that can decrease noise in transcription factor levels. My model suggests that while there are steps that enhance noise in the BMP signaling pathway, there are also multiple mechanisms that function to filter out the noise.

My stochastic model of BMP signaling only studied how the pathway evolves

for one nucleus. It would be interesting to expand this model to study how stochasticity impacts patterning of the dorsal surface. There is a previously published stochastic model that looks at BMP signaling in field of cells, but does not study in detail the downstream network [71]. Our model suggests that the downstream network may be important in the propagation of noise. Thus it would be interesting to create a hybrid of these two models to study stochasticity in morphogen gradient formation. However, simulating the downstream network is computationally very expensive. Thus simplifications will be needed to extend the results to a field of cells based on currently available computing power.

In conclusion I have studied the robustness and feedback control of BMP signaling during early Drosophila development. I have used both mathematical modeling and developmental biology techniques to understand how the BMP signaling pathway is controlled by two different proteins, Nejire and Crossveinless-2. Nejire appears to be required for robust and consistent patterning of the dorsal surface through BMP signaling. Crossveinless-2 is part of a negative feedback loop that helps refine the BMP morphogen gradient on the dorsal surface. Intriguingly, Crossveinless-2 is not a robustness factor, but actually increases the noise in BMP signaling. This finding has been confirmed with a 3-D stochastic model of the BMP signaling pathway. The 3-D stochastic model also predicts that transcription factor formation may also increase noise in the BMP signaling pathway.

However, large number of receptors on the PV space, endocytosis, and nuclear accumulation of transcription factors may be able to buffer noise produced by low copy numbers of signaling molecules and slow steps in the signaling network. While there is noise in BMP signaling, there are several mechanisms that help to filter out that noise to create robust and consistent patterning of target tissues. The work of this theis has allowed us to better understand the feedback control and robustness of BMP signaling during dorsal surface patterning in *Drosophila*.

References

[1] E.C. Délot. Control of endocardial cushion and cardiac valve maturation by BMP signaling pathways. *Molecular genetics and metabolism*, 80(1-2):27–35, 2003.

[2] L. Ye, S.M. Bokobza, and W.G. Jiang. Bone morphogenetic proteins in development and progression of breast cancer and therapeutic potential. *International journal of molecular medicine*, 24(5):591–597, 2009.

[3] J.C. Hardwick, L.L. Kodach, G.J. Offerhaus, and G.R. van den Brink. Bone morphogenetic protein signaling in colorectal cancer. *Nature Reviews Cancer*, 8(10):806–812, 2008.

[4] A. Moustakas and C.H. Heldin. The regulation of TGF-β signal transduction. *Development*, 136(22):3699–3714, 2009.

[5] C. Parada and Y. Chai. Roles of BMP signaling pathway in lip and palate development. *Frontiers of Oral Biology*, 16:60–70, 2012.

[6] D.M. Medeiros and J.G. Crump. New perspectives on pharyngeal dorsoventral patterning in development and evolution of the vertebrate jaw. *Developmental Biology*, 371(2):121–135, 2012.

[7] E. Bier. *Drosophila*, the golden bug, emerges as a tool for human genetics. *Nature Reviews Genetics*, 6(1):9–23, 2005.

[8] G.M. Rubin and E.B. Lewis. A brief history of *Drosophila's* contributions to genome research. *Science*, 287(5461):2216–2218, 2000.

[9] M.D. Adams, S.E. Celniker, R.A. Holt, C.A. Evans, J.D. Gocayne, P.G. Amanatides, S.E. Scherer, P.W. Li, R.A. Hoskins, R.F. Galle, et al. The genome sequence of *Drosophila melanogaster*. *Science*, 287(5461):2185–2195, 2000.

[10] E.W. Myers, G.G. Sutton, A.L. Delcher, I.M. Dew, D.P. Fasulo, M.J. Flanigan, S.A. Kravitz, C.M. Mobarry, K.H.J. Reinert, K.A. Remington, et al. A whole-genome assembly of *Drosophila*. *Science*, 287(5461):2196–2204, 2000.

[11] F.S. Collins, E.S. Lander, J. Rogers, R.H. Waterston, and IHGS Consoortium. Finishing the euchromatic sequence of the human genome. *Nature*, 431(7011):931–945, 2004.

[12] H. Burdett and M. van den Heuvel. Fruits and flies: A genomics perspective of an invertebrate model organism. *Briefings in functional genomics & proteomics*, 3(3):257–266, 2004.

[13] H. Stocker and P. Gallant. An overview on raising and handling *Drosophila*. *Methods in Molecular Biology. Humana Press, Totowa, NJ USA*, 2008.

[14] A.H. Brand and N. Perrimon. Targeted gene expression as a means of altering cell fates and generating dominant phenotypes. *Development*, 118(2):401–415, 1993.

[15] D.A. Elliott and A.H. Brand. The GAL4 system. In *Drosophila*, pages 79–95. Springer, 2008.

[16] E. Ryder and S. Russell. Transposable elements as tools for genomics and genetics in *Drosophila*. *Briefings in functional genomics & proteomics*, 2(1):57–71, 2003.

[17] R.D. St Johnston and W.M. Gelbart. Decapentaplegic transcripts are localized along the dorsal-ventral axis of the *Drosophila* embryo. *The EMBO journal*, 6(9):2785–2791, 1987.

[18] K. Arora, M.S. Levine, and M.B. O'Connor. The screw gene encodes a ubiquitously expressed member of the TGF-β family required for specification of dorsal cell fates in the *Drosophila* embryo. *Genes & development*, 8(21):2588–2601, 1994.

[19] J.L. Neul and E.L. Ferguson. Spatially restricted activation of the SAX receptor by SCW modulates DPP/TKV signaling in *Drosophila* dorsal–ventral patterning. *Cell*, 95(4):483–494, 1998.

[20] M. Nguyen, Sa. Park, G. Marqués, and K. Arora. Interpretation of a BMP activity gradient in *Drosophila* embryos depends on synergistic signaling by two type I receptors, SAX and TKV. *Cell*, 95(4):495–506, 1998.

[21] O. Shimmi, D. Umulis, H. Othmer, and M.B. O'Connor. Facilitated transport of a Dpp/Scw heterodimer by Sog/Tsg leads to robust patterning of the *Drosophila* blastoderm embryo. *Cell*, 120(6):873–886, 2005.

[22] Y.C. Wang and E.L. Ferguson. Spatial bistability of Dpp–receptor interactions during *Drosophila* dorsal–ventral patterning. *Nature*, 434(7030):229–234, 2005.

[23] E. Ruberte, T. Marty, D. Nellen, M. Affolter, and K. Basler. An absolute requirement for both the type II and type I receptors, punt and thick veins, for dpp signaling in vivo. *Cell*, 80(6):889–897, 1995.

[24] A. Letsou, K. Arora, J.L. Wrana, K. Simin, V. Twombly, J. Jamal, K. Staehling-Hampton, F.M. Hoffmann, W.M. Gelbart, J. Massagué, and M.B. O'Connor. *Drosophila* Dpp signaling is mediated by the punt gene product: a dual ligand-binding type II receptor of the TGF-β receptor family. *Cell*, 80(6):899–908, 1995.

[25] H. Mitchell, A. Choudhury, R.E. Pagano, and E.B. Leof. Ligand-dependent and-independent transforming growth factor-β receptor recycling regulated by clathrin-mediated endocytosis and Rab11. *Molecular biology of the cell*, 15(9):4166–4178, 2004.

[26] G.M. Di Guglielmo, C. Le Roy, and J.L. Goodfellow, A.F .and Wrana. Distinct endocytic pathways regulate TGF-β receptor signaling and turnover. *Nature cell biology*, 5(5):410–421, 2003.

[27] P. Xu, J. Liu, and R. Derynck. Post-translational regulation of TGF-β receptor and Smad signaling. *FEBS letters*, 586(14):1871–1884, 2012.

[28] A. Nohe, S. Hassel, M. Ehrlich, F. Neubauer, W. Sebald, Y.I. Henis, and P. Knaus. The mode of bone morphogenetic protein(BMP) receptor oligomerization determines different BMP-2 signaling pathways. *Journal of Biological Chemistry*, 277(7):5330–5338, 2002.

[29] D.J. Sutherland, M. Li, X. Liu, R. Stefancsik, and L.A. Raftery. Stepwise formation of a smad activity gradient during dorsal-ventral patterning of the *Drosophila* embryo. *Development*, 130(23):5705–5716, 2003.

[30] B. Schmierer, A.L. Tournier, P.A. Bates, and C.S. Hill. Mathematical modeling identifies Smad nucleocytoplasmic shuttling as a dynamic signal-interpreting system. *Proceedings of the National Academy of Sciences*, 105(18):6608–6613, 2008.

[31] S. Shi, D.J. de Gorter, W.M Hoogaars, P.A. 't Hoen, and P. ten Dijke. Overactive bone morphogenetic protein signaling in heterotopic ossification and Duchenne muscular dystrophy. *Cellular and Molecular Life Sciences*, 70(3):407–423, 2013.

[32] D. Baldridge, O. Shchelochkov, B. Kelley, and B. Lee. Signaling pathways in human skeletal dysplasias. *Annual review of genomics and human genetics*, 11:189–217, 2010.

[33] T.T. Roberts and A.J. Rosenbaum. Bone grafts, bone substitutes and orthobiologics: The bridge between basic science and clinical advancements in fracture healing. *Organogenesis*, 8(4):0–1, 2012.

[34] J. Cai, E. Pardali, G. Sánchez-Duffhues, and P. ten Dijke. BMP signaling in vascular diseases. *FEBS letters*, 586(14):1993–2002, 2012.

[35] I. Tossidou and M. Schiffer. TGF-β BMP pathways and the podocyte. In *Seminars in Nephrology*, volume 32, pages 368–376. Elsevier, 2012.

[36] Role of the TGF-β/bmp.

[37] M.C. Ramel and C.S. Hill. Spatial regulation of BMP activity. *FEBS letters*, 586(14):1929–1941, 2012.

[38] E.L. Ferguson and K.V. Anderson. Decapentaplegic acts as a morphogen to organize dorsal-ventral pattern in the *Drosophila* embryo. *Cell*, 71(3):451–461, 1992.

[39] H.L. Ashe, M. Mannervik, and M. Levine. Dpp signaling thresholds in the dorsal ectoderm of the *Drosophila* embryo. *Development*, 127(15):3305–3312, 2000.

[40] M.B. O'Connor, D. Umulis, H.G. Othmer, and S.S. Blair. Shaping BMP morphogen gradients in the *Drosophila* embryo and pupal wing. *Development*, 133(2):183–193, 2006.

[41] L. Wolpert. Positional information and the spatial pattern of cellular differentiation. *Journal of theoretical biology*, 25(1):1–47, 1969.

[42] A. Scuderi and A. Letsou. Amnioserosa is required for dorsal closure in *Drosophila*. *Developmental dynamics*, 232(3):791–800, 2005.

[43] L. Wolpert. Diffusible gradients are out-an interview with Lewis Wolpert. interviewed by Richardson, Michael K. *The International journal of developmental biology*, 53(5-6):659, 2009.

[44] R. Dorfman and B.Z. Shilo. Biphasic activation of the BMP pathway patterns the *Drosophila* embryonic dorsal region. *Development*, 128(6):965–972, 2001.

[45] X. Wang, R.E. Harris, L.J. Bayston, and H.L. Ashe. Type IV collagens regulate BMP signalling in *Drosophila*. *Nature*, 455(7209):72–77, 2008.

[46] A. Sawala, C. Sutcliffe, and H.L. Ashe. Multistep molecular mechanism for bone morphogenetic protein extracellular transport in the *Drosophila* embryo. *Proceedings of the National Academy of Sciences*, 109(28):11222–11227, 2012.

[47] C.M. Mizutani, Q. Nie, F.Y.M. Wan, Y.T. Zhang, P. Vilmos, R. Sousa-Neves, E. Bier, J.L. Marsh, and A.D. Lander. Formation of the BMP activity gradient in the *Drosophila* embryo. *Developmental cell*, 8(6):915–924, 2005.

[48] B.Z. Shilo, M. Haskel-Ittah, D. Ben-Zvi, E.D. Schejter, and N. Barkai. Creating gradients by morphogen shuttling. *Trends in Genetics*, 29(6):339–347, 2013.

[49] G. Marqués, M. Musacchio, M.J. Shimell, K. Wunnenberg-Stapleton, K.W.Y. Cho, and M.B. O'Connor. Production of a DPP activity gradient in the early *Drosophila* embryo through the opposing actions of the SOG and TLD proteins. *Cell*, 91(3):417–426, 1997.

[50] O. Shimmi and M.B. O'Connor. Physical properties of Tld, Sog, Tsg and Dpp protein interactions are predicted to help create a sharp boundary in BMP signals during dorsoventral patterning of the *Drosophila embryo*. *Development*, 130(19):4673–4682, 2003.

[51] A. Eldar, R. Dorfman, D. Weiss, H. Ashe, B.Z. Shilo, and N. Barkai. Robustness of the BMP morphogen gradient in *Drosophila* embryonic patterning. *Nature*, 419(6904):304–308, 2002.

[52] D.M. Umulis, M. Serpe, M.B. OConnor, and H.G. Othmer. Robust, bistable patterning of the dorsal surface of the *Drosophila* embryo. *Proceedings of the National Academy of Sciences*, 103(31):11613, 2006.

[53] M. Fujise, S. Takeo, K. Kamimura, T. Matsuo, Toshiro A., S. Izumi, and H. Nakato. Dally regulates Dpp morphogen gradient formation in the *Drosophila* wing. *Development*, 130(8):1515–1522, 2003.

[54] D.J. Bornemann, S. Park, S. Phin, and R. Warrior. A translational block to HSPG synthesis permits BMP signaling in the early *Drosophila* embryo. *Science Signaling*, 135(6):1039–1047, 2008.

[55] R. Vuilleumier, M. Affolter, and G. Pyrowolakis. Pentagone: patrolling BMP morphogen signaling. *Fly*, 5(3):210–214, 2011.

[56] M. Szuperak, S. Salah, E.J. Meyer, U. Nagarajan, A. Ikmi, and M.C. Gibson. Feedback regulation of *Drosophila* BMP signaling by the novel extracellular protein Larval Translucida. *Development*, 138(4):715–724, 2011.

[57] M. Serpe, D. Umulis, A. Ralston, J. Chen, D.J. Olson, A. Avanesov, H. Othmer, M.B. O'Connor, and S.S. Blair. The BMP-binding protein Crossveinless 2 is a short-range, concentration-dependent, biphasic modulator of BMP signaling in *Drosophila*. *Developmental cell*, 14(6):940–953, 2008.

[58] P. Joly, B.H. Jennings, and S.N. Jayasinghe. Development and fertility studies on post-bio-electrosprayed *Drosophila melanogaster* embryos. *Biomicrofluidics*, 3:44107, 2009.

[59] R.R. Dubreuil, P. Wang, S. Dahl, J. Lee, and L.S.B. Goldstein. *Drosophila* β Spectrin functions independently of α Spectrin to polarize the Na, K ATPase in epithelial cells. *Journal of Cell Biology*, 149(3):647–656, 2000.

[60] M. Niepel, S.L. Spencer, and P.K. Sorger. Non-genetic cell-to-cell variability and the consequences for pharmacology. *Current Opinion in Chemical Biology*, 13(5-6):556–651, 2009.

[61] V. Shahrezaei and P.S. Swain. The stochastic nature of biochemical networks. *Current opinion in biotechnology*, 19(4):369–374, 2008.

[62] R. Losick and C. Desplan. Stochasticity and cell fate. *Science*, 320(5872):65–68, 2008.

[63] A. Kurakin. Stochastic cell. *IUBMB life*, 57(2):59–63, 2005.

[64] P.J. Goldschmidt-Clermont, C. Dong, M. West, and D.M. Seo. Of cardiovascular illness and diversity of biological response. *Trends in cardiovascular medicine*, 18(5):194–197, 2008.

[65] G. Tkačik, T. Gregor, and W. Bialek. The role of input noise in transcriptional regulation. *PLoS One*, 3(7):e2774, 2008.

[66] J. Paulsson. Summing up the noise in gene networks. *Nature*, 427(6973):415–418, 2004.

[67] J.J. Tyson and B. Novák. Functional motifs in biochemical reaction networks. *Annual review of physical chemistry*, 61:219–240, 2010.

[68] A. Steinacher and O.S. Soyer. Evolutionary principles underlying structure and response dynamics of cellular networks. In *Evolutionary Systems Biology*, pages 225–247. Springer, 2012.

[69] Y. Dublanche, K. Michalodimitrakis, N. Kümmerer, M. Foglierini, and L. Serrano. Noise in transcription negative feedback loops: simulation and experimental analysis. *Molecular Systems Biology*, 2(1):Epub, 2006.

[70] A. Eldar, R. Dorfman, D. Weiss, H. Ashe, B.Z. Shilo, and N. Barkai. Robustness of the BMP morphogen gradient in *Drosophila* embryonic patterning. *Nature*, 419(6904):304–8, 2002.

[71] M.S. Karim, G.T. Buzzard, and D.M. Umulis. Secreted, receptor-associated bone morphogenetic protein regulators reduce stochastic noise intrinsic to many extracellular morphogen distributions. *Journal of The Royal Society Interface*, 9(70):1073–1083, 2012.

[72] T.G. Kurtz. The relationship between stochastic and deterministic models for chemical reactions. *The Journal of Chemical Physics*, 57(7):2976, 1972.

[73] D.T. Gillespie. Exact stochastic simulation of coupled chemical reactions. *The journal of physical chemistry*, 81(25):2340–2361, 1977.

[74] D.T. Gillespie. Stochastic simulation of chemical kinetics. *Annu. Rev. Phys. Chem.*, 58:35–55, 2007.

[75] K. Arora, M.B. O'Connor, and R. Warrior. BMP signaling in *Drosophila* embryogenesis. *Annals of the New York Academy of Sciences*, 785(1):80–97, 1996.

[76] C.A. Conley, R. Silburn, M.A. Singer, A. Ralston, D. Rohwer-Nutter, D.J. Olson, W. Gelbart, and S.S. Blair. Crossveinless 2 contains cysteine-rich domains and is required for high levels of BMP-like activity during the

formation of the cross veins in *Drosophila*. *Development*, 127(18):3947–3959, 2000.

[77] H. Akimaru, D.X. Hou, and S. Ishii. *Drosophila* CBP is required for dorsal–dependent twist gene expression. *Nature genetics*, 17(2):211–214, 1997.

[78] L. Waltzer and M. Bienz. *Drosophila* CBP represses the transcription factor TCF to antagonize Wingless signalling. *Nature*, 395(6701):521–525, 1998.

[79] B. Florence and W. McGinnis. A genetic screen of the *Drosophila* X chromosome for mutations that modify Deformed function. *Genetics*, 150(4):1497–1511, 1998.

[80] L. Waltzer and M. Bienz. A function of CBP as a transcriptional co-activator during Dpp signalling. *The EMBO journal*, 18(6):1630–1641, 1999.

[81] T. Lilja, D. Qi, M. Stabell, and M. Mannervik. The CBP coactivator functions both upstream and downstream of Dpp/Screw signaling in the early *Drosophila* embryo. *Developmental biology*, 262(2):294–302, 2003.

[82] V.V. Ogryzko, R.L. Schiltz, V. Russanova, B.H. Howard, and Y. Nakatani. The transcriptional coactivators p300 and CBP are histone acetyltransferases. *Cell*, 87(5):953–959, 1996.

[83] A.J. Bannister and T. Kouzarides. The CBP co-activator is a histone acetyltransferase. *Nature*, 384(6610):641–643, 1996.

[84] H. Chen, R.J. Lin, R.L. Schiltz, D. Chakravarti, A. Nash, L. Nagy, M.L. Privalsky, Y. Nakatani, R.M. Evans, et al. Nuclear receptor coactivator ACTR is a novel histone acetyltransferase and forms a multimeric activation complex with P/CAF and CBP/p300. *Cell*, 90(3):569–580, 1997.

[85] T.E. Spencer, G. Jenster, M.M. Burcin, C.D. Allis, J. Zhou, C.A. Mizzen, N.J. McKenna, S.A. Onate, S.Y. Tsai, M.J. Tsai, et al. Steroid receptor coactivator-1 is a histone acetyltransferase. *Nature*, 389(6647):194–198, 1997.

[86] X.J. Yang, V.V. Ogryzko, J. Nishikawa, B.H. Howard, and Y. Nakatani. A p300/CBP-associated factor that competes with the adenoviral oncoprotein E1A. *Nature*, 382(6589):319–324, 1996.

[87] C. Das, M.S. Lucia, K.C. Hansen, and J.K. Tyler. CBP/p300-mediated acetylation of histone H3 on lysine 56. *Nature*, 459(7243):113–117, 2009.

[88] N. Shiama. The p300/CBP family: integrating signals with transcription factors and chromatin. *Trends in cell biology*, 7(6):230–236, 1997.

[89] M. Moser, O. Binder, Y. Wu, J. Aitsebaomo, R. Ren, C. Bode, V.L. Bautch, F.L. Conlon, and C. Patterson. BMPER, a novel endothelial cell precursor-derived protein, antagonizes bone morphogenetic protein signaling and endothelial cell differentiation. *Molecular and cellular biology*, 23(16):5664–5679, 2003.

[90] G. Kolle, K. Georgas, G.P. Holmes, M.H. Little, and T. Yamada. CRIM1, a novel gene encoding a cysteine-rich repeat protein, is developmentally regulated and implicated in vertebrate CNS development and organogenesis. *Mechanisms of development*, 90(2):181–193, 2000.

[91] J. Lin, S.R. Patel, X. Cheng, E.A. Cho, I. Levitan, M. Ullenbruch, S.H. Phan, J.M. Park, and G.R. Dressler. Kielin/chordin-like protein, a novel enhancer of BMP signaling, attenuates renal fibrotic disease. *Nature medicine*, 11(4):387–393, 2005.

[92] M. Matsui, K. Mizuseki, J. Nakatani, S. Nakanishi, and Y. Sasai. Xenopus kielin: A dorsalizing factor containing multiple chordin-type repeats secreted from the embryonic midline. *Proceedings of the National Academy of Sciences*, 97(10):5291–5296, 2000.

[93] M. Ikeya, M. Kawada, H. Kiyonari, N. Sasai, K. Nakao, Y. Furuta, and Y. Sasai. Essential pro-BMP roles of crossveinless 2 in mouse organogenesis. *Development*, 133(22):4463–4473, 2006.

[94] M. Moser, Q. Yu, C. Bode, J.W. Xiong, and C. Patterson. BMPER is a conserved regulator of hematopoietic and vascular development in zebrafish. *Journal of molecular and cellular cardiology*, 43(3):243–253, 2007.

[95] F. Rentzsch, J. Zhang, C. Kramer, W. Sebald, and M. Hammerschmidt. Crossveinless 2 is an essential positive feedback regulator of BMP signaling during zebrafish gastrulation. *Development*, 133(5):801–811, 2006.

[96] M.E. Binnerts, X. Wen, K. Cante-Barrett, J. Bright, H.T. Chen, V. Asundi, P. Sattari, T. Tang, B. Boyle, W. Funk, et al. Human Crossveinless-2 is a novel inhibitor of bone morphogenetic proteins. *Biochemical and biophysical research communications*, 315(2):272–280, 2004.

[97] E. Coles, J. Christiansen, A. Economou, M. Bronner-Fraser, and D.G. Wilkinson. A vertebrate crossveinless 2 homologue modulates BMP activity and neural crest cell migration. *Development*, 131(21):5309–5317, 2004.

[98] M. Kamimura, K. Matsumoto, K. Koshiba-Takeuchi, and T. Ogura. Vertebrate crossveinless 2 is secreted and acts as an extracellular modulator of the BMP signaling cascade. *Developmental dynamics*, 230(3):434–445, 2004.

[99] J. Lin, S.R. Patel, M. Wang, and G.R. Dressler. The cysteine-rich domain protein KCP is a suppressor of transforming growth factor β/activin signaling in renal epithelia. *Molecular and cellular biology*, 26(12):4577–4585, 2006.

[100] S. Matsuda and O. Shimmi. Directional transport and active retention of Dpp/BMP create wing vein patterns in *Drosophila*. *Developmental biology*, 366:153–162, 2012.

[101] K.J.T. Venken, E. Popodi, S.L. Holtzman, K.L. Schulze, S. Park, J.W. Carlson, R.A. Hoskins, H.J. Bellen, and T.C. Kaufman. A molecularly defined duplication set for the X chromosome of *Drosophila melanogaster*. *Genetics*, 186(4):1111–1125, 2010.

[102] R.K. Cook, M.E. Deal, J.A. Deal, R.D. Garton, C.A. Brown, M.E. Ward, R.S. Andrade, E.P. Spana, T.C. Kaufman, and K.R. Cook. A new resource for characterizing X-linked genes in *Drosophila melanogaster*: systematic coverage and subdivision of the X chromosome with nested, Y-linked duplications. *Genetics*, 186(4):1095–1109, 2010.

[103] Y. Zhao, K. Takeyama, S. Sawatsubashi, S. Ito, E. Suzuki, K. Yamagata, M. Tanabe, S. Kimura, S. Fujiyama, T. Ueda, et al. Corepressive action of CBP on androgen receptor transactivation in pericentric heterochromatin in a *Drosophila* experimental model system. *Molecular and cellular biology*, 29(4):1017–1034, 2009.

[104] R. Anderson, J.and Bhandari and J.P. Kumar. A genetic screen identifies putative targets and binding partners of CREB-binding protein in the developing *Drosophila* eye. *Genetics*, 171(4):1655–1672, 2005.

[105] J.P. Kumar, T. Jamal, A. Doetsch, F.R. Turner, and J.B. Duffy. CREB binding protein functions during successive stages of eye development in *Drosophila*. *Genetics*, 168(2):877–893, 2004.

[106] N.T. Takaesu, A.N. Johnson, O.H. Sultani, and S.J. Newfeld. Combinatorial signaling by an unconventional Wg pathway and the Dpp pathway requires Nejire (CBP/p300) to regulate *dpp* expression in posterior tracheal branches. *Developmental biology*, 247(2):225–236, 2002.

[107] T. Lilja, H. Aihara, M. Stabell, Y. Nibu, and M. Mannervik. The acetyltransferase activity of *Drosophila* CBP is dispensable for regulation of the Dpp pathway in the early embryo. *Developmental biology*, 305(2):650–658, 2007.

[108] W.H. Ludlam, M.H. Taylor, K.G. Tanner, J.M. Denu, R.H. Goodman, and S.M. Smolik. The acetyltransferase activity of CBP is required for wingless activation and H4 acetylation in *Drosophila melanogaster*. *Molecular and cellular biology*, 22(11):3832–3841, 2002.

[109] D. Fu, Y. Wen, and J. Ma. The co-activator CREB-binding protein participates in enhancer-dependent activities of bicoid. *Journal of Biological Chemistry*, 279(47):48725–48733, 2004.

[110] F. Hamaratoglu, A.M. de Lachapelle, G. Pyrowolakis, S. Bergmann, and M. Affolter. Dpp signaling activity requires Pentagone to scale with tissue size in the growing *Drosophila* wing imaginal disc. *PLoS biology*, 9(10):e1001182, 2011.

[111] D.M. Umulis, O. Shimmi, M.B. O'Connor, and H.G. Othmer. Organism-scale modeling of early *Drosophila* patterning via Bone Morphogenetic Proteins. *Developmental cell*, 18(2):260–274, 2010.

[112] O. Wartlick, P. Mumcu, A. Kicheva, T. Bittig, C. Seum, F. Jülicher, and M. González-Gaitán. Dynamics of Dpp signaling and proliferation control. *Science*, 331(6021):1154–1159, 2011.

[113] Y. Ogiso, K. Tsuneizumi, N. Masuda, M. Sato, and T. Tabata. Robustness of the dpp morphogen activity gradient depends on negative feedback regulation by the inhibitory Smad, Dad. *Development, growth & differentiation*, 53(5):668–678, 2011.

[114] A. Brooks, W. Dou, X. Yang, T. Brosnan, M. Pargett, L.A. Raftery, and D.M. Umulis. BMP signaling in wing development: A critical perspective on quantitative image analysis. *FEBS letters*, 586(14):1942–1952, 2012.

[115] A. Ralston and S.S. Blair. Long-range Dpp signaling is regulated to restrict BMP signaling to a crossvein competent zone. *Developmental biology*, 280(1):187–200, 2005.

[116] L.H. Frank and C. Rushlow. A group of genes required for maintenance of the amnioserosa tissue in *Drosophila*. *Development*, 122(5):1343–1352, 1996.

[117] M.L. Yip, M.L. Lamka, and H.D. Lipshitz. Control of germ-band retraction in *Drosophila* by the zinc-finger protein HINDSIGHT. *Development*, 124(11):2129–2141, 1997.

[118] T.E. Haerry, O. Khalsa, M.B. O'Connor, and K.A. Wharton. Synergistic signaling by two BMP ligands through the SAX and TKV receptors controls wing growth and patterning in *Drosophila*. *Development*, 125(20):3977–3987, 1998.

[119] A. Hartung, K. Bitton-Worms, M.M. Rechtman, V. Wenzel, J.H. Boergermann, S. Hassel, Y.I. Henis, and P. Knaus. Different routes of bone morphogenic protein (BMP) receptor endocytosis influence BMP signaling. *Molecular and cellular biology*, 26(20):7791–7805, 2006.

[120] S.W. Chung, F.L. Miles, R.A. Sikes, C.R. Cooper, M.C. Farach-Carson, and B.A. Ogunnaike. Quantitative modeling and analysis of the transforming growth factor beta signaling pathway. *Journal of Biophysics*, 96:1733–1750, 2009.

[121] B. Schmierer, A.L. Tournier, P.A. Bates, and C.S. Hill. Mathematical modeling identifies Smad nucleocytoplasmic shuttling as a dynamic signal-interpreting system. *Proceedings of the National Academy of Sciences*, 105(18):6608, 2008.

[122] Z. Zi and E. Klipp. Constraint-based modeling and kinetic analysis of the Smad dependent TGF-β signaling pathway. *PLoS One*, 2(9):e936, 2007.

[123] Z. Zi, Z.and Feng, D.A. Chapnick, M. Dahl, D. Deng, E. Klipp, A. Moustakas, and X. Liu. Quantitative analysis of transient and sustained transforming growth factor-β signaling dynamics. *Molecular systems biology*, 7(1), 2011.

[124] J.M.G. Vilar, R. Jansen, and C. Sander. Signal processing in the TGF-β superfamily ligand-receptor network. *PLoS Computational Biology*, 2(1):e3, 2006.

[125] P. ten Dijke and C.H. Heldin. Smad signal transduction: Smads in proliferation, differentiation and disease. *Proteins and Cell Regulation*, 5, 2006.

[126] B. Schmierer and C.S. Hill. Kinetic analysis of Smad nucleocytoplasmic shuttling reveals a mechanism for transforming growth factor β-dependent nuclear accumulation of Smads. *Molecular and cellular biology*, 25(22):9845, 2005.

[127] B.Y. Qin, B.M. Chacko, S.S. Lam, M.P. de Caestecker, J.J. Correia, and K. Lin. Structural basis of Smad1 activation by receptor kinase phosphorylation. *Molecular cell*, 8(6):1303–1312, 2001.

[128] B. Drawert, S. Engblom, and A. Hellander. URDME: a modular framework for stochastic simulation of reaction-transport processes in complex geometries. *BMC systems biology*, 6(1):76, 2012.

[129] R.A. Anders, S.L. Arline, J.E. Doré, and E.B. Leof. Distinct endocytic responses of heteromeric and homomeric transforming growth factor β receptors. *Molecular biology of the cell*, 8(11):2133–2143, 1997.

[130] D.M. Holloway, F.J. Lopes, L. da Fontoura Costa, B. A. Travençolo, N. Golyandina, K. Usevich, and A.V. Spirov. Gene expression noise in spatial patterning: hunchback promoter structure affects noise amplitude and distribution in *Drosophila* segmentation. *PLoS computational biology*, 7(2):e1001069, 2011.

[131] E.A. Nalefski, E. Nebelitsky, J.A. Lloyd, and S.R. Gullans. Single-molecule detection of transcription factor binding to DNA in real time: specificity, equilibrium, and kinetic parameters. *Biochemistry*, 45(46):13794–13806, 2006.

[132] S. Thomsen, S. Anders, S.C. Janga, W. Huber, and C.R. Alonso. Genome-wide analysis of mRNA decay patterns during early *Drosophila* development. *Genome biology*, 11(9):R93, 2010.

[133] A. Mor, S. Suliman, R. Ben-Yishay, S. Yunger, Y. Brody, and Y. Shav-Tal. Dynamics of single mRNP nucleocytoplasmic transport and export through the nuclear pore in living cells. *Nature cell biology*, 12(6):543–552, 2010.

[134] D.Y. Vargas, A. Raj, S.A.E. Marras, F.R. Kramer, and S. Tyagi. Mechanism of mRNA transport in the nucleus. *Proceedings of the National Academy of Sciences of the United States of America*, 102(47):17008, 2005.

[135] M. Scott. Tutorial: Genetic circuits and noise. `http://www.math.uwaterloo.ca/~mscott/NoiseTutorial.pdf`, 2006.

[136] S. Felder, J. LaVin, A. Ullrich, and J. Schlessinger. Kinetics of binding, endocytosis, and recycling of EGF receptor mutants. *The Journal of cell biology*, 117(1):203–212, 1992.

[137] A.K. Knecht and M. Bronner-Fraser. Induction of the neural crest: a multigene process. *Nature Reviews Genetics*, 3(6):453–461, 2002.

[138] E.M. De Robertis and H. Kuroda. Dorsal-ventral patterning and neural induction in Xenopus embryos. *Annual review of cell and developmental biology*, 20:285–308, 2004.

[139] S. Tozer, G. Le Dreau, E. Marti, and J. Briscoe. Temporal control of BMP signalling determines neuronal subtype identity in the dorsal neural tube. *Development*, 140(7):1467–1474, 2013.

Appendix A

Acronyms

Care has been taken in this thesis to minimize the use of jargon and acronyms, but this cannot always be achieved. This appendix contains a table of acronyms and their meaning.

A.1 Acronyms

Table A.1: Acronyms

Acronym	Meaning
AM	Average Method
A/P	Anterior / Posterior
	Continued on next page

Table A.1 – continued from previous page

Acronym	Meaning
B	BMP in Mathematical Model
BC	B bound to C in Mathematical Model
BCR	B, C, and R in One Complex in Mathematical Model
BMP	Bone Morphogenic Protein
BR	Bound Receptor in Mathematical Model
C	Cv-2 Like Molecule in Mathematical Model
CBP	CREB Binding Protein
CV	Coefficient of Variation
Cv-2	Crossveinless-2
Dpp	Decapentaplegic
D/V	Dorsal / Ventral
FI	Fluorescence Intensity
Gbb	Glass Bottom Boat
GFP	Green Fluorescent Protein
His	Histone
HSPG	Heparan Sulfate Proteoglycan

Continued on next page

Table A.1 – continued from previous page

Acronym	Meaning
L(1)G0232	Lethal (1) G0232
Ltl	Larval Translucida
Me	Medea in Mathematical Model
MM	Mixing Method
Mvent[1]	Maternal Ventralizing Factor-1
Nej	Nejire
PCV	Posterior Crossvein
PI	Propidium Iodide
Pol	Polymerase
PM	Parallel Method
pM3	2 pMad Molecules and 1 Medea in a Complex in the Mathematical Model
pMad	Phosphorylated Mad
pMad2	Dimer of Two pMad Molecules in Mathematical Model
pMMe	Dimer of pMad and Medea in Mathematical Model
Pnt	Punt

Continued on next page

Table A.1 – continued from previous page

Acronym	Meaning
PV	Perivitelline
R	Receptor in Mathematical Model
RM	Ratio Method
RNAp	RNA Polymerase in Mathematical Model
RNAt	RNA Elongation Complex in Mathematical Model
Sax	Saxophone
SC	Staining Control
Scw	Screw
Sog	Short Gastrulation
T	Threshold
TGF-β Tkv	Thickvein
Tld	Tolloid
Tsg	Twisted Gastrulation
V	Volume
W	White
Wt	Wild Type

Continued on next page

Table A.1 – continued from previous page

Acronym	Meaning
*c	Molecule in the Cytoplasm
*n	Molecule in the Nucleus
*p	Molecule in the PV Space